

Greenhouse gas release from nearshore sediments with peat deposits under long and short seawater exposure

Monographische Dissertation

zur

Erlangung des akademischen Grades

doctor rerum naturalium (Dr. rer. nat)

der Mathematisch-Naturwissenschaftlichen Fakultät

der Universität Rostock

vorgelegt von

Daniel Lars Pönisch

geboren am 15. September 1993 in Dresden

Rostock, April 2023



Dieses Werk ist lizenziert unter einer
Creative Commons Namensnennung - Weitergabe unter gleichen Bedingungen
4.0 International Lizenz.

Diese Dissertation entstand am Leibniz-Institut für Ostseeforschung Warnemünde (IOW) unter der Betreuung von Prof. Dr. Gregor Rehder in der Arbeitsgruppe "Biogeochemie Umweltrelevanter Gase" im Zeitraum vom Januar 2019 bis April 2023. Die Arbeit wurde im Rahmen des Graduiertenkollegs „Baltic TRANSCOAST“ durchgeführt und von der Deutschen Forschungsgemeinschaft (DFG) gefördert.

This dissertation was conducted at the Leibniz Institute for Baltic Sea Research Warnemünde (IOW) under the supervision of Prof. Dr. Gregor Rehder in the working group “trace gas biogeochemistry” between January 2019 and April 2023. The work was carried out within the framework of the Research Training Group "Baltic TRANSCOAST" funded by the German Research Foundation (DFG).

Gutachter:

Erster Gutachter: Prof. Dr. Gregor Rehder
Biogeochemie Umweltrelevanter Gase
Leibniz-Institut für Ostseeforschung Warnemünde (IOW)
Rostock, Germany

Zweiter Gutachter: Prof. Dr. Arne Körtzinger
Chemische Ozeanographie
GEOMAR Helmholtz-Zentrum für Ozeanforschung Kiel
Kiel, Germany

Datum der Einreichung: 20.04.2023

Datum der Verteidigung: 14.11.2023

Table of contents

Table of contents	II
Abstract	V
Zusammenfassung	VIII
Publications	XI
List of abbreviations, symbols and variables	XIII
List of figures	XVI
List of tables	XIX
Motivation and aims	XX
1. Introduction	1
1.1 Highly dynamic shallow water areas under pressure	1
1.2 Carbon dioxide	2
1.2.1 Analytical variables of the marine CO ₂ system	3
1.2.2 The marine CO ₂ system.....	4
1.3 Methane	6
1.4 Peatlands.....	9
1.4.1 Peatlands in the climate system.....	9
1.4.2 The impact of peatland rewetting on GHG fluxes and nutrients.....	10
1.5 Methodological challenges in shallow waters.....	12
1.6 The study areas.....	13
1.6.1 The nearshore shallow waters of the Hütelmoor.....	15
1.6.2 The rewetted peatland Drammendorf.....	16
2. Methods.....	17
2.1 The landers as a platform and sensor overview	17
2.1.1 The central data processing unit (DPU)	17
2.1.2 The Instrumentation	18
2.2 The Hütelmoor lander survey.....	19
2.2.1 Deployment of the landers	20
2.2.2 Sensor configuration and data post-processing.....	20
2.2.3 Measures for consistent data acquisition and quality control	22
2.2.4 Discrete sampling.....	23
2.2.5 Supplementary information (water velocity, numerical model, water column measurements) and data handling	23
2.3 The Drammendorf field survey	25

2.4	The Drammendorf lander survey	28
2.4.1	Major lander adaptations and the field deployment	28
2.4.2	Sensor configuration and data post-processing	28
2.4.3	Discrete sampling	31
2.4.4	Supplementary information and data handling	31
2.5	Laboratory analysis of discrete samples	32
2.5.1	Analysis of the inorganic carbon system (C_T , A_T , pH)	32
2.5.2	Dissolved CH_4 and N_2O concentration analysis	33
2.5.3	Analysis of nutrient concentrations (NO_3^- , NO_2^- , NH_4^+ , PO_4^{3-})	33
2.5.4	Analysis of dissolved O_2	34
2.6	Calculated variables and auxiliary data	34
2.7	Atmospheric flux calculation based on air-sea exchange parameterization	34
2.7.1	Air-sea exchange calculation for the Drammendorf field survey	35
2.7.2	Air-sea exchange calculation for the Drammendorf lander survey	36
3.	Results	37
3.1	The Hütelmoor lander survey	37
3.1.1	Characterization of meteorological and hydrographic conditions during the lander survey	37
3.1.2	Time records of biochemical variables at both landers	41
3.1.3	Identification of three event-based system changes	43
3.2	The Drammendorf field survey	47
3.2.1	Surface water properties (temperature, salinity, O_2 , DOC, and chlorophyll <i>a</i>)	49
3.2.2	The inorganic carbon system in the surface water after rewetting	49
3.2.3	CH_4 in the surface water after rewetting	50
3.2.4	N_2O in the surface water after rewetting	51
3.2.5	Nutrient concentrations after rewetting	51
3.2.6	Pre- and post-rewetting GHG fluxes (CO_2 , CH_4 , N_2O)	52
3.3	The Drammendorf lander survey	53
3.3.1	Time series of the variables at lander 1 and lander 2	53
3.3.2	Short-term variability and diurnal cycles	58
3.3.3	Identification of three event-based system changes	60
3.3.4	GHG fluxes derived from high-resolution data at lander 1 and lander 2	63
4.	Discussion	66
4.1	The Hütelmoor lander survey	66

4.1.1	GHG and nutrient distribution in the nearshore area	66
4.1.2	Drivers of nearshore variability.....	68
4.1.3	Implications of these lander deployments.....	71
4.2	Drammendorf field survey	72
4.2.1	Development of the CO ₂ system after flooding	72
4.2.2	The development of CH ₄ after flooding.....	74
4.2.3	The role of brackish water in GHG fluxes – a system shift.....	75
4.2.4	Nutrient dynamics after rewetting.....	78
4.3	The Drammendorf lander survey	78
4.3.1	Temporal and spatial variation of CO ₂ and CH ₄ distribution at lander 1 and lander 2.....	78
4.3.2	Diurnal <i>p</i> CO ₂ and <i>p</i> CH ₄ variability.....	80
4.3.3	Event driven variability in the rewetted peatland.....	81
4.3.4	Derivation of GHG fluxes from sensor measurements	83
4.4	Conceptual assessment of the lander system and data verification.....	85
5.	Summary	87
6.	Outlook.....	90
7.	References	91
	Data availability and interdisciplinary collaborations.....	102
	Danksagung.....	104
	Curriculum Vitae.....	105
	Eidesstattliche Versicherung	106

Abstract

Coastal oceans form unique shallow water habitats as an interface between the marine and terrestrial ecosystems, host a high biodiversity, and fulfill important ecological, social, and economic functions for humankind. The shallow water zones of the Baltic Sea ($\sim 0 - 10$ m) are subjected to wave-induced mixing as well as sediment-water and water-air interactions, but also to strong anthropogenic inputs of nutrients and pollutants. A rising sea level, the increase in extreme weather events, and coastal erosion have already increased the interactions between marine and terrestrial systems and are predicted to become even more intense. This is exemplified by the low-lying terrestrial areas in the Baltic Sea region which are at risk of flooding. However, as these shallow areas are often drained peatlands, the risk of natural flooding can also be used to actively rewet coastal peatlands with seawater. As a result, these peatlands become permanently flooded areas and in turn become part of the shallow water zones. Both shallow water zones and rewetted peatlands can play essential roles in organic matter (OM) sequestration, but long-term data with adequate resolution are lacking. Furthermore, the lack of knowledge about the temporal and spatial variability of the involved processes and their biogeochemical controls leads to uncertain estimates of the contribution of marine greenhouse gases (GHGs) to climate processes from these areas.

In this work, the scientific focus was on the distribution of GHGs (CO_2 , CH_4 , N_2O) at the sediment-water interface of nearshore sediments with peat deposits, including the role of oxygen (O_2) availability and with respect to the biogeochemistry of the water body. Therefore, several physicochemical variables were investigated based on temporal high-resolution sensor measurements in the field and these were combined with conventional discrete sampling of the water body. The methodological focus was on the deployment of two prototype sensor-equipped lander systems at two study sites on the German Baltic Sea coast. One field study was conducted in the shallow waters of the Baltic Sea (Hütelmoor) at around 6 m water depth and the results were evaluated in an interdisciplinary approach. Two additional studies addressed the rewetting of a degraded peatland (Drammendorf) with brackish water, the consequences of which for GHG emissions are largely unknown.

The shallow waters of the Baltic Sea (Hütelmoor) showed considerable temporal changes in GHG distribution, with shifts of up to one order of magnitude within a few hours (7 – 27 h), ranging from 293 to 1383 μatm for $p\text{CO}_2$ and from 9 to 96 μatm ($17 - 143 \text{ nmol L}^{-1}$) for CH_4 . This variability was partly triggered by event-based changes in the water column (tipping

points). One such event consisted of an advection of water masses from nearby, deeper parts of the Baltic Sea, transporting salt- and CO₂-enriched (up to 1000 µatm-CO₂) water to the coast for ~ 24 h, but only below 2 – 3 m water depth. Potential mixing of the water column may cause surface water to become oversaturated, releasing CO₂ into the atmosphere. A second event consisted of a period of calm conditions of ~ 4 days, during which local processes could be established. This led, for example, to an accumulation of CH₄ in the bottom water probably released from the pore water.

The GHG response to rewetting a coastal peatland (Drammendorf) with brackish water was evaluated based on emissions determined before, in the first year, and in the second year of rewetting. CO₂ emissions remained high in the first year after rewetting compared to pre-rewetting conditions, despite they decreased slightly, from $0.29 \pm 0.82 \text{ g m}^{-2} \text{ h}^{-1}$ to $0.26 \pm 0.29 \text{ g m}^{-2} \text{ h}^{-1}$ (comparing the summer/autumn of both 2019 and 2020). At the same time, a decrease in the amplitude (minimum/maximum) of the fluxes prevented peak emissions after rewetting. In the second year (summer 2021), CO₂ fluxes decreased by 1.9-fold compared to the first year after flooding. In general, the CO₂ fluxes after rewetting with brackish water were higher than those after rewetting peatlands with freshwater, the water source normally used. The availability of OM from residual vegetation as no removal of the topsoil was conducted prior to rewetting or that built up via primary production after rewetting was likely the driver of the high CO₂ fluxes. Investigations in the second year after flooding based on high-resolution measurements revealed a considerable temporal fluctuation in the CO₂ distribution, expressed as multi-day, diurnal, and event-based variability. Spatial differences in the flooded peatland occurred for variables dominated by biological processes. CH₄ emissions increased by one order of magnitude, from $0.13 \pm 1.01 \text{ mg m}^{-2} \text{ h}^{-1}$ to $1.74 \pm 7.59 \text{ mg m}^{-2} \text{ h}^{-1}$, during the transition from dry to flooded conditions in the first year but decreased by 2.6-fold during the second year. Despite the immediate increase after rewetting, CH₄ emissions were lower compared to studies that examined rewetting with freshwater. Although CH₄ formation was favored by the presence of OM, this was offset by the effects of (i) the availability of O₂ due to water column mixing and the sulfate present in the brackish water, both of which suppressed CH₄ production and (ii) both of which resulted in aerobic and anaerobic CH₄ oxidation. The high-resolution measurements in the second year revealed strong multi-day, short-term (< 1 day), and event-based variability in *p*CH₄. The event-based variability of CO₂ and CH₄ in the flooded peatland occurred in response to a

storm, precipitation, and water level changes that resulted in fast changes in the water body biogeochemistry and GHG partial pressures.

This dissertation expands the general understanding of the distribution and temporal variability of GHGs in coastal regions. It also sheds light on possible control mechanisms of the marine carbon cycle in coastal areas. Given the temporal scales at which significant changes in variables occurred (i.e., few hours), it becomes obvious that these could only be captured using the new and adapted methods such as those employed here. The development and establishment of centralized sensor-based measurements using two lander systems was critical to this work, although improvements to the systems are still needed. The results of this work pointed to directions for further coastal research that take into account the control of GHG concentrations by tipping points and by pronounced day-night shifts. Furthermore, the lower CH₄ fluxes in the peatland examined in this dissertation, along with a trend of decreasing GHG fluxes, demonstrate the favorable impact of rewetting with brackish water rather than freshwater, and thus the potential of this rewetted area to serve as a carbon sink.

Zusammenfassung

Die Küstenmeere bilden einzigartige Flachwasserlebensräume als Schnittstelle zwischen marinen und terrestrischen Ökosystemen, beherbergen eine hohe genetische Vielfalt und erfüllen wichtige ökologische, soziale und wirtschaftliche Funktionen für die Menschheit. Der Flachwasserbereich der Ostsee ($\sim 0 - 10$ m) ist durch wellenbedingte Durchmischung sowie Sediment-Wasser- und Wasser-Luft-Wechselwirkungen gekennzeichnet, aber auch einem starken anthropogenen Eintrag von Nähr- und Schadstoffen ausgesetzt. Ein steigender Meeresspiegel, die Zunahme extremer Wetterereignisse und die Küstenerosion haben die Interaktionen zwischen marinen und terrestrischen Systemen bereits verstärkt und werden voraussichtlich noch intensiver werden. Im Ostseeraum sind beispielsweise die niedrig gelegenen Gebiete an Land, bei denen es sich häufig auch um entwässerte Moore handelt, von Überschwemmungen bedroht. Diese möglichen, natürlichen Überschwemmungen können allerdings für aktive Wiedervernässungen von Küstenmooren mit Seewasser genutzt werden, was zur Folge hat, dass die so entstandenen Flächen ein Teil des Flachwasserbereichs werden können. Obwohl Flachwasserzonen und wiedervernässte Torfgebiete eine wesentliche Rolle bei der Sequestrierung von organischem Material (OM) einnehmen können, fehlen für aktuelle Schätzungen langfristige Daten mit angemessener Auflösung. Daher ist das Wissen über die zeitliche und räumliche Variabilität der beteiligten Prozesse und die biogeochemischen Kontrollmechanismen begrenzt, was zu Unsicherheiten bei der Abschätzung des Beitrages mariner Treibhausgase (THG) aus diesen Gebieten zum Klimageschehen führt.

In dieser Arbeit lag der wissenschaftliche Schwerpunkt auf der Verteilung und den Mechanismen der Treibhausgasfreisetzung (CO_2 , CH_4 , N_2O) an der Sediment-Wasser-Grenzfläche von küstennahen Sedimenten mit Torfablagerungen sowie der Rolle der Verfügbarkeit von Sauerstoff (O_2) und im Hinblick auf die Biogeochemie des Wasserkörpers. Zu diesem Zweck wurden eine Vielzahl physikalisch-chemischer Variablen mit zeitlich hochauflösenden sensorischen Messungen im Feld untersucht und diese mit konventionellen Einzelbeprobungen des Wasserkörpers kombiniert. Der methodische Schwerpunkt lag auf dem Einsatz von zwei, mit Sensoren ausgestatteten, Prototypen-Landersystemen, die an zwei Standorten der deutschen Ostseeküste eingesetzt wurden. Eine Feldstudie wurde im Flachwasser der Ostsee (Hütelmoor) in etwa 6 m Wassertiefe durchgeführt und die Ergebnisse in einem interdisziplinären Ansatz bewertet. Zwei weitere Studien befassten sich

mit der Wiedervernässung eines degradierten Mooregebietes (Drammendorf) mit Brackwasser, deren Folgen für die Treibhausgasemissionen weitgehend unbekannt sind.

Das Flachwasser der Ostsee (Hütelmoor) zeigte beträchtliche zeitliche Veränderungen in der THG-Verteilung, mit Änderungen bis zu einer Größenordnung innerhalb weniger Stunden (7–27 h), die sich im Falle von CO_2 von 293 – 1383 μatm und für CH_4 von 9 – 96 μatm (17 – 143 nmol L^{-1}) erstreckte. Diese Variabilität wurde teilweise durch ereignisgesteuerte Veränderungen in der Wassersäule (Kippunkte) ausgelöst. Ein solches Ereignis bestand in der Advektion von Wassermassen aus nahegelegenen, tieferen Teilen der Ostsee. Dabei wurde salz- und CO_2 -angereichertes Wasser von bis zu 1000 $\mu\text{atm-CO}_2$ für etwa 24 h an die Küste transportiert, allerdings wurde dieses Signal nur unterhalb von 2 – 3 m Wassertiefe detektiert. Das ist insofern bedeutend, als dass eine potentielle Durchmischung zu übersättigten Bedingungen an der Wasseroberfläche führen kann und somit Treibhausgase in die Atmosphäre abgegeben werden können. Ein zweites Ereignis bestand aus einer Periode ruhiger Bedingungen von ~ 4 Tagen, in der lokale Prozesse, die Einfluss auf die THG-Verteilung nahmen, an Bedeutung gewannen. Dies führte beispielsweise zu einer Anreicherung von CH_4 im Bodenwasser, welches wahrscheinlich aus Porenwasser freigesetzt wurde.

Die THG-Reaktion auf die Wiederbefeuchtung eines Küstenmoores (Drammendorf) mit Brackwasser wurde anhand der Emissionen bewertet, die vor, im ersten und im zweiten Jahr der Wiederbefeuchtung ermittelt wurden. Die CO_2 Emissionen blieben im ersten Jahr nach der Vernässung im Vergleich zu den Verhältnissen vor der Vernässung hoch, obwohl sie leicht von $0.29 \pm 0.82 \text{ g m}^{-2} \text{ h}^{-1}$ auf $0.26 \pm 0.29 \text{ g m}^{-2} \text{ h}^{-1}$ sanken (Vergleich Sommer/Herbst der Jahre 2019 und 2020). Gleichzeitig verhinderte eine Abnahme der Amplitude der Flüsse Spitzenemissionen nach der Vernässung. Im zweiten Jahr (Sommer 2021) sanken die CO_2 Flüsse im Vergleich zum ersten Jahr um das 1.9-fache. Im Allgemeinen waren die CO_2 Flüsse nach der Wiederbefeuchtung höher als in Studien, die die Auswirkungen von Wiederbefeuchtungen mit Süßwasser, das normalerweise verwendet wird, untersuchen. Die Verfügbarkeit von OM aus der Restvegetation (keine Entfernung der Deckschicht vor der Vernässung) oder OM, das nach der Vernässung über die Primärproduktion aufgebaut wurde, war wahrscheinlich die Ursache für die hohen CO_2 Flüsse. Darüber hinaus ergaben Untersuchungen im zweiten Jahr nach der Überflutung mit hochauflösenden Messungen eine beträchtliche zeitliche Fluktuation in der CO_2 Verteilung, die sich als mehrtägige,

tageszeitliche und ereignisbezogene Variabilität äußerte. Räumliche Unterschiede im gefluteten Moor traten bei Variablen auf, die von biologischen Prozessen dominiert wurden. Die CH₄ Emissionen stiegen beim Übergang von trockenen zu überfluteten Bedingungen im ersten Jahr um eine Größenordnung von $0.13 \pm 1.01 \text{ mg m}^{-2} \text{ h}^{-1}$ auf $1.74 \pm 7.59 \text{ mg m}^{-2} \text{ h}^{-1}$ an, nahmen aber im zweiten Jahr um das 2.6-fache ab. Trotz des unmittelbaren Anstiegs nach der Vernässung, waren die CH₄ Emissionen im Vergleich zu ähnlichen Studien, bei denen Süßwasser zur Wiederbefeuchtung genutzt wurde, geringer. Obwohl die CH₄ Bildung durch das Vorhandensein von OM begünstigt wurde, wurde dies durch die Auswirkungen von (i) dem verfügbaren O₂ aufgrund der Durchmischung der Wassersäule und dem im Brackwasser vorhandenen Sulfat ausgeglichen, die beide die CH₄ Produktion unterdrückten und (ii) zu einer aeroben und anaeroben CH₄ Oxidation führten. Die hochauflösenden Messungen im zweiten Jahr ergaben eine starke mehrtägige, kurzfristige (< 1 Tag) und ereignisbezogene Variabilität in der CH₄ Verteilung. Im Allgemeinen war die ereignisbedingte Variabilität von CO₂ und CH₄ die Folge eines Sturms, eines Niederschlages und von Änderungen des Wasserstandes, die zu schnellen Veränderungen der Biogeochemie des Wasserkörpers und der Treibhausgaskonzentrationen führten.

Diese Dissertation erweitert das allgemeine Verständnis der Verteilung und zeitlichen Variabilität von Treibhausgasen in Küstenregionen. Sie wirft auch ein Licht auf mögliche Kontrollmechanismen des marinen Kohlenstoffkreislaufs im Flachwasser. In Anbetracht der zeitlichen Skalen, auf denen signifikante Veränderungen der Variablen stattgefunden haben (d.h. wenige Stunden), wird deutlich, dass diese nur mit den hier eingesetzten neuen und angepassten Methoden erfasst werden konnten. Daher war die Entwicklung und erstmalige Etablierung der zentralisierten sensorbasierten Messung mit zwei Landersystemen von entscheidender Bedeutung, wenngleich Verbesserungen an den Systemen erforderlich sind. Die Ergebnisse dieser Arbeit zeigen Richtungen für die weitere Küstenforschung auf, die die Steuerung der Treibhausgaskonzentrationen durch Kipppunkte und ausgeprägte Tag-Nacht-Verschiebungen berücksichtigen sollten. Darüber hinaus deuten die niedrigeren CH₄ Flüsse in dem untersuchten Torfgebiet, zusammen mit einem Trend von abnehmenden Treibhausgasflüssen, auf eine günstige Auswirkung des Brackwassers anstelle von Süßwasser hin und dies zeigt eine Entwicklung des Gebiets hin zu einer potenziellen Kohlenstoffsenke.

Publications

Article in a peer-reviewed journal

Pönisch, D. L., Breznikar, A., Gutekunst C. N., Jurasinski, G., Voss, M., Rehder, G.: Nutrient release and flux dynamics of CO₂, CH₄, and N₂O in a coastal peatland driven by actively induced rewetting with brackish water from the Baltic Sea, *Biogeosciences*, 20 (2), 295–323, <https://doi.org/10.5194/bg-20-295-2023>, 2023. With supplementary data:

(1) Pönisch, D. L. and Breznikar, A.: Supplementary data of the discrete water sampling used in the publication “Nutrient release and flux dynamics of CO₂, CH₄, and N₂O in a coastal peatland driven by actively induced rewetting with brackish water from the Baltic Sea”, IOW [data set], <https://doi.org/10.12754/data-2022-0003>, 2022.

(2) Pönisch, D. L. and Gutekunst, C. N.: Supplementary data for greenhouse gas emissions used in the publication “Nutrient release and flux dynamics of CO₂, CH₄, and N₂O in a coastal peatland driven by actively induced rewetting with brackish water from the Baltic Sea”, IOW [data set], <https://doi.org/10.12754/data-2022-0004>, 2022.

Conferences and presentations

Jurasinski, G., Gutekunst, C. N., Liebner, S., Jenner, A.-K., Racasa, E. D., Knorr, K.-H., Anthony, E. S., **Pönisch, D. L.**, Böttcher, M. E., Janssen, M., Kallmeyer, J., Keobsch, F., Rehder, G.: Changes of greenhouse gas fluxes and microbial community groups upon rewetting of a coastal peatland with brackish water. EGU, 23 – 24 April 2023, Vienna, talk

Pönisch, D. L., Breznikar, A., Gutekunst, C. N., Jurasinski, G., Rehder, G., Voss, M.: Greenhouse gas response to rewetting with brackish water in a coastal peatland. Scientific Advisor Board, 2022, IOW, poster

Breznikar, A., **Pönisch, D. L.**, Dippner, W D., Jurasinski, G., Rehder, G., Voss, M.: Short- vs. long-term rewetting effects on nutrient and nitrous oxide release – Comparison of two coastal peatlands on the Baltic Sea, Scientific Advisor Board, 2022, IOW, poster

Pönisch, D. L., Breznikar, A., Gutekunst, C. N., Jurasinski, G., Rehder, G., Voss, M.: Flux dynamics of CO₂, CH₄, and N₂O in a highly degraded coastal peatland during transition from drained to inundated conditions by rewetting with brackish waters. 4th Baltic Earth Conference, 30 May – 03 June 2022, Jastarnia, Poland, poster

Pönisch, D. L., Breznikar, A., Gutekunst, C. N., Jurasinski, G., Rehder, G., Voss, M.: Brackwasservernässte Küstenmoore – die bessere Alternative zur Süßwasservernässung? Meeresumweltsymposium, 18 – 19 May 2022, Hamburg, Germany, poster

Gutekunst, C. N., Jenner, A.-K., **Pönisch, D. L.**, Breznikar, A., Böttcher, M. E., Jansen, M., Kallmeyer, J., Knorr, K.-H., Koebsch, F., Liebner, S., Racasa, E. D., Rehder, G., Voss, M., Juasinski, G.: Development of greenhouse gas emissions and microbial community of a saltwater rewetted coastal peatland. ECSA 58, 06 – 10 September 2021, online conference, talk

Pönisch, D. L., Bittig, H. C., Aßmann, S., Meyer, M., Rehder, G.: A lander system for long-term and high-resolution determination of trace gases (CH₄, CO₂), nutrients and physical parameters in flat coastal water. Wetscapes, 10 – 13 September 2019, Rostock, Germany, poster

List of abbreviations, symbols and variables

[]	Concentration, equivalent to c
<U²>	Average squared wind speed
AOM	Anaerobic methane oxidation
ASE	Air-Sea Exchange
A_T	Total alkalinity
C	Carbon
c_a	Concentration of GHGs at the top of the liquid boundary layer adjacent to the atmosphere
Ca²⁺	Calcium(II) ion
CaCO₃	Calcium carbonate
cCH₄	Concentration of CH ₄
CDOM	Colored dissolved organic matter
CH₃COOH	Acetic acid
CH₄	Methane
cN₂O	Concentration of N ₂ O
CO₂	Carbon dioxide
CO₂[*]	Sum of CO _{2,(aq)} and H ₂ CO _{3,(aq)}
CO_{2,(aq)}	CO ₂ physically dissolved in seawater
CO_{2,(g)}	CO ₂ in the gas phase
CO₃²⁻	Carbonate ion
CRM	Certified Reference Material
C_T	Total amount of dissolved inorganic carbon
CTD-O₂	Conductivity, temperature, pressure, oxygen
c_w	Concentration of GHGs in the bulk liquid layer
DOC	Dissolved organic carbon
DPU	Data processing unit
DWD	Deutscher Wetterdienst
ECD	Electron capture detector
F	Flux (mass area ⁻¹ time ⁻¹)
fCO₂	Fugacity of CO ₂
Fe³⁺	Iron(III) ion
FID	Flame ionization detector
GHG	Greenhouse gas
GML	Global Monitoring Laboratory
H⁺	Hydrogen ion

H₂	Hydrogen gas
H₂CO₃	Carbonic acid
H₂S	Hydrogen sulfide
HC-CH₄	HydroC-CH ₄ sensor
HC-CO₂	HydroC-CO ₂ sensor
HCO₃⁻	Hydrogen carbonate ion
HELCOM	Baltic Marine Environment Protection Commission
HgCL₂	Mercury(II) chloride
http	Hypertext Transfer Protocol
ICOS	Integrated Carbon Observation System
IOW	Leibniz Institute for Baltic Sea Research Warnemünde
k	Gas transfer velocity
K₀	Solubility coefficient
K₁	First dissociation constant of the marine CO ₂ system
K₂	Second dissociation constant of the marine CO ₂ system
K_f	Acid dissociation constant of [HF]
K_s	Acid dissociation constant for HSO ₄ ⁻
MARNET	Marines Umweltmessnetz in Nord- und Ostsee des Bundesamts für Seeschifffahrt und Hydrographie
MEB	Mecklenburg Bight
Mn⁴⁺	Manganese(IV) ion
N	Nitrogen
N₂	Nitrogen gas
N₂O	Nitrous oxide
NDIR	Non-dispersive infrared spectrometry
NH₄⁺	Ammonium ion
NO₂⁻	Nitrite
NO₃⁻	Nitrate
NOAA	National Oceanic and Atmospheric Administration
O₂	Oxygen
OH⁻	Hydroxide ion
OM	Organic matter
pCH₄	Partial pressure of CH ₄
pCO₂	Partial pressure of CO ₂
pct	percentiles

pH_T	pH on the total scale
pO₂	Partial pressure of O ₂
PO₄³⁻	Phosphate
r_s	Spearman coefficient
Sc	Schmidt number
SD	Standard deviation
SFTP	Secure File Transfer Protocol
SO₄²⁻	Sulfate ion
SRB	Sulfate-reducing bacteria
TDLAS	Tunable diode laser absorption spectroscopy
TEA	Terminal electron acceptor
THG	Treibhausgas
UTC	Coordinated Universal Time
UV	Ultraviolet
WMO-ID	Stations list of the DWD
τ	Response time

List of figures

Figure 1: Overview of the two study areas, located in **(a)** the southern Baltic Sea and **(b)** at the coastline of *Mecklenburg-Vorpommern*. **(c)** The bathymetry of the Hütelmoor site, together with the lander positions deployed in the shallow area of the Baltic Sea in front of the *Hütelmoor* and *Heiligensee* in autumn of 2019 (data retrieved from Kreuzburg et al., 2018). **(d – f)** The topography of Drammendorf and the resulting bathymetry after flooding at normal water level. Two surveys were conducted in Drammendorf: a field survey (2019/2020) and a lander survey (summer 2021). **(d, e)** Overview of the stations during the Drammendorf field survey. The stations in the inner bay are shown in purple and those of the peatland in black. **(e)** The transect belonging to that survey, which was sampled for GHG fluxes to the atmosphere by flux chamber measurements (before - and accordingly dry, and after rewetting), and for surface water GHG concentration measurements (after rewetting). **(f)** The locations of the two landers, deployed one year later. The new dike is shown in dark red.

Figure 2: Technical description and instrumentation of the landers. **(a)** Schematic overview of the lander and the modular frames for the sensors (left and right) and the central yellow battery container. **(b)** Summary of the sensor configuration used in the Hütelmoor lander survey. A dashed line represents the equipment used only at lander 1. The captions at the arrows describe the resolution of the data acquisition; s: seconds, m: minutes. **(c)** Lander 1 at the sediment-water interface in Hütelmoor after ~ 15 days of deployment. **(d)** Overview of the setup and technical adjustments made for the Drammendorf lander survey, including the key components of a wired land-based electrical power supply and powerline communication (right top) as well as remote accessibility (right bottom). The respective hardware was bundled in the “Octopus” device on both landers (left). In **(d)**, the dashed line represents the equipment used at the actual lander and the captions describe the resolution. **(e)** The set-up of the lander in the central area of the Drammendorf lander survey, using a lift construction.

Figure 3: The photographs of Drammendorf illustrate the strong shift from **(a)** a drained *Polder* (March 2019) to a flooded area due to the active removal of a section of a dike. **(b)** Construction of the boardwalk before flooding and the site of the transect where the GHG samples were collected. Flooding due to excavation on 26 November 2019 is shown in **(c)**, with the artificial connecting ditch in the foreground and the Baltic Sea (*Kubitzer Bodden*) in the background. **(d)** The result of flooding in the summer of 2021 is framed in red and the artificial connecting ditch (the removed part of the dike) is well visible in the center. **(e)** Field work and discrete sampling from a small boat (April 2020). **(f)** The lander before its recovery on the last day of the Drammendorf lander deployment (summer 2021).

Figure 4: High resolution time series of lander 1 (black) and lander 2 (red) together with wind data. Results from discrete bottle data are indicated by asterisks, together with the color of the respective lander. **(a – k)** Post-processed data of **(a)** $p\text{CO}_2$ (μatm), **(b)** $p\text{CH}_4$ (μatm), **(c)** water temperature ($^{\circ}\text{C}$), **(d)** salinity, **(e)** $p\text{O}_2$ (mbar), **(f)** depth and smoothed depth (hydrostatic pressure; dbar) together with the standard deviation (SD) of the pressure (right axis; dbar), **(g)** chlorophyll *a* concentration ($\mu\text{L L}^{-1}$), **(h)** turbidity (NTU), **(i)** NO_3^- concentration ($\mu\text{mol L}^{-1}$), **(j)** PO_4^{3-} concentration ($\mu\text{mol L}^{-1}$), **(k)** water velocity (m s^{-1}), **(l)** wind speed (m s^{-1}) and wind direction (right axis; degrees). In k and l, the crossshore direction is shown in gold and the alongshore direction in red. The three gray rectangles highlight the events referred to as FINN-I – FINN-III.

Figure 5: Time series of temperature and saturation of O₂ at both landers measured continuously in high-resolution 1 and 3 m above the sediment by PME miniDOT instruments (in red and turquoise, respectively) compared to the time series of the temperature and O₂ measured at the lander. The inlet of the latter (i.e., CTD-O₂ measurements of the lander) were ~ 0.70 cm above the sediment, and hence the lowest point of measurements in the water column.

Figure 6: Development of salinity in the water column as derived from numerical model simulations (top). (a – c) Snapshots of (a) shortly before, (b) during, and (c) after the event FINN-I.

Figure 7: Spearman correlation coefficients (r_s) between the measured variables at lander 1 and auxiliary data (i.e., wind speed, wind direction and solar irradiance) for the entire deployment. A significance level of 0.001 was applied to remove non-correlating relationships (empty fields). Cohen's convention was used to interpret the effect size (Cohen, 1988). Black stars represent a large effect size and hence a strong correlation, and brown stars represent a medium effect size.

Figure 8: Spearman correlation coefficients (r_s) between the measured variables at lander 1 and auxiliary data for the period corresponding to FINN-I. A significance level of 0.001 was applied to remove non-correlating relationships (empty fields). Cohen's convention was used to interpret the effect size (Cohen, 1988). Black stars represent a large effect size and hence a strong correlation, and brown stars represent a medium effect size.

Figure 9: Spearman correlation coefficients (r_s) between the measured variables at lander 1 and auxiliary data, for the period corresponding to FINN-II. A significance level of 0.001 was applied to remove non-correlating relationships (empty fields). Cohen's convention was used to interpret the effect size (Cohen, 1988). Black stars represent a large effect size and hence a strong correlation, and brown stars a medium effect size.

Figure 10: Spearman correlation coefficients (r_s) between the measured variables at lander 1 and auxiliary data, for the period corresponding to FINN-III. A significance level of 0.001 was applied to remove non-correlating relationships (empty fields). Cohen's convention was used to interpret the effect size (Cohen, 1988). Black stars represent a large effect size and hence a strong correlation, and brown stars a medium effect size.

Figure 11: Time series of the mean (a) temperature, (b) salinity, (c) O₂ saturation, (d) DOC concentration, and (e) chlorophyll *a* concentration (\pm standard deviations) in the surface water after rewetting, as measured from December 2019 to December 2020. Data from the flooded peatland are shown in blue and data from the inner bay in black. The vertical black line indicates the rewetting event.

Figure 12: Time series of the mean (a) total CO₂ (C_T), (b) total alkalinity (A_T), and (c) pH (\pm standard deviations) in the surface water after rewetting, as measured from December 2019 to December 2020. Data from the flooded peatland ($n = 6$) are shown in blue and data from the inner bay (until March $n = 1$, thereafter: $n = 2$) in black. The vertical black line indicates the rewetting event.

Figure 13: Time series of the mean (a) pCO_2 , (b) CH₄ concentration (cCH_4), and (c) N₂O concentration (cN_2O) (\pm standard deviations) after rewetting in the surface water, as measured from December 2019 to December 2020. Data from the flooded peatland ($n = 6$) are shown in blue and data from the inner bay (until March $n = 1$, thereafter: $n = 2$) in black. The vertical black line indicates the rewetting event.

Figure 14: Time series of the mean **(a)** CO₂, **(b)** CH₄, and **(c)** N₂O fluxes (\pm standard deviations) from June 2019 to December 2020. Fluxes of the permanently water-filled drainage ditch are shown in purple, and fluxes derived from the flooded, formerly dry peatland in green. In both cases, the two methods (i.e., fluxes measured using chambers and fluxes derived from wind-parameterization) were applied. The vertical black line indicates the rewetting event.

Figure 15: High-resolution time series from lander 1 (black) and lander 2 (red). Results from discrete bottle data are indicated by asterisks, together with the color of the respective lander. **(a – j)** Post-processed data of **(a)** $p\text{CO}_2$ (μatm), **(b)** $p\text{CH}_4$ (μatm), **(c)** water temperature ($^{\circ}\text{C}$), **(d)** salinity, **(e)** O₂ saturation (%), **(f)** pressure (depth; dbar), **(g)** chlorophyll *a* concentration ($\mu\text{L L}^{-1}$), **(h)** turbidity (NTU), **(i)** PO₄³⁻ concentration ($\mu\text{mol L}^{-1}$), **(j)** wind speed (m s^{-1}), and precipitation (mm). The sensor signals of $p\text{CO}_2$ and $p\text{CH}_4$ were additionally smoothed, as represented by the black and red lines, respectively. The gray rectangles highlight three periods of system changes.

Figure 16: Spearman correlation coefficients (r_s) between the measured variables determined by both landers, wind speed and solar irradiance. A significance level of 0.001 was applied to remove non-correlating relationships (empty fields). The Cohen convention was used to interpret the effect size (Cohen, 1988). Black stars represent a large effect size and hence a strong correlation, and brown stars a medium effect size. Wind speeds were retrieved from the *Putbus* station (WMO-ID 10093) and solar irradiance from *Rostock-Warnemünde* (WMO-ID 10170; both DWD).

Figure 17: Distribution and mean values of $p\text{CO}_2$, $p\text{CH}_4$, temperature, O₂, and wind speed calculated for each hour of the daily cycle over 24 h during the deployment, highlighting diurnal patterns. The box plots show the median and the 25 / 75 % quantiles; the whiskers indicate the 5 / 95 % percentiles, and the red points the mean values.

Figure 18: Spearman correlation coefficients (r_s) between the measured variables at lander 1, wind speed, and solar irradiance, limited to time period (I). A significance level of 0.001 was applied to remove non-correlating relationships (empty fields). Cohen's convention was used to interpret the effect size (Cohen, 1988). Black stars represent a large effect size and hence a strong correlation, and brown stars a medium effect size. Wind speeds were retrieved from *Putbus* station (WMO-ID 10093) and solar irradiance from *Rostock-Warnemünde* (WMO-ID 10170; both DWD).

Figure 19: Spearman correlation coefficients (r_s) between the measured variables at lander 1, wind speed, and solar irradiance, limited to time period (II). A significance level of 0.001 was applied to remove non-correlating relationships (empty fields). Cohen's convention was used to interpret the effect size (Cohen, 1988). Black stars represent a large effect size and hence a strong correlation, and brown stars a medium effect size. Wind speeds were retrieved from *Putbus* station (WMO-ID 10093) and solar irradiance from *Rostock-Warnemünde* (WMO-ID 10170; both DWD).

Figure 20: Spearman correlation coefficients (r_s) between the measured variables at lander 1, wind speed, and solar irradiance, limited to time period (III). A significance level of 0.001 was applied to remove non-correlating relationships (empty fields). Cohen's convention was used to interpret the effect size (Cohen, 1988). Black stars represent a large effect size and hence a strong correlation, and brown stars a medium effect size. Wind speeds

were retrieved from *Putbus* station (WMO-ID 10093) and solar irradiance from *Rostock-Warnemünde* (WMO-ID 10170; both DWD).

Figure 21: Calculated GHG fluxes for CO₂ and CH₄ at both landers using the wind parameterization approach of Wanninkhof (2014). Smoothing was used to highlight the trend and differences between the data from the two landers.

Figure 22: Summary of the results in Drammendorf. Schematic overview of (a) literature-based GHG fluxes after rewetting with freshwater, (b) measured GHG fluxes in the drained condition, and (c) measured GHG fluxes after rewetting with brackish water.

List of tables

Table 1: Overview of the sensors, manufacturers, abbreviations, detector types, and the variables measured with each unit.

Table 2: Summary of the methodology used for the Hütelmoor lander survey.

Table 3: Summary of the methodology used for the Drammendorf field survey.

Table 4: Summary of the methodology used for the Drammendorf lander survey.

Table 5: Summary of the mean, standard deviation, minimum and maximum of the measured variables determined by lander 1 and lander 2. The concentration of CH₄ (nmol L⁻¹) was calculated from *p*CH₄ (µatm). Some data at lander 2 are not considered because they had to be removed after quality assessment.

Table 6: Summary of the measured and calculated variables of the Drammendorf field survey. (a) Seasonal summary of the measured surface water means ± standard deviations (SD) in the peatland after rewetting (n = the number of observations) and (b) the derived GHG fluxes determined in chamber measurements and wind-based parameterization before and after rewetting.

Table 7: Summary of the mean, standard deviation, minimum and maximum (as 0.98th and 0.02th percentiles) of available data from lander 1 and lander 2. The mean, minimum and maximum of the calculated daily variability are also shown (Sect. 3.3.2). The CH₄ concentration (nmol L⁻¹) was calculated from *p*CH₄ (µatm). NO₃⁻ concentrations could not be determined due to strong interferences from CDOM.

Table 8: Greenhouse gas fluxes calculated for both lander positions and by using different data sets. The fluxes were calculated based on the sensor data⁽¹⁾ (bold) and, for comparison, using the bottle data⁽²⁾. GHG fluxes were also calculated based on the sensor data for daytime⁽³⁾ and nighttime⁽³⁾ in order to show the impact of diurnal effects. The sensor data for daytime and nighttime were averaged by ± 1 h. Data from the Drammendorf field survey were used to calculate the ASE for the corresponding period in 2020⁽⁴⁾ (column “data from 2020”). For maximum comparability, the ASE based on the sensor data (lander survey) for the period between 09:00 and 15:00 UTC (the main sampling period in the Drammendorf field survey) was calculated⁽⁵⁾. The calculation procedure of (1) – (5) is described in Sect 2.4.4.

Motivation and aims

Coastal areas exhibit a wide range of ecological and chemical characteristics due to numerous interacting processes such as hydrologic exchange, solute transport, and biogeochemical processes. These processes all occur at different temporal and spatial scales, resulting coastal zones to be highly heterogeneous. In addition, some coastal areas are sources of atmospheric greenhouse gases (GHGs; e.g., CO₂ and CH₄), although accurate estimates are not possible due to the lack of long-term data with adequate resolution. The semi-enclosed Baltic Sea is of particular interest because of an excess supply of nutrients, mostly of anthropogenic origin, which promote the formation of organic matter (OM) in coastal and open waters. The subsequent sedimentation and microbial turnover of the OM increase oxygen (O₂) consumption in bottom waters, resulting in the expansion of hypoxic and anoxic zones. The impacts on aerobic benthic organisms and on the distribution of CO₂ and CH₄ are significant, since the production of both gases is strongly controlled by the availability of O₂. Other important characteristic of coastal areas include mechanical stress at the sediment surface and water column mixing, both of which can affect the transport of soluble compounds and GHGs within the water column.

In addition to the processes in the shallow water column, coastal waters are directly connected to the terrestrial compartment, allowing energy, water, and substance exchange. Some of these low-lying onshore areas are at constant risk of flooding, partly due to human activities. For example, onshore areas with already drained peatlands are particularly affected due to ongoing peat loss and associated land mass subsidence, with the peat loss also causing the release of large amounts of CO₂. The renaturation of drained peatlands can stop the release of CO₂, but using freshwater for this purpose often causes the release of large amounts of CH₄. For coastal peatlands, brackish water is available for rewetting and its salinity could limit CH₄ emissions while flooding could stop CO₂ emissions, but this has not yet been investigated intensively in field studies.

As coastal areas are often methodologically difficult to reach, data collection is limited, and the resulting uncertainties in estimating sources and sinks for atmospheric GHGs make it difficult to consider these areas in global upscaling approaches. Systematic, high-resolution, long-term studies and a better description of local heterogeneity are therefore needed, especially for the detection of events that act as tipping points. This can only be achieved with an integrated approach that allows a wide range of information to be taken into account, for

example, through the integration of model simulations. Thus, the objective of the research conducted for this dissertation was to investigate the temporal and spatial variability of CO₂ and CH₄ in shallow waters. This included incorporating the effects of biogeochemical properties at the sediment-water interface (e.g., O₂) on the distribution of greenhouse gases. The dependence of GHG distributions on nutrients availability as well as hydrodynamic forces and the role of peat deposits was also examined. Guided by the deficiencies in our understanding of the coastal areas of the Baltic Sea, this dissertation has three work packages:

Work package I: The **Hütelmoor lander survey** involved the deployment of two sensor-equipped landers at two nearshore locations for around four weeks in autumn 2019. At this site, which is representative of the sandy and soft sediments that are widely distributed in the southern Baltic Sea, stationary measurements of key marine variables ($p\text{CO}_2$, $p\text{CH}_4$, temperature, salinity, hydrostatic pressure, O₂, chlorophyll *a*, turbidity, NO₃⁻, PO₄³⁻) were obtained at high-resolution. These autonomous measurements contribute to closing the knowledge gap resulting from inadequately described GHG distributions in coastal areas. By combining these sensor measurements with supporting information, potential drivers of the expected variability can be evaluated. Therefore, data from the stationary measurements were combined with data obtained from discrete sampling, additional high-resolution water column measurements, atmospheric data, water velocity measurements, and numerical model simulations.

Work package II: The **Drammendorf field study** was based on the frequent discrete sampling of (mainly) the surface water from a coastal peatland during the first year after the rewetting. The collected data provide the scientific basis for assessing GHG development in a coastal peatland actively rewetted with brackish water, and thus for following the transformation from dry to inundated conditions. Measurements of GHG concentrations (CO₂, CH₄, N₂O) were combined with physical information (e.g., temperature, salinity), nutrient determinations (e.g., NO₃⁻, PO₄³⁻) and the derivation of GHG exchange between the water surface and the atmosphere. The comparison of these GHG fluxes before and after rewetting allowed a detailed analysis of the effect of brackish water rewetting on GHG distributions and fluxes under field conditions.

Work package III: The **Drammendorf lander survey** used two sensor-equipped landers to measure key marine variables ($p\text{CO}_2$, $p\text{CH}_4$, temperature, salinity, depth, O₂, chlorophyll *a*, turbidity, NO₃⁻, PO₄³⁻) in the water column of the peatland rewetted with brackish water.

Autonomous measurements were made for about nine weeks in the summer of 2021, the second year after rewetting. The main objective was to determine the temporal scales of variability and cyclicity, especially of GHGs. Spatial heterogeneity in the flooded peatland was assessed by deploying the landers at two positions differing in their hydrographic conditions. The results extended the findings from the Drammendorf field study (i.e., work package II) and tracked the progressive development of GHGs under brackish water conditions using a different approach than in the first year after rewetting. It was anticipated that the discrete sampling approach used in the field study would not be well suited for this heterogeneous field environment, as the distribution of GHGs in the water column was expected to be highly variable.

1. Introduction

1.1 Highly dynamic shallow water areas under pressure

Coastal areas fulfil essential global functions and are important habitats for flora, fauna, and humans. Due to their interactions with adjacent terrestrial and marine compartments, they represent heterogeneous environments with high turnover rates of carbon (C) and nutrients, which explains the high productivity of coastal regions (Field, 2002; Doney, 2010). Although coastal areas cover only a limited fraction of the global surface, ~ 10 % of the world's population lives in areas < 10 m above sea level or ~ 40 % lives within 100 km of the coast, such that coastal areas are closely associated with human activities (Field, 2002; Small and Nicholls, 2003; The Ocean Conference, 2017). Consequently, coastal areas, but also the marine environment overall, are under intense anthropogenic pressure in the form of rising atmospheric carbon dioxide (CO₂) levels, increased nutrient inputs, and pollution, all of which affect the marine chemistry (Doney, 2010). Further, the rising sea level, sinking coasts, and changing precipitation patterns are altering hydrodynamic gradients as well as sea-land exchanges. Coastal peatlands are particularly vulnerable because many have been drained for decades, causing land mass subsidence and exposing these sites and their immediate terrestrial catchment areas to flooding.

The Baltic Sea, as a semi-enclosed marginal sea, is under strong pressure from excess nutrient inputs, pollution, overfishing, and construction activities (e.g., HELCOM, 2018). The large supply of nutrients in coastal areas and estuaries promotes the formation of organic matter (OM) through the increased growth of algae and plants, the process referred to as eutrophication (Nixon, 1995). The sedimentation and subsequent turnover of the abundantly produced OM increase oxygen (O₂) consumption in bottom waters, with the potential to expand hypoxic and anoxic zones and displace aerobic benthic organisms (Rosenberg, 1985; Vallius, 2006). The distribution of the climate-relevant trace gases CO₂, methane (CH₄), and nitrous oxide (N₂O) is also affected because their formation is strongly controlled by the availability of O₂ (Bange et al., 2010; Gelesh et al., 2016). Although it is difficult to estimate the impact of eutrophication on the changing distribution of marine greenhouse gases (GHGs), coastal areas have been identified as a major source of atmospheric GHGs (e.g., Bange et al., 1994; Heyer and Berger, 2000; Bange, 2006; Stokowski et al., 2020). Conversely, coastal areas can act not only as C sources but also as C sinks, through the

establishment of vegetation and the long-term deposition of OM in sediments, by the acquisition and storage of C from the atmosphere. This stored carbon is known as “blue carbon” and its formation is a feature of mangrove forests, seagrass beds, and salt marshes (e.g., Mcleod, 2011; Roth et al., 2022). Thus, coastal areas can act as both sinks and sources of GHGs, but these are not well constrained as the areas exhibit large temporal and spatial variability (e.g., Heyer and Berger, 2000; Borges et al., 2016; Humborg et al., 2019; Stokowski et al., 2020). This circumstance complicates scaling processes and therefore coastal areas are not well-implemented in the global C budget (Saunois et al., 2020).

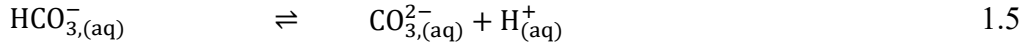
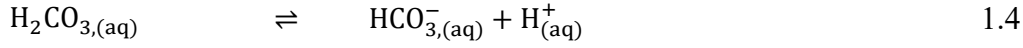
1.2 Carbon dioxide

Carbon dioxide is the most chemically oxidized form of C, is soluble in water, and is the most potent GHG on Earth after water vapor. From pre-industrial times to 2022, atmospheric CO₂ increased by 51 % (Friedlingstein et al., 2022). This increase is strongly associated with anthropogenic activities such as fossil fuel burning, cement production (Sabine et al., 2004), and deforestation (Houghton and Hackler, 2001). The marine environment, however, has a CO₂ inventory that is more than 50 times larger than that of the atmosphere (Archer, 2005) such that its uptake capacity buffers changes in atmospheric CO₂ concentration. Nonetheless, the increased uptake of atmospheric CO₂ alters the sensitive and complex chemical equilibria in the marine environment and finally influences resident organisms. This is even more pronounced in coastal areas because the response time is shorter than in the open ocean. In turn, the knowledge of CO₂ levels in nearshore waters and changes therein is limited due to the challenges posed by scientific investigations of coastal areas.

The dissolution of atmospheric CO₂ into the water and subsequent equilibrium reactions affect the acid-base system in seawater. The physical dissolution of CO₂ in water (Eq. 1.1) leads to the formation of carbonic acid (H₂CO₃; Eq. 1.2). Since the concentration of H₂CO₃ in water is very low (Zeebe and Wolf-Gladrow, 2001) and is difficult to distinguish analytically from the dissolved CO_{2,(aq)} concentration, the two species are combined as the [CO₂*] term (Eq. 1.3). The carbonic acid immediately dissociates into bicarbonate (Eq. 1.4), and carbonate ions (Eq. 1.5), with the respective chemical reactions providing protons (H⁺).



$$[\text{CO}_2^*] = [\text{CO}_{2,(aq)}] + [\text{H}_2\text{CO}_{3,(aq)}] \quad 1.3$$



The equilibrium conditions between the dissociated species as shown in Eq. 1.4 and Eq. 1.5 are described by the equilibrium constants K_1 and K_2 (e.g., Millero, 2010), as shown in Eqs. 1.6 and 1.7, where brackets represent the stoichiometric concentrations:

$$K_1 = \frac{[\text{HCO}_3^-] \cdot [\text{H}^+]}{[\text{CO}_2^*]} \quad 1.6$$

$$K_2 = \frac{[\text{CO}_3^{2-}] \cdot [\text{H}^+]}{[\text{HCO}_3^-]} \quad 1.7$$

The CO_2^* concentration (Eq. 1.3) is directly related to the fugacity of CO_2 in seawater ($f\text{CO}_2$), where K_0 is the solubility constant (Eq. 1.8):

$$K_0 = \frac{[\text{CO}_2^*]}{f\text{CO}_2} \quad 1.8$$

The direction of CO_2 gas exchange between the atmosphere and seawater is controlled exclusively by differences in the $f\text{CO}_2$ in the two compartments.

1.2.1 Analytical variables of the marine CO_2 system

The state of the marine CO_2 system can be characterized by four measurable key variables (Dickson et al., 2007): total dissolved inorganic carbon (C_T), total alkalinity (A_T), pH, and the partial pressure of CO_2 ($p\text{CO}_2$). In the open ocean, any two of these variables together with the equilibrium constants of all the acid-base systems involved, are sufficient to describe the CO_2 system and allow the other two variables of the CO_2 system to be calculated. In coastal systems, deviations might occur, e.g., due to organic acid-base systems or deviations from the salt composition of seawater (e.g., Kuliński et al., 2014).

C_T is the sum of all inorganic CO_2 species dissolved in seawater; hence, it is also called dissolved inorganic carbon (DIC), defined as shown in Eq. 1.9:

$$C_T = [\text{CO}_2^*] + [\text{HCO}_3^-] + [\text{CO}_3^{2-}] \quad 1.9$$

C_T is strongly coupled to the formation and mineralization of OM. Thus, CO_2 uptake via primary production, e.g., by growing organisms (phytoplankton), leads to a decrease in C_T , and mineralization (e.g., microbial turnover) to an increase in C_T .

A_T is defined as an excess of proton acceptors over donors relative to the amount of hydrogen ions which are required to neutralize proton acceptors (Dickson, 1981). The largest contribution to A_T comes from the HCO_3^- species (Eq. 1.10):

$$A_T = [HCO_3^-] + 2[CO_3^{2-}] + [B(OH)_4^-] + [OH^-] + [HPO_4^{2-}] + 2[PO_4^{3-}] + [SiO(OH)_3^-] + [NH_3] + [HS^-] - [H^+]_F - [HF] - [HSO_4^-] - [H_3PO_4] + [\text{minor bases} - \text{minor acids}] \quad 1.10$$

In general, the contributions of hydroxide, phosphate, silicate, and other bases are very small, but in the case of the Baltic Sea, their effect may be enhanced. Both C_T and A_T are mainly determined by HCO_3^- and are conservative variables of the marine CO_2 system. Hence, if they are determined as the units of mol kg^{-1} , they do not change as a function of temperature or pressure, unlike pH and pCO_2 (Zeebe and Wolf-Gladrow, 2001).

pH is generally defined as the negative decadic logarithm of the H^+ concentration (Eq. 1.11).

$$pH = -\log[H^+] \quad 1.11$$

In this study, the total scale of the pH (pH_T) was applied to the hydrogen ion concentration. pH_T is measured on concentration scales derived relative to the standard composition of a seawater matrix and includes the amount of free H^+ ions and the protonated form of sulfate ion (Dickson, 1990).

The pCO_2 is directly related to fCO_2 (Eq. 1.8). The difference between the two quantities is very small, but fCO_2 is more realistic because it takes into account the non-ideal behavior of the CO_2 gas.

1.2.2 The marine CO_2 system

The marine C cycle, of which CO_2 is an important component, is controlled by three major processes in a changing global surrounding (Hansell and Carlson, 2014). (i) The solubility pump is driven by changes in gas solubility as a function of temperature and salinity. In addition, pressure, salinity, and temperature determine the dissociation constants of carbonic acid and change the dissociation equilibria such that more CO_2 is taken up at lower temperatures. Lower temperatures also lead to higher water density, causing these water masses to sink and thus pump atmospheric carbon into the deep sea. (ii) The organic pump

involves the fixation of inorganic C (DIC) into organic C by photosynthesis, which is mainly carried out by phytoplankton. The subsequent partial sinking of the produced OM transports C into deeper waters or buries it in shallow sediments. (iii) The carbonate pump describes the biogenic formation of CaCO_3 from bicarbonate and calcium (Ca^{2+}) ions by surface marine organisms such as coccolithophorids (Zeebe and Wolf-Gladrow, 2001). However, during sedimentation, up to 50 % of solid CaCO_3 structures are redissolved (deep ocean; Feely et al., 2004).

In the decade between 2012 and 2021, the ocean was a sink for $2900 \pm 400 \text{ Tg C yr}^{-1}$, corresponding to 26 % of total CO_2 emissions (Friedlingstein et al., 2022). However, a detailed examination revealed a large heterogeneity in terms of whether the marine environment, especially marginal areas, acts locally as a CO_2 sink or source. For example, it has been reported that the Baltic Sea, as a marginal sea located in a dynamic region, acted as a CO_2 source in pre-industrial times, but today it is both a sink and a source (Omstedt et al., 2009).

1.2.2.1 Baltic Sea

The marine C cycle of the Baltic Sea corresponds to that of the ocean but has some peculiarities that need to be taken into account. The CO_2 system in the Baltic Sea is influenced by the water balance between incoming seawater and freshwater inputs from rivers. This estuarine circulation forms a unique hydrographic configuration in which limited inflows of high-density oxygen-rich water from the North Sea and concurrent positive river discharge result in brackish conditions. Furthermore, this setting leads to stratification through the formation of a strong (permanent) halocline and a (seasonal) thermocline in the Baltic Sea basins (e.g., Schneider and Müller, 2018). Stratification inhibits vertical mixing, which in combination with the topography of the Baltic Sea, consisting of individual basins separated by sills, limits the mineralization of OM to deeper waters of the Baltic Sea Proper. As a result, O_2 is depleted, and CO_2 and CH_4 accumulate under the stagnant conditions (e.g., Schmale et al., 2010; Gülzow et al., 2014; Schneider and Otto, 2019). The estuarine circulation also results in a surface salinity gradient in the Baltic Sea between its western parts (i.e., the Kattegat region), with a salinity of ~ 30 , and the northern parts, with a salinity of ~ 2 (Schneider and Müller, 2018).

The hydrography of the Baltic Sea also influences the coastal zones, through the transport of water from different areas, the amount and impact of which are strongly coupled to weather

conditions. As a result, the salinity of the coastal waters around the German Baltic Sea is particularly variable. For example, salinity at the monitored station *Darsser Schwelle* (in the vicinity of the study areas Hütelmoor and Drammendorf) during the period 2012 – 2022 ranged from 7 to 19 (MARNET, data originator Leibniz Institute for Baltic Sea Research Warnemünde, Germany, 54.42° N, 12.42° E). In addition, coastal areas of the Baltic Sea are also affected by upwelling processes that can transport mineralization signals (i.e., high CO₂ and/or CH₄ concentrations) from deeper waters toward the coasts (Jacobs et al., 2021).

River runoff affects not only the distribution of salinity, but rivers also transport soluble chemical compounds and have a strong impact on the coastal CO₂ system. The riverine transport of large amounts of dissolved GHGs leads to a variable CO₂ and CH₄ distribution in the coastal mixing zone (Stokowski et al., 2020). Coastal alkalinity, a significant component of the CO₂ system, is affected by CaCO₃ (limestone) weathering. The latter leads mainly to the formation of HCO₃⁻, which is transported by rivers and thus has local effects on the nearshore C cycle. The weathering and the potential transport by rivers depends on the catchment area and is most pronounced in southern parts of the Baltic Sea (Schneider and Müller, 2018). Hence, A_T is closely linked to salinity and can be described by A_T-S correlations (Beldowski et al., 2010). Moreover, rivers are usually enriched with nutrients because some catchment areas are heavily urbanized and industrialized, and increased nutrient supply promotes higher rates of primary production in coastal zones. Subsequent mineralization of the produced OM may cause a shift in these areas such that they are oversaturated in CO₂ and CH₄ with respect to atmospheric values.

1.3 Methane

Methane is the most abundant organic molecule on Earth, the most chemically reduced form of C, and the most potent GHG after CO₂ and water vapor. It has a residence time of 9 – 11 years and its concentration in the atmosphere over the past 300 years has increased by ~ 260 % (Whiticar, 2020). The global warming potential of CH₄ is 28 times higher than that of CO₂ over a 100-year lifetime (Crutzen, 1991; Myhre et al., 2014; Whiticar, 2020). In general, most CH₄ is produced biogenically, by microbially mediated OM degradation (methanogenesis), and by abiotic sources in the form of thermogenic (breakup of OM under high temperature and pressure) and pyrogenic (incomplete combustion of OM) processes (Whiticar, 2020). The primary natural sources of CH₄ include wetlands and freshwater environments (Saunois et al., 2020). Anthropogenic contributions, mainly from biogenic (e.g.,

livestock), pyrogenic (e.g., biomass burning), and thermogenic (e.g., fossil fuel industry), sources accounted for 50 – 65 % of the global emissions in 2000 – 2009 (Saunois et al., 2020). The main sinks for CH₄ are the oxidation by hydroxyl radicals in the atmosphere (Ehhalt, 2022), microbial oxidation in terrestrial soils (Dutaur and Verchot, 2007), and photochemical reactions.

Global CH₄ emissions to the atmosphere from the open ocean and coastal sources (biogenic, geological, and hydrate emissions), excluding estuaries, are in the range of 5 – 17 Tg CH₄ yr⁻¹ (Saunois et al., 2020). When estuaries are included, the emissions increase to 9 – 22 Tg CH₄ yr⁻¹ (Saunois et al., 2020). In general, coastal regions and estuaries contribute substantially to total marine CH₄ emissions, estimated at 75 % (Bange et al., 1994), although the literature has large uncertainties in estimating marine emissions. However, these emissions from oceanic and coastal sources are modest compared to emissions from wetlands, which are in the range of 149 – 181 Tg CH₄ yr⁻¹ (e.g., Saunois et al., 2020) and include emissions from peatlands. Moreover, current peatland rewetting efforts may result in larger CH₄ emissions but also greater uncertainties in their amounts, as emissions typically increase after rewetting. Furthermore, an increase in the exchange between coastal waters and low-lying onshore areas is expected through unintended (sea-level rise) or intended (rewetting) changes that are likely to result in altered contributions of CH₄ emissions from affected areas. Therefore, identifying local sinks and sources of CH₄ emission in the coastal environment remains a significant challenge.

Methane levels in the oceanic environment are affected by a variety of formation and consumption processes, with methane formed by microbially mediated methanogenesis in anoxic sediments being the most abundant source. The substrates for methanogens, derived from previous degradation of OM, are acetate, CO₂, and hydrogen (H₂). These substrates are mainly converted into methane by hydrogenotrophic methanogens, which use CO₂ instead of O₂ as the electron acceptor during anaerobic respiration (i.e., $\text{CO}_2 + 4\text{H}_2 \rightarrow \text{CH}_4 + 2\text{H}_2\text{O}$), and by acetoclastic methanogens (i.e., $\text{CH}_3\text{COOH} \rightarrow \text{CO}_2 + \text{CH}_4$). Hydrogenotrophic methanogens are mostly active in marine environments whereas acetoclastic methanogens are the main source of global CH₄ production (Deppenmeier, 2002; Reeburgh, 2007). A third general CH₄ formation pathway, methylotrophic methanogenesis, uses non-competitive substrates, such as methanol, methylamine, and methylsulfides, in the upper anoxic sediment layer, where the concentration of SO₄²⁻ is usually high (e.g., Thauer et al., 2008; Lang et al.,

2015). CH₄ can also be produced locally in oxic zones of the water column, thus contributing to CH₄ supersaturation in the oxygenated water column, as widely reported for ocean and freshwater environments (Reeburgh, 2007; Karl et al., 2008; Grossart et al., 2011). Among the processes reported for oxic CH₄ production are classical methanogenesis in the gut of zooplankton and the demethylation of organic phosphonates, dimethylsulfoniopropionate, (DMSP) or methylamines (Repeta et al., 2016; Bižić et al., 2020).

The main pathways of methane formation are closely linked to the competitive degradation of OM and depend on the availability of terminal electron acceptors (TEAs), such as NO₃⁻, manganese (Mn⁴⁺), iron (Fe³⁺), and SO₄²⁻, as the energy derived from the respective processes controls the establishment of organisms. Since dissolved SO₄²⁻ is a major component in seawater, CH₄ formation in sediments is strongly affected by the microbial reduction of SO₄²⁻ by sulfate-reducing bacteria (SRB), which in OM degradation effectively outcompete methanogens for available H₂ (i.e., 4H₂ + SO₄²⁻ → HS⁻ + OH⁻ + 3H₂O) (Reeburgh, 2007). Consequently, CH₄ production occurs predominantly in SO₄²⁻ depleted sediments. For example, in Eckernförde Bay, a well-studied coastal area in the Baltic Sea, the SO₄²⁻ depleted zone begins at 25 cm depth, although the penetration of SO₄²⁻ varies depending on the marine environment (Treude et al., 2005; Reeburgh, 2007).

The availability of TEAs in the sediments and overlying water column also determines the rate of CH₄ oxidation by methanotrophic microorganisms (bacteria and archaea) under oxic and anoxic conditions, using mainly O₂ and SO₄²⁻ (i.e., CH₄ + SO₄²⁻ → HCO₃⁻ + HS⁻ + H₂O), respectively (e.g., Jørgensen et al., 2001; Reeburgh, 2007). These oxidation processes form an essential barrier for the rising CH₄ from the sediment to the water surface. In addition to oxidation in the upper sediment layers, oxidation in the water column is supported by stable (e.g., Baltic Sea) or seasonal (North Sea) haloclines and pycnoclines, allowing CH₄ to persist for an extended time in the water column (Schmaljohann, 1996; Boetius et al., 2000; Jørgensen et al., 2001; Bange, 2006; Schmale et al., 2010). However, this physical barrier is often disrupted, such that the oxidation potential decreases when water column mixing prevents the formation of density gradients, which is often the case in coastal regions and estuaries. Consequently, the sources of dissolved and atmospheric CH₄ from these areas are strengthened (Bange, 2006; Borges et al., 2016; Gelesh et al., 2016).

1.4 Peatlands

Peatlands occupy a small part (~ 3 %) of the Earth's land surface and are unevenly distributed throughout the world, with ~ 80 % located in the northern hemisphere, mostly in boreal and subarctic zones, 10 % in tropical areas, and another 10 % in temperate zones (e.g., Frohking et al., 2011). Despite their low spatial coverage, peatlands account for many active and passive ecosystem functions, for example:

- Water management, such as water storage, filtration, supply, and the mitigation of floods and drought (e.g., Sierszen et al., 2012)
- Retention of nutrients and sediment
- Biological niches for endemic or endangered plant and animal species, and thus important reservoirs for genetic biodiversity (Mäkilä and Saarnisto, 2008)
- Stabilization of the microclimate (e.g., local cooling due to evaporation) and macroclimate (as a CO₂ sink)
- Accumulation of large amounts of C, as the rate of primary production in peatlands historically exceeded OM decomposition, such that peatlands in their natural state act as a C sink (e.g., Turunen et al., 2002; Mäkilä and Saarnisto, 2008)

However, peatlands are subject to strong anthropogenic pressure that has led to their destruction and disappearance. In some countries, including Germany, almost all of these areas have disappeared as they have been converted into agricultural land (Joosten and Clarke, 2002; Parish et al., 2008). Lowering of the water column as the main measure leads to aerobic conditions in the peat soil, which result in OM degradation and thus in massive CO₂ release. Nevertheless, worldwide peatlands still represent the largest reservoir of terrestrial C, up to 550 Gt, which is twice the C stock of the worldwide forest biomass (Moore et al., 1998; Kaat and Joosten, 2009). Therefore, the protection of peatlands, including the restoration of those that have been drained, offers enormous potential for mitigating GHG emissions, by increasing water levels and changing land management strategies (Parish et al., 2008).

1.4.1 Peatlands in the climate system

Exchange of the GHGs CO₂, CH₄, and N₂O in peatlands is sensitive to changes in the prevailing biochemical and physical conditions in the soil, which in turn are strongly connected with the vegetation, the water level, and consequently, the occurrence of oxic and anoxic conditions (Parish et al., 2008; Kaat and Joosten, 2009). Pristine peatlands are

permanently or frequently saturated with water and act as a natural sink for CO₂ (evidenced by peat accumulation) while also retaining nutrients (e.g., NO₃⁻) in the form of microbial biomass (Martikainen et al., 1993), because the rates of primary production and OM deposition exceed those of decomposition. The anoxic conditions of the waterlogged peat are highly favorable for CH₄ and N₂O production, such that global peatlands are moderate sources of ~ 30 Tg CH₄ yr⁻¹ and 0.02 Tg N₂O yr⁻¹ (Frolking et al., 2011). However, when the total C budget is considered, undisturbed peatlands are a weak C sink, with uptakes of around 100 Tg C yr⁻¹ (Frolking et al., 2011).

The drainage of peatlands leads to the infiltration of O₂ into the peat layers and aerobic OM decomposition, which is associated with increased CO₂ emissions (e.g., Joosten and Clarke, 2002). As a result, drained peatlands become a strong CO₂ source whereas CH₄ emissions are either reduced or negligible (e.g., water level < 20 cm) because production is strongly coupled to the water level (Kaat and Joosten, 2009). In Germany, where > 85 % of the peatland areas are disturbed (i.e., drained), 32 Tg CO₂ yr⁻¹ (or 53 Tg CO₂-equivalents per year¹) are released. These emissions account for ~ 5 – 7 %² of the total CO₂ emissions of Germany over an area that covers only ~ 4.7 % of the land surface (Kaat and Joosten, 2009). CO₂ emissions are even more pronounced in *Mecklenburg Vorpommern*, where peatlands cover ~ 12.5 % of the land area. These drained areas account for ~ 30 % (6.2 Tg CO₂-equivalents yr⁻¹) of the state's total annual CO₂ emissions (LU M-V, 2009). While drainage generally increases CO₂ emissions and decreases CH₄ emissions, N₂O emissions are coupled to the cycling of nitrogen (N) and are therefore mainly controlled by substrate availability (e.g., NO₃⁻), which is low in peatlands. However, availability can be raised by inputs from external sources (e.g., from agriculture) or by stimulating mineralization (e.g., Martikainen et al., 1993; Parish et al., 2008).

1.4.2 The impact of peatland rewetting on GHG fluxes and nutrients

Although the rewetting of degraded peatlands would be expected to decrease CO₂ and N₂O emissions due to waterlogged peat and anoxic conditions in the peat soil, in practice, it often

¹ CO₂-equivalents are the amount of CO₂ emissions that would cause the same integrated radiative forcing of a mixture of GHGs over a given time horizon. A CO₂-equivalent is obtained by multiplying the emissions of a gas by its global warming potential. The sum of the equivalent CO₂ emissions of a gas mixture that includes CO₂, CH₄, and N₂O is called CO₂-equivalent (IPCC, 2013).

² The lower limit (~ 5 %) refers to 2008 and was reported by Kaat and Joosten, 2009 and the upper limit (~ 7 %) refers to the Umweltbundesamt, 2022.

leads to increased CH₄ emissions while CO₂ emissions can remain consistently high. This behavior is often related to the rapid degradation of young plant material after rewetting and is likely a transient phenomenon (Kaat and Joosten, 2009). Nevertheless, the response of GHG emissions to rewetting can vary widely depending on the preconditions and rewetting strategies, even several years after rewetting. For example, an important factor is whether the humified peat was removed prior to rewetting. The source of water and the strategy of rewetting can also lead to different responses, resulting in either permanent flooding with freshwater, episodic flooding with saltwater, or permanent flooding with saltwater.

In rewetted peatlands, CO₂ emissions are controlled by primary production or the decomposition of OM (Parish et al., 2008; Oertel et al., 2016). In anoxic, water-saturated zones, OM degradation formerly induced by oxygen is slowed and relies on the availability of TEAs, for example, NO₃⁻ and SO₄²⁻, resulting in lower CO₂ emissions (Strack, 2008; Dean et al., 2018). In turn, methanogenesis may gain in importance as the final step of OM mineralization, because in water-saturated, anoxic soil layers CH₄ is produced mainly by archaea, when all other TEAs are depleted (Schönheit et al., 1982; Oremland, 1988; Segers and Kengen, 1998). Thus, rewetted peatlands are often significant sources of CH₄ (Hahn et al., 2015). By contrast, in coastal peatlands rewetted with seawater the contribution of methanogenesis may be lower, because the availability of SO₄²⁻ transported by seawater allows SRB to outcompete methanogenic archaea (Bartlett et al., 1987; Capone and Kiene, 1988; Oremland, 1988; Jørgensen, 2006) and CH₄ production shifts to deeper parts of the sediment. The availability of SO₄²⁻ also favors the anaerobic oxidation of methane (AOM) associated with SO₄²⁻ reduction (e.g., Boetius et al., 2000; Knittel and Boetius, 2009). Although rewetting coastal peatlands with brackish water is expected to have beneficial effects on limiting GHG emissions compared to peatlands rewetted with freshwater, due to the availability of SO₄²⁻, the impact on GHG emissions remains still unclear.

Whether rewetted peatlands release or take up nutrients depends on several factors. Release after rewetting is related, for example, to the degree of previous peat degradation and to the availability of decomposable OM after rewetting, both of which can lead to nutrient accumulation in the topmost layers (Zak and Gelbrecht, 2007). In addition, water level fluctuations (i.e., redox conditions; Duhamel et al., 2017) and salinity (Liu and Lennartz, 2019) determine nutrient release or uptake. The release of NH₄⁺ and PO₄³⁻ after rewetting is generally higher in areas where drainage, and thus peat degradation has been intense

(Duhamel et al., 2017). Therefore, removal of the humified topsoil is recommended as an effective measure to reduce nutrient release after rewetting (Harpenslager et al., 2015; Zak et al., 2017).

The general sea level rise and a simultaneous increase in storm surge events in the Baltic Sea region (Vousdoukas et al., 2016) have strengthened the coupling of marine and terrestrial compartments. In some cases, this coupling, which includes the transport of water and material between the two, is actively promoted, as in the Drammendorf coastal peatland study area. Reasons for the expansion of such coastal wetlands include the peat growth with a rising sea level (Karstens et al., 2016) and the restoration of water and nutrient retention, biodiversity, and C storage functions. However, the outcome of coupling coastal peatlands with seawater through a permanent hydrological connection is largely unknown.

1.5 Methodological challenges in shallow waters

Although some coastal areas in the Baltic Sea are a significant source of atmospheric GHGs (e.g., Bange et al., 1998; Heyer and Berger, 2000; Stokowski et al., 2020), systematic long-term data with an appropriate resolution are scarce, as previous studies focused on open waters and estuaries. Moreover, they mostly relied on discrete sampling (one-point recording), an approach that in coastal areas is questionable because the methods are usually not well adapted to coastal conditions, including the fact that they do not take into account for spatial and temporal heterogeneity and the role of mechanical forces. Therefore, new techniques and interdisciplinary scientific approaches are needed to uncover the blind spots created by discrete sampling and thus to more robustly connect terrestrial and marine compartments.

The deployment of autonomous in situ sensors can significantly increase the resolution in data acquisition and maintain data collection even under bad weather conditions. However, there are challenges associated with this approach, such as battery power limitations and the need for sophisticated procedures to sensor installation and data verification during data post-processing. In addition to these sensor-based techniques and to address the associated issues, model simulation should be implemented that can simulate small-scale and large-scale processes. Therefore, by combining field measurements and modelling, short-term or extreme events (e.g., storms, droughts) that are expected to occur more frequently in coastal areas can be captured, tracked and evaluated (e.g., Gräwe and Burchard, 2012; BACC II Author Team,

2015; Vousdoukas et al., 2016). However, presently there is no network for autonomous sensor-based measurements in coastal areas, such as those established for open waters (e.g., ARGO floats, ships of opportunity), or the high-resolution data obtained from the sensors only can cover a few marine variables (e.g., Canning et al., 2021; Roth et al., 2022).

In this work, two lander systems were used that can be considered as modern, advanced technology for underwater monitoring applications. The systems are designed to deploy various sensors and can be customized for the desired application. In addition, sensor operation and sensor data acquisition were controlled by a central data processing unit, which enabled efficient processing of incoming data even during long-term missions. To support for the lander measurements, a wide range of additional information was collected, including data obtained from extensive discrete sampling, meteorological data, and model simulations.

1.6 The study areas

The content of Sect. 1.6.2 and the Figure 1 d, e were published in Pönisch et al., 2023. Nutrient release and flux dynamics of CO₂, CH₄, and N₂O in a coastal peatland driven by actively induced rewetting with brackish water from the Baltic Sea, Biogeosciences, 20 (2), 295–323, <https://doi.org/10.5194/bg-20-295-2023>. The respective text was changed for linguistic and conceptual reasons to conform with the overall style of this dissertation.

The three work packages of this dissertation were carried out at two sites located in the northeastern German Baltic Sea, on the coast of *Mecklenburg-Vorpommern*. Both sites encompassed shallow water areas (< 10 m) and were influenced by peat deposits (Figure 1a, b). They included (i) a shallow coastal area of the Baltic Sea located offshore of the nature reserve *Hütelmoor* and *Heiligensee* (Figure 1c), and (ii) a recently rewetted peatland in the *Polder Drammendorf* (Figure 1d – f), hereafter referred to as *Hütelmoor* and *Drammendorf*, respectively. The terrestrial and marine areas of the *Hütelmoor* have been the subjects of intensive scientific research for several years (e.g., Jurasinski et al., 2018; Kreuzburg et al., 2018). Further, the offshore area is representative of many coastal areas in the Baltic Sea, due to its marine vegetation and sediment characteristics. In *Drammendorf*, a rewetting using brackish water from the adjacent *Kubitzer Bodden* was implemented for the first time. This measure allows to compare the consequences of rewetting with brackish water with studies in which freshwater was used. Freshwater is commonly used for the rewetting of peatlands and has been the subject of several studies (e.g., Hahn-Schöfl et al., 2011; Koebisch et al., 2013).

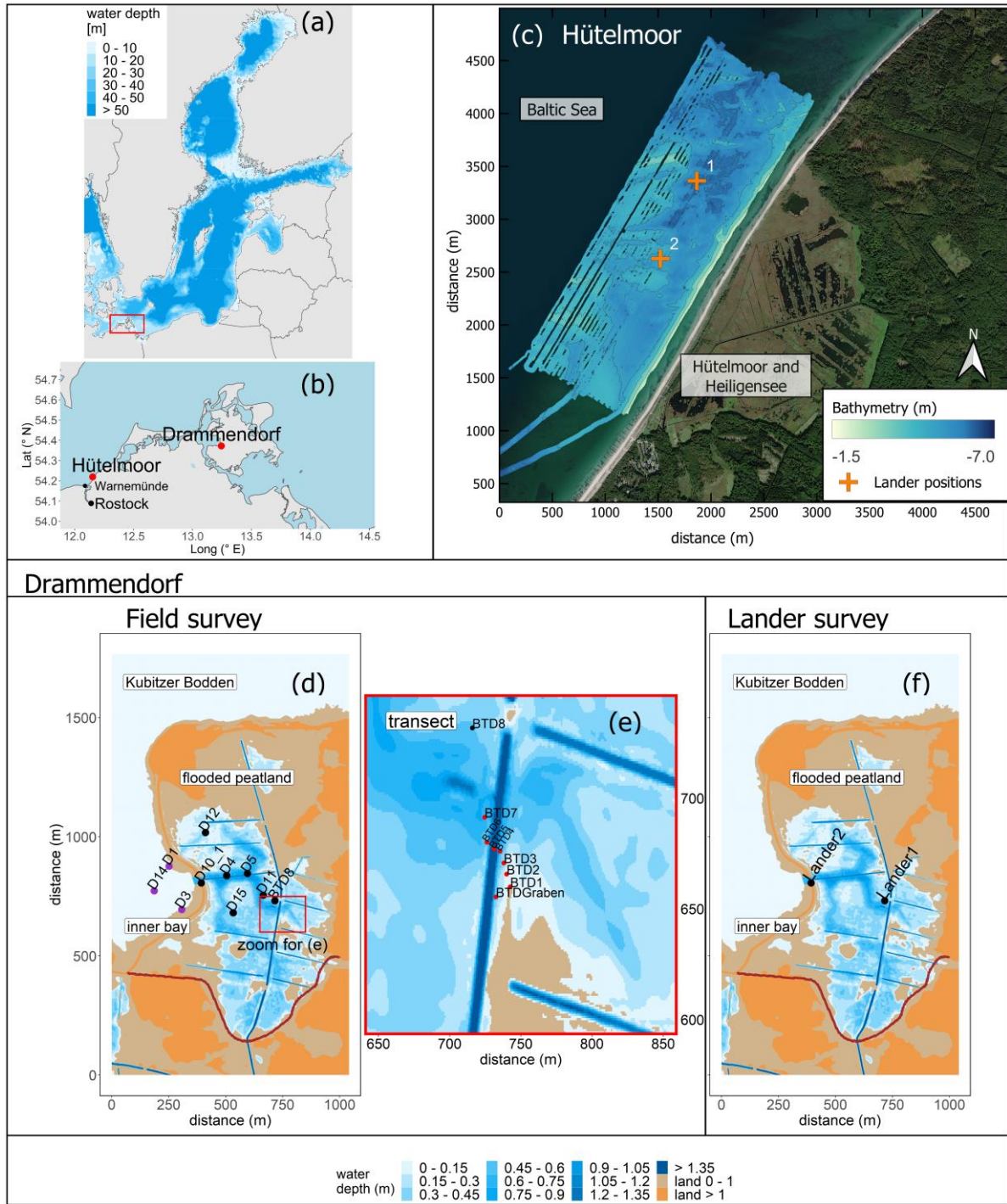


Figure 1: Overview of the two study areas, located in (a) the southern Baltic Sea and (b) at the coastline of *Mecklenburg-Vorpommern*. (c) The bathymetry of the Hütelmoor site, together with the lander positions deployed in the shallow area of the Baltic Sea in front of the *Hütelmoor* and *Heiligensee* in autumn of 2019 (data retrieved from Kreuzburg et al., 2018). (d – f) The topography of Drammendorf and the resulting bathymetry after flooding at normal water level. Two surveys were conducted in Drammendorf: a field survey (2019/2020) and a lander survey (summer 2021). (d, e) Overview of the stations during the Drammendorf field survey. The stations in the inner bay are shown in purple and those of the peatland in black. (e) The transect belonging to that survey, which was sampled for GHG fluxes to the atmosphere by flux chamber measurements (before - and accordingly dry, and after rewetting), and for surface water GHG concentration measurements (after rewetting). (f) The locations of the two landers, deployed one year later. The new dike is shown in dark red.

1.6.1 The nearshore shallow waters of the Hütelmoor

The Hütelmoor is located ~ 15 km northeast of Rostock and comprises an area of ~ 2 km in the north-south direction, extending ~ 1 km offshore, where the depth is ~ 6 m (Figure 1c). The bathymetry and the properties of the sediment surface are described elsewhere (Kreuzburg et al., 2018) and both are heterogeneous. In the Hütelmoor, sand and sill ridges emerge seawards parallel to the coastline. The seafloor composition ranges from well-sorted fine sand to medium sand, poorly sorted coarse sand, and gravel with medium vegetation (e.g., seagrass). Analyses of sediment cores indicated that the offshore subsurface structure partly consists of organic layers in the sediment and outcropping peat at the beach (Kreuzburg et al., 2018).

The water column of the Hütelmoor is influenced by two major mechanisms, acting at different scales, that affect its physical and biochemical conditions: (i) large-scale interactions with the open Baltic Sea that result in the transport of physical and biochemical signals typical for the shallow coasts of the Baltic Sea and (ii) local interactions between sea-land and sea-sediment interfaces (Jurasinski et al., 2018). The influence of large-scale water masses is reflected by the changes in surface water salinity determined at the adjacent monitoring station *Darsser Schwelle* between 2012 and 2022, which ranged between 7 and 19 (MARNET, Sect. 1.2.2). This variability is caused by the influence of different water bodies, including the less saline water from the northern part of the Baltic Sea and the more saline water from the North Sea (Sect. 1.2.2.1). Another possible source of impact is the *Warnow* plume, which enters ~ 10 km west of the study site and transports recalcitrant substrates toward the Hütelmoor (Jurasinski et al., 2018). Local processes determined by interactions at the sea-sediment interface also play an important role in the Hütelmoor. These include mechanical forces caused by wave action, which may induce pore water flows and occur at time scales ranging from minutes to days (Jurasinski et al., 2018). In addition, stagnant conditions can lead to water stratification, resulting in an accumulation of dissolved compounds at the bottom and thus to small spatial gradients of salinity and temperature in the near-coastal area of the Hütelmoor (Jurasinski et al., 2018).

1.6.2 The rewetted peatland Drammendorf

Drammendorf is a low-lying, highly degraded coastal peatland located in the western part of the island of *Rügen* (Figure 1b). The site was converted from a drained and agriculturally used *Polder* to a brackish wetland in November 2019. This was part of an active rewetting effort aimed at restoring biodiversity, preventing CO₂ emissions from peat degradation, and, in the long-term, establishing C-storage, and is described in detail in Pönisch et al. (2023). Flooding occurred immediately after the removal of a ~ 20-m-wide section of the dike, by dredging a channel down to the sediment level of the *Kubitzer Bodden*, which is part of the Baltic Sea (Figure 3d). This measure created a partially flooded area with a water depth of ~ 0.5 – 1 m, covering ~ 0.5 km² (Figure 1d – f). The preceding intensive drainage initiated in the 1960s had resulted in oxic peat degradation and peat loss, which led to the formation of a local land depression below mean sea level and thus, after flooding, to the establishment of a permanent water column. Soil in the area has a high organic content since vegetation, topsoil, or the remaining ditch system were not removed prior to rewetting. The topsoil of the central part consists of a highly degraded peat layer of up to 50 – 70 cm followed by a well-preserved peat layer of up to 100 cm, and a maximum peat deposit of 220 cm was found in the western part (Brisch, 2015). A dike, a drainage ditch, and a pumping station were built prior to rewetting. The pump station is used to pump water from the adjacent drainage areas into the rewetted area. However, inputs of dissolved compounds (e.g., nutrients, OM) are not considered to be significant (T. Schulze, *Wasser- und Bodenverband Rügen*, personal communication, 2020).

Rewetting and the establishment of a hydrological connection enabled the transport of water with a salinity of ~ 6 – 8. At usual water levels, surface water exchange between the flooded peatland and *Kubitzer Bodden* takes place only via this channel. Consequently, the extent of inundation, and thus the water level in the peatland, is directly coupled to the water level of the Baltic Sea. For example, a small change in the Baltic Sea water level from – 0.5 to + 0.5 m, as occasionally occurs in the area, expands the inundated area from 0.08 to 0.7 km² (Pönisch et al., 2023). Furthermore, the water level of the flooded peatland follows that of the *Kubitzer Bodden* without detectable signal delay (Pönisch et al., 2023).

2. Methods

Coastal ecosystems connect terrestrial and marine compartments and exhibit rapid element cycling, which is enhanced by terrestrial loads (e.g., nutrients, GHGs) and intense water column mixing. As a result, coastal areas are heterogeneous and thus represent environments that are methodologically difficult to evaluate. The shallow areas of the Baltic Sea (0 – 10 m) are particularly challenging because existing methods are often not adjusted to brackish water conditions and the shallow water column hinders the access of research vessels and the use of heavy equipment. Innovative methodological approaches are therefore needed. The methodology of this work relied on the deployment of two novel sensor-equipped landers to obtain autonomous measurements with high temporal resolution. These measurements were complemented by intensive discrete sampling campaigns from a small working boat.

2.1 The landers as a platform and sensor overview

The landers are modular platforms (i.e., for components and sensors) and consist of the lander framework and the hardware and software required for autonomous underwater monitoring applications. They were designed as advanced stationary observatories to be deployed at the sediment-water interface for the autonomous study of physical and biochemical processes, and are particularly adapted for studies in shallow waters (> 1 m water depth). Integrated high-resolution measurements using commercially available sensors were conducted with the landers (Figure 2a). The lander concept was developed in cooperation with Kongsberg Maritime Contros GmbH (Kiel, Germany) and subsequently realized by the latter. Nevertheless, extensive improvements regarding power supply, data handling and software had to be developed as part of this work in order to increase system reliability in shallow water applications. In the Hütelmoor survey, the landers were deployed under battery power (Sect. 2.2), while in the Drammendorf survey power was provided through a permanent, wired supply line (Sect. 2.4). A detailed technical description is provided in Figure 2.

2.1.1 The central data processing unit (DPU)

The most innovative feature of the landers is the data processing unit (DPU), which provides the power infrastructure and software needed for autonomous sensor measurements. The DPU is capable of managing up to ten sensors. Each sensor is controlled by an individual schedule for measurements that can be adjusted during the deployment via cable connection. Because the sensors are integrated through centralized time synchronization, accurate data processing

and the subsequent integration of auxiliary data, e.g., wind information, are possible. DPU data management is based on a SQLite database, with additional access via a web user interface.

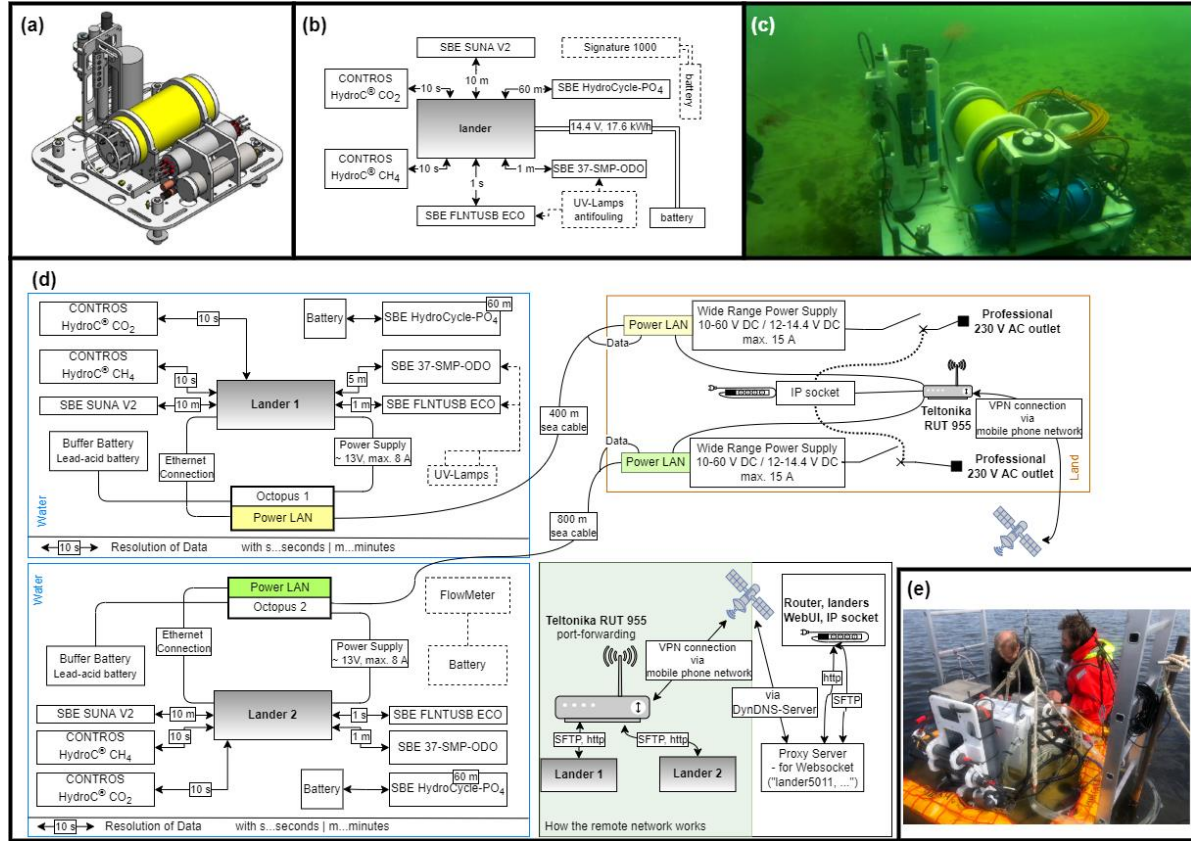


Figure 2: Technical description and instrumentation of the landers. **(a)** Schematic overview of the lander and the modular frames for the sensors (left and right) and the central yellow battery container. **(b)** Summary of the sensor configuration used in the Hütelmoor lander survey. A dashed line represents the equipment used only at lander 1. The captions at the arrows describe the resolution of the data acquisition; s: seconds, m: minutes. **(c)** Lander 1 at the sediment-water interface in Hütelmoor after ~ 15 days of deployment. **(d)** Overview of the setup and technical adjustments made for the Drammendorf lander survey, including the key components of a wired land-based electrical power supply and powerline communication (right top) as well as remote accessibility (right bottom). The respective hardware was bundled in the “Octopus” device on both landers (left). In **(d)**, the dashed line represents the equipment used at the actual lander and the captions describe the resolution. **(e)** The set-up of the lander in the central area of the Drammendorf lander survey, using a lift construction.

2.1.2 The Instrumentation

Each lander was equipped with six state-of-the-art sensors measuring the partial pressure of CO₂ and CH₄, temperature, salinity, hydrostatic pressure (depth), turbidity, O₂, and the concentrations of NO₃⁻, PO₄³⁻, and chlorophyll *a* (Figure 2b, d). The sensors and their characteristics are summarized in Table 1. In addition to the measurements using the integrated sensors on the landers, other sensors were included to obtain supplemental information (e.g., water velocity; Table 1).

Table 1: Overview of the sensors, manufacturers, abbreviations, detector types, and the variables measured with each unit.

Model	Manufacturer	Abbreviation	Detector type	Variable	Unit
CONTROS HydroC® CO ₂	-4H- JENA Engineering GmbH, Jena, Germany	HC-CO ₂	non-dispersive infrared spectrometry (NDIR)	partial pressure of CO ₂	µatm
CONTROS HydroC® CH ₄		HC-CH ₄	tunable diode laser absorption spectroscopy (TDLAS)	partial pressure of CH ₄	µatm
HC-CO ₂ and HC-CH ₄ were equipped with SBE-5M and SBE-5T pumps, which provided active water circulation across the sensor membranes. They are different in power consumption and water flow rate. Details can be found in the respective chapters on the two lander surveys.					
SBE 37-SMP- ODO MicroCAT	Sea-Bird Electronics Inc, Bellevue, WA, USA	CTD-O ₂	conductivity cell	salinity	NA
			thermistor	temperature	°C
			hydrostatic probe	hydrostatic pressure	dbar
			fluorescence quenching	oxygen	µmol kg ⁻¹
SBE SUNA V2		SUNA-NO ₃ ⁻	UV-Spectroscopy	concentration of NO ₃ ⁻	µmol L ⁻¹
SBE HydroCycle- PO4		HCycle-PO ₄	IR-Spectroscopy	concentration of PO ₄ ³⁻	µmol L ⁻¹
SBE-FLNTUSB ECO		NA	fluorescence	chlorophyll <i>a</i>	µg L ⁻¹
			back scatter	turbidity	NTU
The following instruments were used to gather additional information and were not used as integrated sensors on the landers. The Signature 1000 and the PME miniDOT instruments were only used during the Hütelmoor lander survey.					
Signature 1000	Nortek AS, Norway	NA	Acoustic Doppler	water velocities	m s ⁻¹
PME miniDOT	Precision Measurement Engineering, Inc., California, USA	NA	thermistor	temperature	°C
			optical (luminescent)	oxygen	mg L ⁻¹
Within the three surveys a HACH HQ40D multimeter (HACH Lange GmbH, Düsseldorf Germany) was used to analyze water temperature, salinity and dissolved oxygen concentration. The multimeter was equipped with two outdoor electrodes (LDO10105, CDC40105) with a precision of the temperature, salinity and O ₂ saturation of ± 0.3°C, 0.1 and 0.8 %, respectively.					

NA means not applicable

2.2 The Hütelmoor lander survey

The survey included the deployment of the two landers for a period of approximately four weeks (04 September 2019 to 04 October 2019), accompanied by discrete water sampling. The landers were deployed ~ 400 m offshore, with a distance of ~ 700 m between them (Figure 1c). $p\text{CO}_2$, $p\text{CH}_4$, temperature, salinity, hydrostatic pressure (depth), O₂, turbidity, and the concentrations of NO₃⁻, PO₄³⁻, and chlorophyll *a* were measured at high-resolution and stationarily at the landers. Lander 1 was deployed at ~ 6 m water depth in a northern direction, where the sediment mostly consisted of medium sand and gravely coarse sand deposits. The location was associated with nearshore peat deposits. However, seismic profiles showed no peat deposits in the immediate vicinity of the lander (Kreuzburg et al., 2018). Lander 2 was deployed at ~ 5 m water depth and in a more southern location, where fine sand predominates and an influence of peat was unlikely. The sensors, the resolution of the acquired data, and the measured variables are summarized in Figure 2b and Table 1. An overview of this survey is provided in Table 2.

2.2.1 Deployment of the landers

The landers were assembled in the laboratory and deployed with administrative assistance from the *Wasserstraßen- und Schifffahrtsverwaltung des Bundes* (Stralsund) using a buoy tender. The systems were powered by lithium primary cells with a capacity of 17.6 kWh and had to be initialized by scientific divers using a magnetic switch. After 15 days, the observatories and sensors were serviced by divers, including cleaning and data downloading, with the latter achieved using a 50-m Ethernet cable connection.

2.2.2 Sensor configuration and data post-processing

The partial pressures CO_2 and CH_4 were determined using different CONTROS HydroC[®] sensors, whereby the measurements were based on equilibration of the gases in the seawater with the sensor headspace through a membrane. The subsequent optical detection was achieved by non-dispersive infrared spectrometry (NDIR, HC- CO_2) and tunable diode laser absorption spectroscopy (TDLAS, HC- CH_4), respectively (Fietzek et al., 2014). The membrane was continuously flushed by pumped sea water. For both instruments, the frequency of data acquisition was adjusted to 10 seconds (s). Each data point represented an average of 10 measurements and was calculated by the sensor software.

***p*CO₂ measurements with HC-CO₂**

The HC- CO_2 sensors were factory calibrated before and after their deployment for a range of 200 – 1000 μatm (post-deployment calibration for the HC- CO_2 at lander 1 was not possible due to a transport-related defect of the NDIR). The sensors were equipped with external 1.0 W pumps (SBE-5M). The instruments recorded zeroing values for 120 s by removing CO_2 from the gas stream at regular intervals every 12 hours (h). After zeroing, a flush period continued (flagged in the data for 780 s), and the signal recovered to environmental conditions. Zero and flush intervals were removed from the continuous data set prior to biogeochemical interpretation. The post-processing of *p*CO₂ values included consideration of regular zeroing signals, pre- and post-calibration (HC- CO_2 at lander 2 included additional span drift correction) as described by Fietzek et al. (2014), and the response time (τ) was corrected according to Fiedler et al. (2013) and Bittig et al. (2014). The response time was determined using in situ data for each flush period by fitting an exponential function to the signal recovery. A rolling mean was applied to the response time correction to suppress short-term noise.

***pCH₄* measurements with HC-CH₄**

The two HC-CH₄ sensors were factory calibrated in water before their deployment for a range of 1 – 40000 μatm ; the response time determined by the manufacturer was 3540 s (59 minutes, min). The sensors were equipped with external 1.0 W pumps (SBE-5M). The response time was used to correct the signal delay for each recorded *pCH₄* as described by Fiedler et al. (2013) and Bittig et al. (2014), following the same procedure as described for the HC-CO₂ sensors. Signal artifacts due to a daily midnight sensor shut-off and the correction procedure were excluded.

CTD-O₂ measurements

Conductivity, temperature, and depth (CTD) and dissolved O₂ measurements were carried out using SBE 37-SMP-ODO MicroCAT instruments (CTD-O₂). The resolution of the acquired data was 1 min for lander 1 and 10 min for lander 2. Pre-deployment calibration was conducted by the manufacturer. Post-deployment calibration for conductivity, temperature, and O₂ was carried out in the accredited calibration laboratory of the IOW two months after deployment. To counteract oxygen optode drift between the manufacturer's calibration and sensor deployment, in-air oxygen optode measurements before the deployment were conducted. Then, a slope correction was performed based on measured values in-air and the calculated atmospheric partial pressure following Bittig and Körtzinger (2015). The correction coefficient for O₂ values were of 1.04 at lander 1 and 1.06 at lander 2. O₂ and conductivity data were removed from lander 2 as of 15 September 2019, due to an unexpected drop in variables and a discrepancy with the discrete sample. This issue was likely related to air entrapment that impeded the undisturbed circulation of pumped seawater along the O₂ optode and conductivity cell. Temperature and pressure were unaffected due to the exposed position of the respective probes at the sensors.

NO₃⁻ measurements with SUNA-NO₃⁻

Nitrate measurements were carried out using SBE SUNA V2 instruments (SUNA-NO₃⁻), with a measurement resolution of 10 min. Individual data points consist of 15 – 21 individual measurements with a resolution of 1 s. The SUNA UV absorption spectra were processed according to Sakamoto et al. (2009) using the manufacturer-provided calibration data. Specifically, the in-situ temperature-corrected salinity absorbance (bromide absorption) was subtracted from the total measured absorbance. After subtraction of the salinity contribution,

the absorbance in the wavelength range of 217 – 240 nm was used in a regression analysis with NO_3^- absorptivity and a linear baseline as components. The linear baseline assumption from Sakamoto et al. (2009), rather than a sophisticated treatment of colored dissolved organic matter (CDOM) interference in the Baltic Sea, was used due to the lack of a characterization of the CDOM spectral shape in the UV range. Technical drift of the light source intensity during the deployment was compensated by measuring the UV absorption spectra of MilliQ water before and after deployment, as a valid linear baseline correction. NO_3^- data were offset-adjusted to the discrete bottle data following Johnson et al. (2013); the offset was in the range of 5.02 – 4.19 $\mu\text{mol L}^{-1}$.

PO_4^{3-} measurements with HCycle- PO_4

Dissolved phosphate (PO_4^{3-}) was measured using SBE HydroCycle- PO_4 sensors. The determinations were based on the wet-chemical formation of a blue colored compound in the sensor cuvette, which is a standard laboratory method, described, for example, in Grasshoff et al. (2009). The concentration of dissolved PO_4^{3-} was determined by absorption measurements of the colored compound in conjunction with measurements of an on-board calibration standard. The frequency of sample measurements was 60 min, with calibration measurements after six determinations. Pre-deployment calibration was conducted by the manufacturer.

Chlorophyll *a* und turbidity measurements

Turbidity and the chlorophyll *a* concentration were measured using SBE-FLNTUSB ECO sensors. Measurements were carried out with ~ 1 Hz for 240 s followed by a 60-s sequence of bio-wiper/UV light treatment (see Sect. 2.2.3 for the UV lights). After processing, the average values of ~ 240 individual measurements were calculated, using calibration data provided by the manufacturer.

2.2.3 Measures for consistent data acquisition and quality control

Sensor-based measurements in nearshore conditions are challenging for several reasons. For example, sediment transport may affect the performance of water pumps, and biofouling may negatively impact the measurements. Further, it is often the case that reference measurements cannot be taken at a frequency that allows optimal drift correction as also occurred during the Hütelmoor survey. The following measures were part of a significant effort aimed at the collection of reliable data:

- In situ clean-up and video documentation of the observatories by scientific divers during deployment
- Discrete water samples for validation of continuous sensor sampling
- Calibrations, sensor drift assessments, additional in-house characterizations
- Response time (τ) analysis of $p\text{CO}_2$ series to identify any drift, induced, for example, by biofouling
- Biofouling is a major issue for data quality in moored systems, particularly in shallow, productive waters. Therefore, two in-house developed UV light antifouling devices were used at lander 1 to improve data quality. The optics were adapted to fit the CTD- O_2 and SBE-FLNTUSB ECO instruments. During the deployment, the UV-lamps were switched on every 10 min for 25 s.

2.2.4 Discrete sampling

Sensor validation was performed using discrete bottle samples collected at each lander position on 19 and 25 September 2019. Sampling was conducted near the sediment surface ($\sim 5 - 6$ m) and at the sea surface at 2 m water depth. Validation was scheduled more frequently but often had to be canceled due to poor weather conditions. Water was sampled manually using a 5 L Niskin bottle, and subsamples were filled directly in the field with sample overflow. Subsamples were taken for dissolved O_2 (50 mL), CH_4 , pH, and C_T (each 250 mL). Poisoning was performed in the laboratory, except for O_2 , where fixation was conducted on board. Nutrient subsamples (NO_3^- , PO_4^{3-} ; 200 mL) were filtered in the field using combusted glass-fiber filters ($0.7 \mu\text{m}$, GF/F, Whatman[®]) and stored at -20°C . Details of the laboratory analysis are provided in Sect. 2.5. Water temperature and salinity were measured using a HACH HQ40D multimeter (see Table 1 for details).

2.2.5 Supplementary information (water velocity, numerical model, water column measurements) and data handling

Lander 1 was additionally equipped with an upward-facing acoustic current profiler (Signature 1000) powered by an external battery, with data recorded on the instrument. The instrument sampled water velocities between 1.8 m and 5.8 m above the sediment using 1 m bins. Bins above 5.8 m were contaminated by interferences with the sea surface (e.g., the sidelobe effect). Along- and cross-shore velocities were derived by rotating the vertically averaged velocities such that the crossshore velocity, averaged over the deployment period, was zero. The angle of rotation was 59.52° .

Numerical simulations were used to derive major three-dimensional water flow information at high temporal and spatial resolution from the Hütelmoor study area and the nearby marine catchment. Model simulations were performed for the entire deployment time. In addition, the salinity and temperature distributions of the water column were derived from lander 1. The model simulations were based on a validated model setup used in previous studies (Buer et al., 2018; Enders et al., 2019), with 25 bottom-following vertical layers, a horizontal resolution of 20 m, and the adaptation described in Lange et al. (2020).

Along with the lander CTD-O₂ measurements, the water column temperature and dissolved O₂ were measured at high-resolution using PME miniDOT instruments (Table 1). The measurements were carried out at 1 and 3 m above the sediment surface in the vicinity of each lander and were used to identify possible stratification of the water column; the measurement frequency was 1 Hz. The time series of each PME miniDOT were corrected by individual factors derived from an offset to the calibrated CTD-O₂ instruments deployed at the lander. The correction factors ranged between 1.046 and 1.066.

Spearman correlation coefficients (r_s) were calculated to obtain a first-order overview of the linear relationships between the measured variables (Figure 7). A significance level of 0.001 was applied to identify non-correlating variables (empty fields). In addition, a p-value adjustment was performed using the R package *corrplot* (Wei and Simko, 2021), appropriate for a multi-variable correlation approach. The Cohen (1988) convention was used to interpret the strength of the relationship between the variables, by introducing effect sizes in the correlations. A large effect size was defined as $r_s \geq 0.5$ and $r_s \leq -0.5$ and indicated a strong correlation (represented by black stars in the figures). A medium effect size and correlation were defined as $r_s \geq 0.3$ and $r_s \leq -0.3$ (represented by brown stars in the figures).

Table 2: Summary of the methodology used for the Hütelmoor lander survey.

Used method	Comments and survey outcomes
Lander deployment	<ul style="list-style-type: none"> -landers under battery power supply -High-resolution data of $p\text{CO}_2$, $p\text{CH}_4$, O₂, temperature, salinity, water pressure, turbidity, and concentrations of chlorophyll <i>a</i> and NO₃⁻ -PO₄³⁻ and O₂ restricted data availability -water velocity measurements
Discrete sampling and laboratory analysis	-bottle data of $p\text{CO}_2$ (C_T/pH), $p\text{CH}_4$ ($c\text{CH}_4$), O ₂ , temperature, salinity, NO ₃ ⁻ , PO ₄ ³⁻
Additional information	<ul style="list-style-type: none"> -high-resolution water column measurements of temperature and salinity from 1 and 3 m above the sediment -auxiliary data of solar irradiance, wind speed and direction retrieved from the station <i>Rostock-Warnemünde</i> (DWD, WMO-ID 10170) -numerical model simulation of water column salinity and temperature distribution
Data analysis	-linear relationships based on correlation coefficients (Spearman)

2.3 The Drammendorf field survey

The content of the Sect. 2.3 was published in Pönisch et al., 2023. Nutrient release and flux dynamics of CO₂, CH₄, and N₂O in a coastal peatland driven by actively induced rewetting with brackish water from the Baltic Sea, Biogeosciences, 20 (2), 295–323, <https://doi.org/10.5194/bg-20-295-2023>. The following text was changed for linguistic and conceptual reasons to conform with the overall style of this dissertation.

The response of the GHG fluxes to flooding of the drained peatland with brackish water was assessed by determining the fluxes before (CO₂, CH₄) and after (CO₂, CH₄, N₂O) flooding. Because field conditions changed from dry/soil to flooded/water column, two different methods to determine GHG fluxes had to be used, with supporting variables (e.g., nutrients, O₂) were intensively sampled after flooding. To cover this system shift, four samplings schemes were applied: (1: before flooding) GHG flux measurements from dry soil sampled using chambers at a transect (Figure 1e, Figure 3b), (2: after flooding) GHG sampling from surface water and calculation of GHG fluxes at the transect, (3: after flooding), GHG sampling from surface water and calculation of GHG fluxes distributed throughout the flooded peatland (Figure 1d, Figure 3d, e), and (4: after flooding) surface water sampling for nutrients distributed throughout the flooded peatland. Strategies 1 – 4 are described in the following and summarized in Table 3.

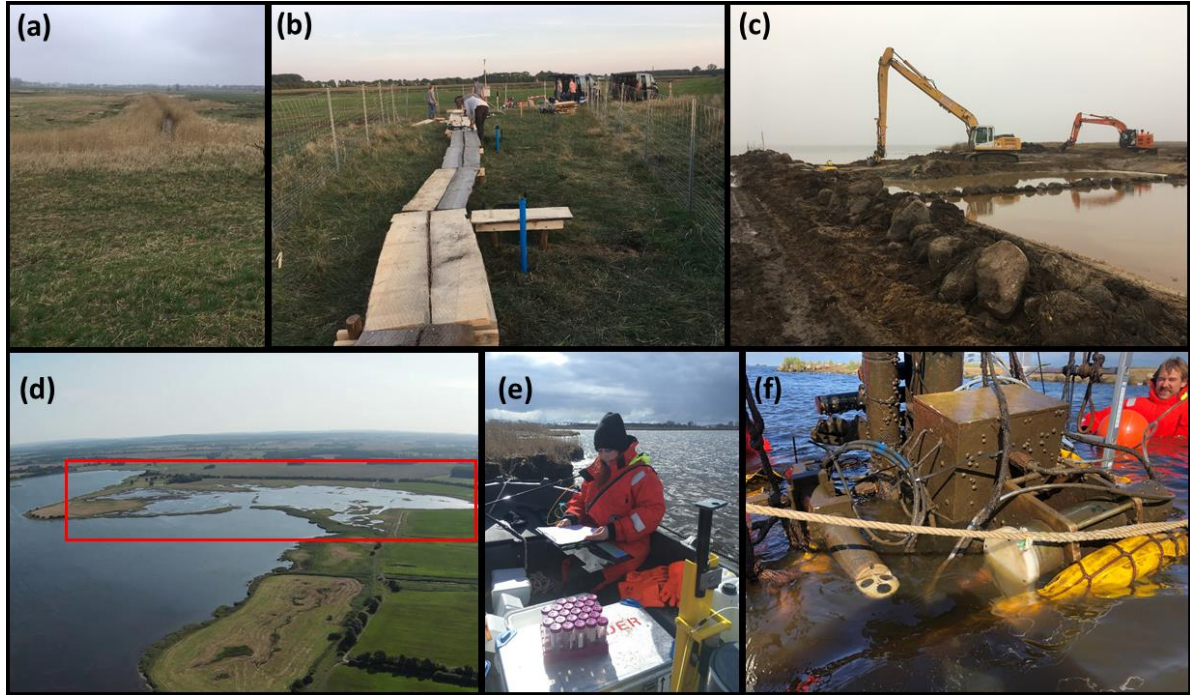


Figure 3: The photographs of Drammendorf illustrate the strong shift from (a) a drained *Polder* (March 2019) to a flooded area due to the active removal of a section of a dike. (b) Construction of the boardwalk before flooding and the site of the transect where the GHG samples were collected. Flooding due to excavation on 26 November 2019 is shown in (c), with the artificial connecting ditch in the foreground and the Baltic Sea (*Kubitzer Bodden*) in the background. (d) The result of flooding in the summer of 2021 is framed in red and the artificial connecting ditch (the removed part of the dike) is well visible in the center. (e) Field work and discrete sampling from a small boat (April 2020). (f) The lander before its recovery on the last day of the Drammendorf lander deployment (summer 2021).

The transect-covering GHG sampling before and after flooding (schemes 1 – 2)

GHG sampling was conducted along a transect consisting of eight stations, with two stations each representing a continuously water-filled ditch in a north-south direction before and after flooding (Figure 1e). Measurements began six months before flooding, with the stations representing a soil moisture gradient (Figure 3b). After flooding, measurements continued for twelve months (December 2019 to December 2020), with the stations then representing a soil elevation gradient that fell dry at low water levels or remained permanently inundated. Before flooding, chamber measurements (CO_2 , CH_4) were conducted twice monthly using opaque and transparent chambers at installed collars to cover (for CO_2) photosynthetic and respiration activity (Livingston and Hutchinson, 1995). After flooding, chamber measurements were made at the same stations using floating opaque chambers and were supplemented by the simultaneous sampling of surface water (CO_2 , CH_4 , N_2O). From the latter, the GHG concentrations were used to calculate the air-sea exchange (ASE), using a wind-based parameterization (Sect. 2.7). In Pönisch et al. (2023), in which the results of this field survey are published, one representative station (BTD7) after flooding was chosen for a statistical comparison between the two methods (i.e., chamber and wind-based parameterization). The

results showed that the two methods were statistically indistinguishable, thus allowing data pooling after rewetting and direct comparisons of GHG fluxes before and after rewetting.

The area-covering surface water sampling of the flooded peatland (schemes 3 – 4)

Discrete surface water sampling was carried out for twelve months from a small boat (Figure 3e) and covered the area of the flooded peatland, with the samples collected using a horizontally positioned 5-L Niskin bottle. Three stations in the inner bay (Figure 1d, purple) served as baselines, but they were unlikely to have been completely unaffected by water from the rewetted peatland. Seven stations in the flooded peatland were sampled as well (Figure 1d, black). The first sampling took place one week after rewetting and was continued at weekly (December 2019 to January 2020), biweekly (February 2020 to September 2020, except for August), and monthly (October 2020 to December 2020) intervals, resulting in a total of 25 observations.

In situ measurements of temperature, salinity, and dissolved O_2 in the surface water and, depending on the prevailing water depth, 15 cm above the soil surface (bottom water) were conducted using a HACH HQ40D multimeter (see Table 1 for details). Subsamples from the surface water were taken for analyses of C_T , A_T , pH, CH_4 , and N_2O (all 250 mL) and filled with sample overflow. Poisoning was carried out in the laboratory ~ 6 h after sampling. Nutrient subsamples (200 mL; NO_3^- , NO_2^- , NH_4^+ , PO_4^{3-}) were filtered in the field with combusted glass-fiber filters (0.7 μm , GF/F, Whatman®) and stored at $-20^\circ C$. Concentrations of chlorophyll *a* and dissolved organic carbon (DOC) were analyzed in collaboration with other laboratories. Details of the laboratory analyses are described in Section 2.5.

Table 3: Summary of the methodology used for the Drammendorf field survey.

Used method	Comments and survey outcomes
Discrete sampling and laboratory analysis	-discrete data of C_T , A_T , pH, cCH_4 , cN_2O , O_2 , temperature, salinity, NO_3^- , NO_2^- , NH_4^+ , PO_4^{3-} , chlorophyll <i>a</i> , DOC
Additional information	-Nutrient export calculation between the flooded peatland and the <i>Kubitzer Bodden</i> (Pönisch et al., 2023)
Data analysis	-Calculation of pCO_2 from C_T and A_T -GHG fluxes based on two methods for comparison of fluxes before (dry) and after (flooded) rewetting

2.4 The Drammendorf lander survey

The survey was conducted in the second summer after flooding, with the two landers deployed for a period of around nine weeks (02 June 2021 to 09 August 2021), during which time nine discrete sampling campaigns were combined simultaneously with lander/sensor maintenance. Lander 1 was deployed in the central part (station BT8 during the field survey) of the flooded peatland, at a water depth of ~ 0.6 m (Figure 1f). Despite the measured frequent changes in the water level height (Figure 15e), water velocities were assumed to be low and local processes were pronounced at this location. Lander 2 was installed in the middle of the excavated channel at a water depth of ~ 0.9 m and thus at the interface between the Baltic Sea and the peatland. This location enabled monitoring of the exchanging water masses. Due to the narrow channel and indications by previous investigations of the Drammendorf field study (Pönisch et al., 2023), high, intermittent water flow velocities were assumed.

2.4.1 Major lander adaptations and the field deployment

A prerequisite for this survey was the development of the necessary infrastructure and significant adjustments of the landers compared to the Hütelmoor lander survey. This included coordinating a professionally constructed land station to provide a reliable wired power supply to the landers. Modifications were also made to the landers to replace the less sustainable and expensive lithium primary cells with wired power (Figure 2d). This was done using 400 m and 800 m cables, which allowed for a longer (potentially unlimited) measurement time than was possible with battery power. A buffer battery was integrated to compensate for the consumption peaks of the sensors. The IOW-developed power supply unit “Octopus”, installed directly on the landers, also enabled powerline communication with SFTP and HTTP requests and thus on-air schedule adjustments and data excess. Data were transmitted via a VPN connection using a mobile network. The landers were deployed and maintained using a small boat, inflatable floats, and a lift system (Figure 2e).

2.4.2 Sensor configuration and data post-processing

The same sensors used for the Hütelmoor land survey were used to measure the variables $p\text{CO}_2$, $p\text{CH}_4$, temperature, salinity, hydrostatic pressure (depth), O_2 , turbidity, NO_3^- , PO_4^{3-} , and chlorophyll a in this survey (Sect. 2.2.2; Table 1). Comparable configurations and the same data post-processing techniques were also used. Adjustments and changes made for this survey are summarized in the following.

***pCO₂* measurements with HC-CO₂**

- Pre- and post-calibration were in the range of 200 – 6000 μatm
- Sensors were equipped with external 1.0 W pumps (SBE-5M)
- A mean response time (τ) of 329 s and 380 s was calculated for lander 1 and lander 2, respectively. These values were higher than the ~ 70 s normally stated for these sensors. Analysis of the pump power consumption during the deployment showed an occasional drop to minimum values of ~ 0.5 W (data not shown), resulting in a lower flow rate at the membrane and likely caused by sediment clogging of the filter basket and/or pump propeller. As a result, signal recovery to environmental conditions was delayed, and the selection criterion (standard deviation < 5 μatm in a series of 3 measurements) was not achieved at every zeroing interval. Hence, some of the in situ determinations of the response times had to be discarded.

***pCH₄* measurements with HC-CH₄**

- Sensors were equipped with external 7.5 W pumps (SBE-5T), which resulted in a τ of 2400 s (40 min).
- The *pCH₄* measurements were also affected by a temporarily decreased flow rate, which led to an increased τ . Based on laboratory tests, pump consumption (W) was converted to a water flow rate (L min^{-1}) and was simulated in an experiment with a SBE-5T pump between ~ 5 W (maximal pump capacity) and ~ 3 W (restricted pump capacity) due to artificial clogging of the filter basket. The decrease in the water flow rate from ~ 8 L min^{-1} to ~ 3 L min^{-1} followed a linear slope ($R^2 = 0.83$), and the lower limit of the water flow rate was equivalent to that of a SBE-5M pump under maximal pump capacity. Based on this observation and to correct the in situ *pCH₄* values, the response times for the HC-CH₄ were determined using the respective response times from the SBE-5T and SBE-5M pumps. The response time of the SBE-5M pump was higher by a factor of 1.7 (due to lower water flow across the membranes). Hence, the response time to correct for in situ *pCH₄* was linearly interpolated between the two limits (maximum pump power of ~ 6 W and 3 W) and extrapolated when measured pump power was below the threshold of 3 W. (N. Kinski, -4H- JENA Engineering GmbH, personal communication, 2022). Since biofouling could be neglected (regular maintenance and cleaning), the response time was not additionally affected. The interpolated/extrapolated response time ranged between 2400 s and 4800 s and was used to correct the signal delay. A rolling mean

(median) with a window width of 180 (50) measurements before (after) the calculation of the in situ $p\text{CH}_4$ value was applied to remove short-term noise. Measurement interruptions and artifacts from post-processing lasting longer than 180 measurements were removed from the continuous data.

CTD-O₂ measurements

- The resolution of data acquisition was 5 min for lander 1 and 10 min for lander 2.
- The O₂ coefficients from slope correction (i.e., to counteract oxygen optode drift) were 1.056 and 1.033 for lander 1 and lander 2, respectively. In some sections of the time series, O₂ and conductivity measurements had to be removed from the data because their time series showed a steep drop and a discrepancy with discrete samples. This was related to air bubbles entering the measurement circuit. Although measures were taken to avoid air bubbles during maintenance, the low pumping capacity of the CTD-O₂ was unable to maintain continuous, undisturbed air-free transport. Temperature and depth were unaffected, due to the exposed location of the probes on the sensors.

NO₃⁻ measurements with SUNA-NO₃⁻

- Post-processing, including discrete colored dissolved organic matter (CDOM) measurements (data not shown), showed that the sensor spectra were dominated by CDOM interferences, which was not unexpected in the flooded peatland. At present, there are no advanced methods to distinguish between CDOM interference and NO₃⁻ absorbance suitable for application in the Baltic Sea or a peatland area. As a result, the SUNA data were assumed to be unsuitable for the derivation of NO₃⁻ concentrations (H. Bittig, IOW, personal communication, 2023).

PO₄³⁻ measurements with HCycle-PO4

- Measurements with external battery supply and data logging
- Five-point laboratory calibration performed prior to deployment and linear correction of the field data ($R^2 = 0.9979$ and 0.9987 , respectively)

Chlorophyll *a* und turbidity measurements

- No adjustments

2.4.3 Discrete sampling

Discrete bottle samplings to validate most of the sensor-based measurements were conducted in the central peatland area (lander 1) and in the connecting channel (lander 2). This task was achieved by sampling bottom water close to the landers with as little disturbance as possible and with an exact timestamp. Water was taken manually from a small working boat using a horizontally positioned 5 L Niskin bottle. Subsamples were filled directly in the field by sample overflow. Subsamples for CH₄, pH, and C_T/A_T (each 250 mL) were taken, and poisoning was conducted in the laboratory ~ 6 h after sampling. Nutrient subsamples (NO₃⁻, PO₄³⁻; 200 mL) were filtered in the field with combusted glass-fiber filters (0.7 µm, GF/F, Whatman®) and stored at - 20 °C. Details of the laboratory analysis are provided in Sect. 2.5. Water temperature and salinity were measured using a HACH HQ40D multimeter (for details, see Table 1).

2.4.4 Supplementary information and data handling

The relationships between the measured variables were analyzed by calculating Spearman correlation coefficients (r_s), as described in Sect. 2.2.5, to obtain a first-order overview of the linear relationship.

The air-sea exchange was calculated (Sect. 2.7) based on the fully available data from both landers and taking into account different scenarios. The latter was carried out mainly to consider the effect of the heterogeneous peatland environment on the derivation of the ASE. The results are presented in Table 8:

- (1) ASE derived from fully available high-resolution time series from the Drammendorf lander survey
- (2) ASE using only the bottle data from the Drammendorf lander survey
- (3) ASE derived from high-resolution time series from the Drammendorf lander survey by isolating a daily average for ± 1 h from 00:00 and 12:00 UTC, respectively, thus representing the day-night-bias (resulted in ~ 200 data points for each calculation).
- (4) ASE derived from the Drammendorf field survey (Pönisch et al., 2023), determined for the period of the Drammendorf lander survey but one year earlier.
- (5) ASE derived from high-resolution time series from the Drammendorf lander survey by isolating a daily average between 09:00 and 15:00 UTC. This time period represents the

period of bottle data sampling in the Drammendorf field survey (Pönisch et al., 2023) and allowing a direct comparison of the ASE evaluation described under (4)

Table 4: Summary of the methodology used for the Drammendorf lander survey.

Used method	Comments and survey outcomes
Lander deployment	-landers under major adjustment in terms of power supply and communication/accessibility -Measurements at high-resolution of $p\text{CO}_2$, $p\text{CH}_4$, O_2 , temperature, salinity, water pressure, turbidity, and chlorophyll a concentration - NO_3^- and PO_4^{3-} are restricted in data availability
Discrete sampling and laboratory analysis	-bottle data of $p\text{CO}_2$ ($\text{C}_\text{T}/\text{pH}$), $p\text{CH}_4$ (cCH_4), O_2 , temperature, salinity, NO_3^- , PO_4^{3-}
Additional information	-auxiliary data of wind speed and direction retrieved from <i>Putbus</i> (DWD, WMO-ID 10093) and solar irradiance from <i>Rostock-Warnemünde</i> (DWD, WMO-ID 10170)
Data analysis	-linear relationships due to correlation coefficients (Spearman) -ASE calculation from high-resolution data and various scenarios -diurnal cycles

2.5 Laboratory analysis of discrete samples

2.5.1 Analysis of the inorganic carbon system (C_T , A_T , pH)

Samples were poisoned in the laboratory with 200 μl of saturated mercury(II) chloride (HgCl_2) solution and stored in the dark at 4 °C.

Total CO_2 (C_T) was measured using an automated infrared inorganic carbon analyzer (AIRICA, MARIANDA, Kiel, Germany). The analysis is based on the stripping of CO_2 from the sample with the carrier gas N_2 (99.999 %) after acidification with 10 % phosphoric acid. The gas is dried using a Peltier cooler and a Nafion[®] drying tube (Perma Pure Nafion[®], Ansyco GmbH, Karlsruhe, Germany). The released CO_2 is detected by an LI-COR-7000 infrared detector (LI-COR Environmental GmbH, Bad Homburg, Germany). Triplicate sample measurements and a comparison with certified reference material (CRM; Scripps Institution of Oceanography, University of California, San Diego, USA; Dickson et al., 2003), allowed calculation of the C_T with a precision of $\pm 5 \mu\text{mol kg}^{-1}$.

Total alkalinity (A_T) was analyzed by open cell titration (glass electrode type LL Electrode plus 6.0262.100, Metrohm, Filderstadt, Germany) as described in Dickson et al. (2007) and involved a two-step titration. After the initial addition of hydrochloric acid to achieve a pH of 4 – 3.5, A_T was determined during a stepwise titration to a pH of 3, with the pH recorded potentiometrically. Calibration was performed with the same CRM used for C_T and resulted in the same precision ($\pm 5 \mu\text{mol kg}^{-1}$).

The pH (total scale) was spectrophotometrically measured as described in Dickson et al. (2007) and Carter et al. (2013) and using the pH-sensitive indicator dye m-cresol purple

(2 mmol L⁻¹; -4H-Jena Engineering GmbH, Jena, Germany). Absorption was measured using an Agilent 8453 UV-visible spectroscopy system (Agilent Technology, Waldbronn, Germany). The pH parameterization for brackish waters after Müller and Rehder (2018) was used to calculate the pH value. A brackish buffer solution (salinity of 20) was prepared according to Müller et al. (2018), and an external buffer solution with a salinity of 35 (Scripps Institution of Oceanography, University of California, San Diego, USA) served as quality control.

2.5.2 Dissolved CH₄ and N₂O concentration analysis

Samples were poisoned in the laboratory with 500 µl of saturated HgCl₂ solution and stored in the dark at 4 °C.

Dissolved CH₄ and N₂O concentrations were measured using an Agilent 7890B gas chromatograph (Agilent Technologies, Santa Clara, USA) coupled with a flame ionization detector (FID) and an electron capture detector (ECD). The analytical method was based on the purge-and-trap technique described in Sabbaghzadeh et al. (2021) and Pönisch et al. (2023). In brief, a purified helium gas stream purges the target molecules from a seawater sample. Subsequently, the gas stream is dried by passing a Nafion[®] tube (Perma Pure Nafion[®], Ansyco GmbH, Karlsruhe, Germany) and a SICAPENT[®] tube (Merck KGaA, Darmstadt, Germany). The relevant compounds are enriched by cryofocusing at – 120 °C on a trap filled with HayeSep D[®] (CS Chromatographie Service GmbH, Langerwehe, Germany) and desorbed after ten minutes by heating. Subsequently, CH₄ and N₂O are separated via two capillary columns and a Deans switch (Pönisch, 2018). The quality is controlled by daily measurement of a calibration gas (9.9379 ± 0.0159 ppm CH₄ and 1982.07 ± 3.77 ppb N₂O) before and after the measurements.

2.5.3 Analysis of nutrient concentrations (NO₃⁻, NO₂⁻, NH₄⁺ PO₄³⁻)

Nutrient concentrations were analyzed according to the standard photometric methods described in Grasshoff et al. (2009). The measurements were performed using a continuous segmented flow analyzer (SEAL Analytical QuAAtro, SEAL Analytical GmbH, Norderstedt, Germany). The detection limits were 0.2 µmol L⁻¹ for NO₃⁻, 0.05 µmol L⁻¹ for NO₂⁻, 0.5 µmol L⁻¹ for NH₄⁺, and 0.1 µmol L⁻¹ for PO₄³⁻.

2.5.4 Analysis of dissolved O₂

Dissolved O₂ was determined according to the potentiometric titration method of Winkler (1888), with various improvements (e.g., Carpenter, 1965), using a Metrohm 916 Ti-Touch (Metrohm AG, Herisau, Switzerland). Chemical fixation was performed directly in the field, and measurements were made within 8 h after sampling, achieving a precision of ± 0.25 %. This analysis was conducted only during the Hütelmoor lander survey.

2.6 Calculated variables and auxiliary data

The partial pressure of CO₂ ($p\text{CO}_2$) in the water phase was calculated from bottle data using C_T and pH. This calculation was performed in addition to the sensor measurements and served to verify the sensor data or to derive the air-sea exchange depending on the respective survey. The calculation was performed using R (R Core Team, 2022) and the package seacarb (Gattuso et al., 2019), with K_1 and K_2 from (Millero, 2010), K_s from (Dickson, 1990), and K_f from (Dickson and Riley, 1979).

Auxiliary data, such as wind speed for the calculation of ASE (Sect. 2.7) as well as solar radiation and precipitation for biogeochemical interpretation, were retrieved from the open data portal of the *Deutscher Wetterdienst* (DWD). The wind data and solar irradiance used for the Hütelmoor lander survey were retrieved from the station *Rostock-Warnemünde* (WMO ID 10170), and the wind and precipitation data used for the Drammendorf investigations from the station *Putbus* (WMO ID 10093). Solar irradiance data were also retrieved from *Rostock-Warnemünde*.

2.7 Atmospheric flux calculation based on air-sea exchange parameterization

Gas exchange between the atmosphere and seawater was calculated for both of the Drammendorf surveys. The ASE direction represents the uptake of GHGs from the atmosphere (negative sign convention) or their release into the atmosphere and is controlled by the differences in partial pressure between the two compartments. The exchange depends on the state of the sea surface, typically estimated based on wind speed. In the Drammendorf field survey, the ASE calculations were based on the partial pressures of the gases (CO₂, CH₄, N₂O), derived from the quantities C_T/pH , $c\text{CH}_4$, and $c\text{N}_2\text{O}$ (Sect. 2.7.1) as measured ~ 0.2 m

below the water surface. In the Drammendorf lander survey, the partial pressures (CO₂, CH₄) were measured ~ 0.6 – 0.9 m below the water surface by sensors (Sect. 2.7.2).

Due to the lack of an appropriate parameterization for small enclosed areas such as Drammendorf, the general approach developed for the open ocean by Wanninkhof (2014) was used in both studies. Although this approach may be of reduced applicability, a direct comparison of the determined fluxes with those directly measured using floating chambers showed high agreement during the Drammendorf field study, as reported in Pönisch et al. (2023). This agreement between the two approaches supported the decision to use the ASE calculation based on Wanninkhof (2014).

2.7.1 Air-sea exchange calculation for the Drammendorf field survey

The content of the Sect. 2.7.1 was published in Pönisch et al., 2023. Nutrient release and flux dynamics of CO₂, CH₄, and N₂O in a coastal peatland driven by actively induced rewetting with brackish water from the Baltic Sea, Biogeosciences, 20 (2), 295–323, <https://doi.org/10.5194/bg-20-295-2023>. The following text was changed for linguistic and conceptual reasons to conform with the overall style of this dissertation.

The air-sea gas exchange (F , g m⁻² h⁻¹) is a function of the gas transfer velocity (k) and the concentration difference between the bulk liquid (c_w) and the top of the liquid boundary layer adjacent to the atmosphere (c_a). It was calculated using the equation for the general boundary layer flux (Eq. 2.1) described by Wanninkhof (2014):

$$F = k * (c_w - c_a) \quad 2.1$$

where k describes the efficiency of the transfer process and is parameterized as a function of the wind speed $\langle U^2 \rangle$, an empirical relationship between the gas transfer coefficient (0.251) and the Schmidt number (Sc), as expressed by Eq. 2.2:

$$k = 0.251 \langle U^2 \rangle (Sc/666)^{-0.5} \quad 2.2$$

The Schmidt number was approximated by a linear interpolation between the freshwater and seawater values. Atmospheric-equilibrium concentrations (c_a) were calculated using the atmospheric data for CO₂ and CH₄ obtained from the ICOS station “Utö” (Finnish Meteorological Institute, Helsinki). Due to seasonal changes in the atmospheric dry molar fraction of CO₂ and CH₄, mean values for each season were computed. For N₂O, the atmospheric dry mole fraction from station Mace Head was selected (National University of Ireland, Galway; data from the NOAA Global Monitoring Laboratory (GML) Carbon Cycle Cooperative Global Air Sampling Network; Dlugokencky et al., 2019a, 2019b). A mean value

of the atmospheric N_2O concentration during the investigation period was calculated, due to its minor seasonality. Equilibrium concentrations were then calculated using the solubility coefficient (K_0) from Weiss and Price (1980). Wind speeds were retrieved from the nearby monitoring station *Putbus* (~ 15 km away) and measured at 15 m height (DWD; WMO-ID 10093). The wind speed was averaged over a time interval of ± 3 h from midday, since sampling was usually performed during this period.

2.7.2 Air-sea exchange calculation for the Drammendorf lander survey

The ASE was calculated as described above, but data handling was slightly different because sensor-derived measurements of $p\text{CO}_2$ and $p\text{CH}_4$ with high temporal resolution were used: All involved variables (i.e., GHGs, wind speed, temperature, salinity, atmospheric GHG equilibrium conditions) were averaged for one hour to obtain robust values and matching timestamps. Since salinity was not continuously available at both landers, the values from the two landers were combined by interleaving those from lander 1 with those from lander 2. This combination was justified because the two lander locations were connected by strong water exchange, resulting in very similar salinity conditions that were also detected in the Drammendorf field survey (Pönisch et al., 2023).

3. Results

3.1 The Hütelmoor lander survey

In the summer/autumn of 2019, autonomous, temporally high-resolution measurements of physicochemical variables were carried out at the sediment-water interface of the Baltic Sea at two locations and at a water depth of ~ 6 m. The measurements addressed the insufficiently described temporal and spatial variability of GHG distributions in coastal areas. An additional goal was to identify the biogeochemical controls of the expected pronounced variability. For this purpose, stationary high-resolution measurements were supported by: (i) water column measurements of temperature and O_2 , (ii) atmospheric data, (iii) water velocity measurements, and (iv) numerical model simulations. This approach revealed three system changes that occurred following an event-driven change of conditions in the water column (tipping point).

3.1.1 Characterization of meteorological and hydrographic conditions during the lander survey

On average, wind speeds were low to moderate, with values of 5.5 m s^{-1} , but they showed strong fluctuations during the deployment period of the landers. For example, wind speeds during a 4-day storm (15 – 19 September 2019) were up to 19 m s^{-1} , mainly from crossshore winds (Figure 4l). At the end of the deployment, there was a prolonged period of low wind speeds with velocities $< 5 \text{ m s}^{-1}$. Wind speeds during the deployment showed a strong positive correlation with turbidity ($r_s = 0.60$) and a relationship with the chlorophyll *a* concentration ($r_s = 0.29$; Figure 7). Solar irradiance, as an essential factor for diurnal cycles of primary production, had no influence on the bottom pCO_2 level (Figure 7).

Alongshore flow velocities in the water column were predominantly northeasterly in their direction, with maximum values of $\sim 0.35 \text{ m s}^{-1}$ (Figure 4k; negative values indicate flow velocities in the southwesterly direction). The highest values in the northeasterly direction were recorded at the beginning of the deployment, during a period of moderate wind speeds. In the second half of the time series (from 22 September 2019), alongshore water velocities decreased and were accompanied by low wind speeds.

The water column was predominantly well mixed during the deployment, indicated by (i) non-significant differences in the high-resolution measurements of water temperature and O_2 within the water column at 1 and 3 m above the sediment (Figure 5) and (ii) a numerical model analysis of the salinity distribution (Figure 6, top). However, two distinct periods of

short-term differences in temperature, O₂ (both Figure 5), and salinity (Figure 6, top) between the bottom and overlying water masses were identified. These periods, around 09 September 2019 and 25 – 29 September 2019, indicated a stratification and delineated the events FINN-I and FINN-III, described in Sect. 3.1.3.

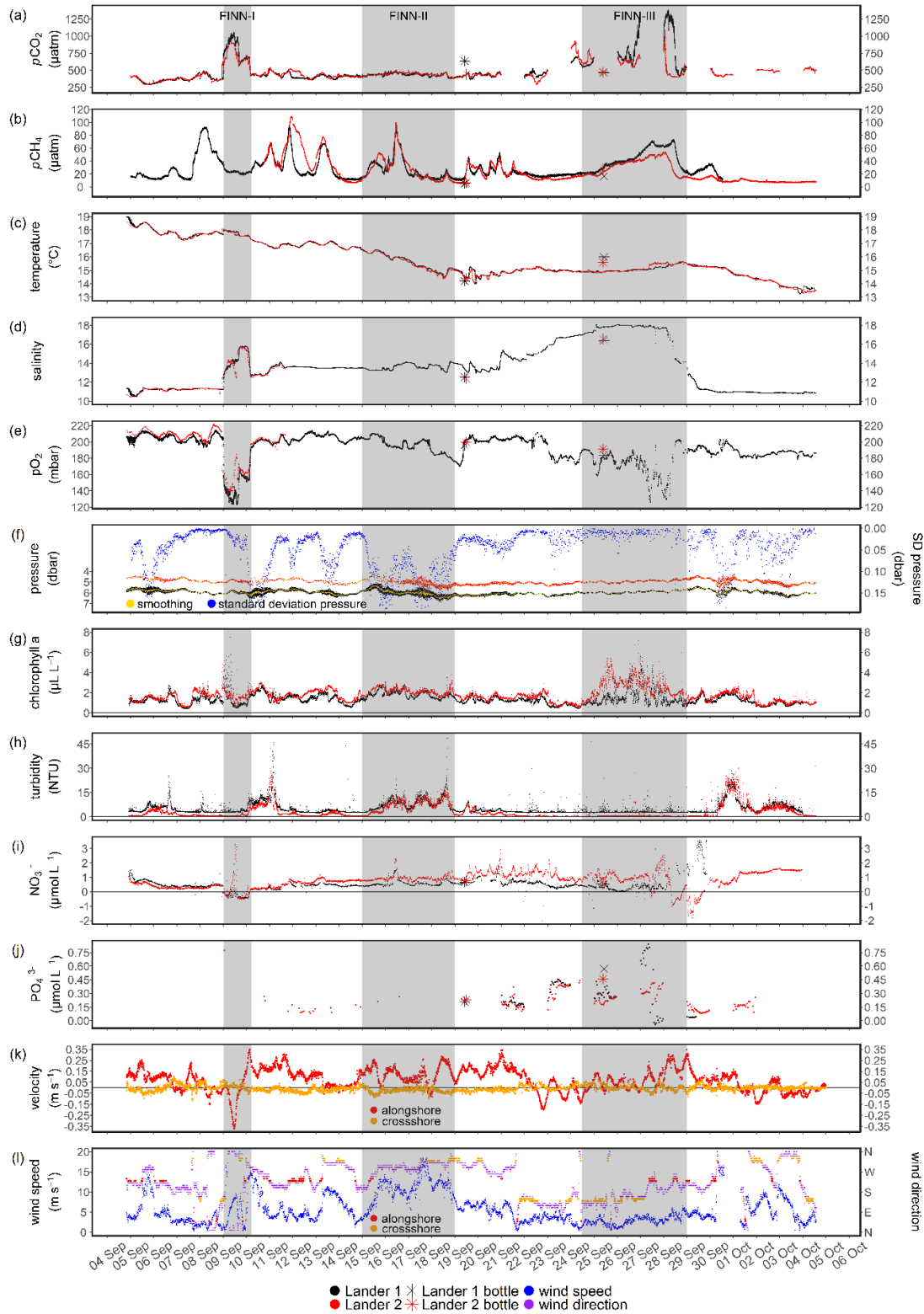


Figure 4: High resolution time series of lander 1 (black) and lander 2 (red) together with wind data. Results from discrete bottle data are indicated by asterisks, together with the color of the respective lander. (a – k) Post-processed data of (a) $p\text{CO}_2$ (μatm), (b) $p\text{CH}_4$ (μatm), (c) water temperature ($^{\circ}\text{C}$), (d) salinity, (e) $p\text{O}_2$ (mbar), (f) depth and smoothed depth (hydrostatic pressure; dbar) together with the standard deviation (SD) of the pressure (right axis; dbar), (g) chlorophyll *a* concentration ($\mu\text{L L}^{-1}$), (h) turbidity (NTU), (i) NO_3^- concentration ($\mu\text{mol L}^{-1}$), (j) PO_4^{3-} concentration ($\mu\text{mol L}^{-1}$), (k) water velocity (m s^{-1}), (l) wind speed (m s^{-1}) and wind direction (right axis; degrees). In k and l, the crossshore direction is shown in gold and the alongshore direction in red. The three gray rectangles highlight the events referred to as FINN-I – FINN-III.

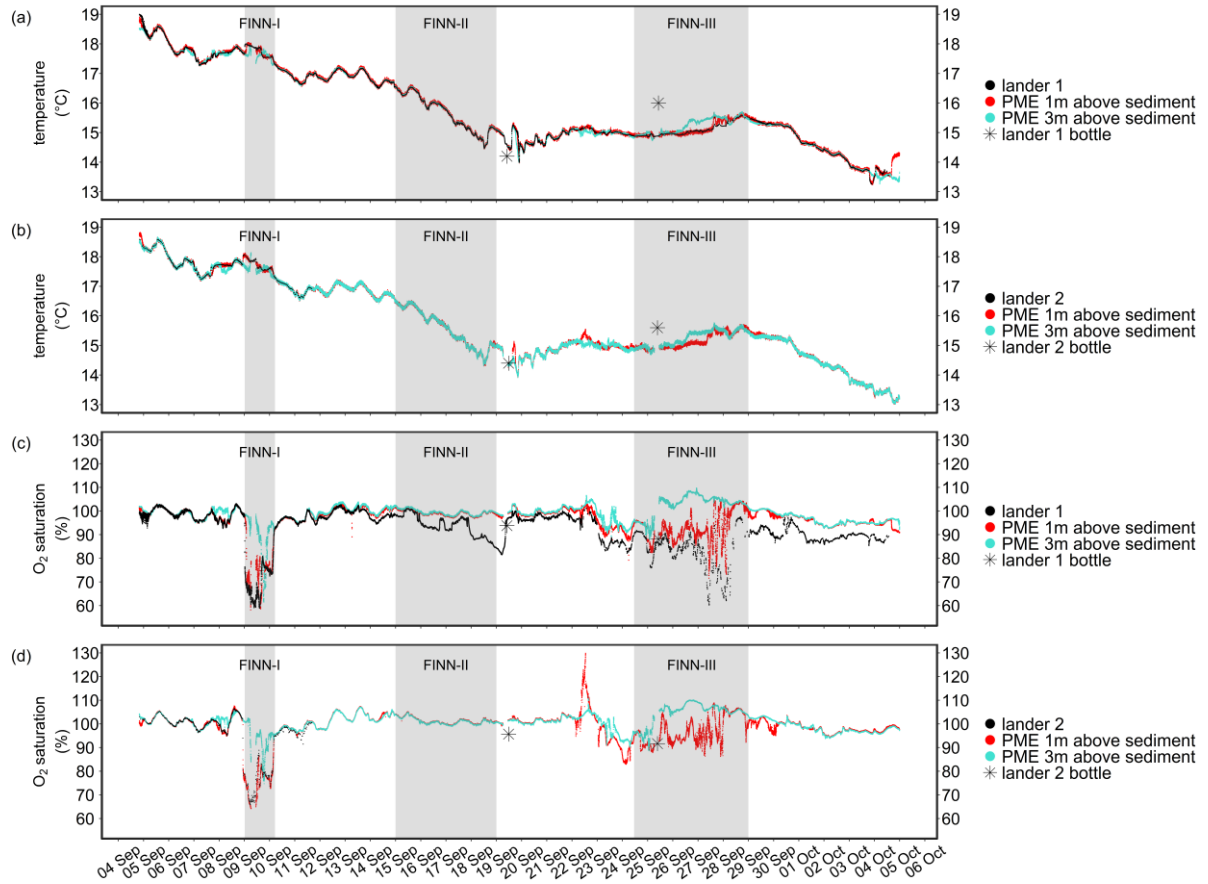


Figure 5: Time series of temperature and saturation of O₂ at both landers measured continuously in high-resolution 1 and 3 m above the sediment by PME miniDOT instruments (in red and turquoise, respectively) compared to the time series of the temperature and O₂ measured at the lander. The inlet of the latter (i.e., CTD-O₂ measurements of the lander) were ~ 0.70 cm above the sediment, and hence the lowest point of measurements in the water column.

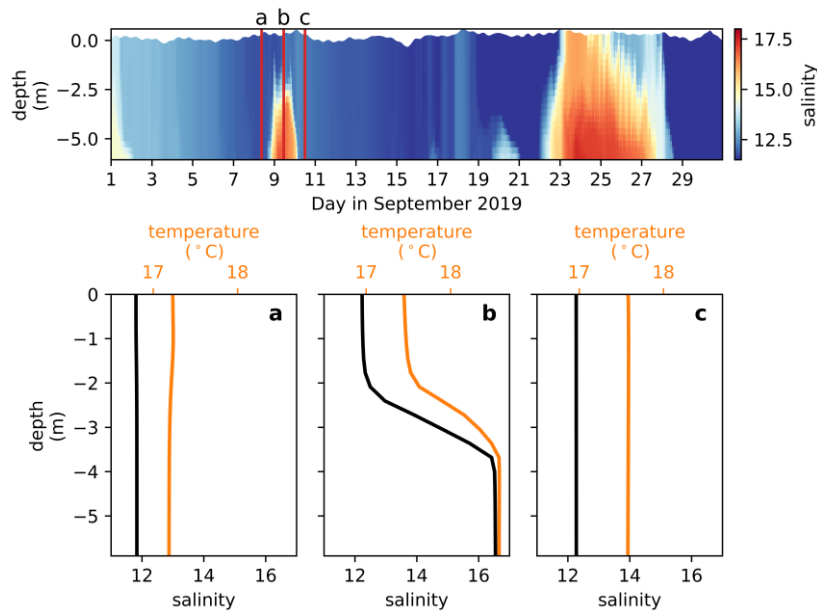


Figure 6: Development of salinity in the water column as derived from numerical model simulations (top). (a – c) Snapshots of (a) shortly before, (b) during, and (c) after the event FINN-I.

3.1.2 Time records of biochemical variables at both landers

Data on the $p\text{CO}_2$ collected by the two landers were almost indistinguishable, with the exception of small variations of the signal and differences during rapid changes (peaks) that resulted in slightly higher mean values and a higher variability at lander 1 (Table 5). Nevertheless, pronounced peaks in $p\text{CO}_2$ were reached rapidly at both landers. For example, $p\text{CO}_2$ measured at lander 1 on 09 September 2019 increased from 350 μatm to 1050 μatm within 12 h, returning to the initial value of ~ 420 μatm after ~ 30 h (Figure 4a). A much faster decline occurred at the end of the deployment (28 September 2019) at lander 1, when the $p\text{CO}_2$ dropped from ~ 1248 μatm to 419 μatm within 6.5 h. The mean diurnal variabilities of $p\text{CO}_2$ and $p\text{CH}_4$ over the entire deployment were calculated by dividing the high-resolution data into 24-h intervals, each starting at midnight. Then, for each interval, the difference between the minimum and maximum was determined. Subsequent calculations of the mean, minimum and maximum yielded an approximation of the diurnal variability. The average daily variability of $p\text{CO}_2$ at lander 1 was 228 μatm , ranging from 43 to 972 μatm . $p\text{CO}_2$ correlated positively (with a large effect size) with salinity ($r_s = 0.60$), and negatively with $p\text{O}_2$ ($r_s = -0.71$, large effect size) and temperature ($r_s = -0.42$, medium effect size; Figure 7).

The pattern for $p\text{CH}_4$ resembled that of $p\text{CO}_2$, such that at both landers a similar mean $p\text{CH}_4$ was measured (Table 5), with differences occurring only during peaks. Nevertheless, the variations in $p\text{CH}_4$ measured at lander 2 were slightly larger, mainly due to higher values during peaks (Figure 4b). The measurements revealed large, rapid variations within a short period at lander 1 and lander 2, for example: $\sim 60 - 80$ μatm within 12 – 17 h and 70 – 90 μatm within 21 – 27 h, respectively. The calculated average daily variability at lander 1 during the deployment was 30 μatm , ranging from 6 to 74 μatm . Furthermore, a positive correlation with a medium effect size was found between $p\text{CH}_4$ and $p\text{CO}_2$ ($r_s = 0.43$) and $p\text{CH}_4$ and the chlorophyll *a* concentration ($r_s = 0.37$), and a weak negative correlation of $p\text{CH}_4$ with water pressure ($r_s = -0.25$; Figure 7). For both, $p\text{CO}_2$ and $p\text{CH}_4$, the sensor data were in line with discrete bottle data (Figure 4a, b; asterisks).

A comparison of the chlorophyll *a* concentrations and turbidity values between the two landers showed slight differences, with lower chlorophyll *a* and higher turbidity values at lander 1 (Table 5). High chlorophyll *a* concentrations occurred during periods of increased salinity and low wind speeds, but the correlations with salinity and wind speed were weak

($r_s = -0.1$ and $r_s = 0.29$; Figure 7). In turn, turbidity showed a strong dependence on wind speed, as it was high at high wind speeds. This finding was supported by the positive correlations with a large effect size between turbidity and both wind speed ($r_s = 0.6$) and the standard deviation of the water pressure ($r_s = 0.78$). The latter serves as an indicator of wave height and was calculated from the high-resolution pressure data.

Sensor measurements of NO_3^- are challenging in coastal zones because optical measurements are affected by other absorbing species. Therefore, the signal from the instruments must be adjusted to the offset to the discrete samples and this is the reason for negative values (Figure 4i). In addition, variability in NO_3^- time series may be due to the nitrogen species themselves or to interferences, like CDOM.

The amount of PO_4^{3-} determinations was low and irregularly distributed because the instruments experienced a power cycle (i.e., power on/off) due to a hardware malfunction, which complicated direct comparisons between the two landers. Nevertheless, the sensor data agreed with the bottle data and showed an increasing trend during the calm conditions in the water column at the end of the deployment (Figure 4j).

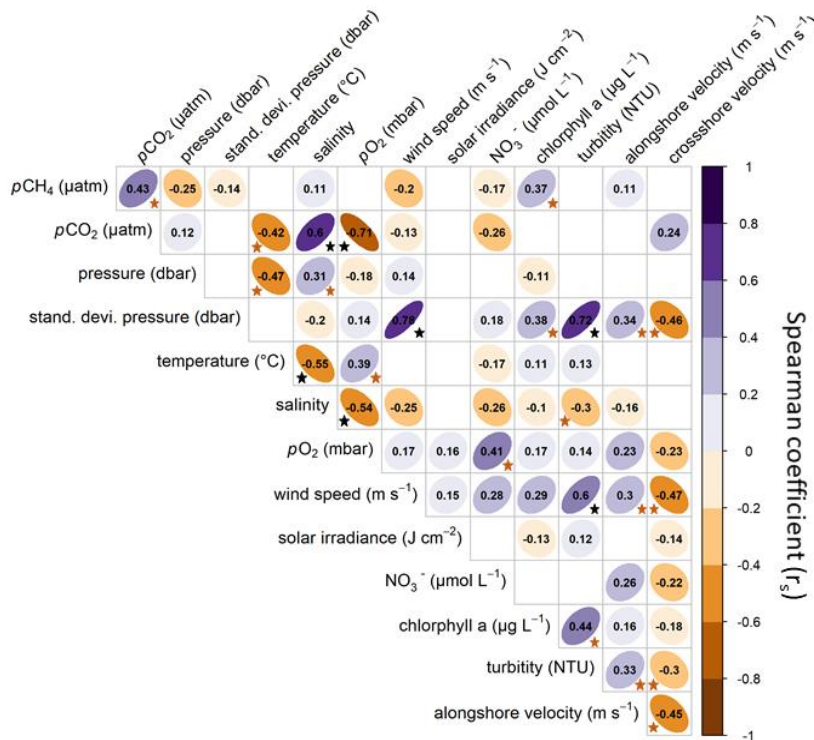


Figure 7: Spearman correlation coefficients (r_s) between the measured variables at lander 1 and auxiliary data (i.e., wind speed, wind direction and solar irradiance) for the entire deployment. A significance level of 0.001 was applied to remove non-correlating relationships (empty fields). Cohen's convention was used to interpret the effect size (Cohen, 1988). Black stars represent a large effect size and hence a strong correlation, and brown stars represent a medium effect size.

Table 5: Summary of the mean, standard deviation, minimum and maximum of the measured variables determined by lander 1 and lander 2. The concentration of CH₄ (nmol L⁻¹) was calculated from *p*CH₄ (μatm). Some data at lander 2 are not considered because they had to be removed after quality assessment.

		Lander 1	Lander 2
<i>p</i> CO ₂ (μatm)	mean ± SD	486 ± 181	465 ± 111
	minimum – maximum	293 – 1383	289 – 1091
<i>p</i> CH ₄ (μatm)	mean ± SD	30 ± 18	25 ± 19
	minimum – maximum	9.4 – 96	5.3 – 109
cCH ₄ (nmol L ⁻¹)	mean ± SD	45 ± 27	N/A
	minimum – maximum	17 – 143	N/A
Temperature (°C)	mean ± SD	16.4 ± 1.3	15.2 ± 1.1
	minimum – maximum	13.3 – 19.0	13.3 – 18.6
Pressure (mbar)	mean ± SD	6.0 ± 0.2	5.0 ± 0.2
	minimum – maximum	5.1 – 6.9	4.2 ± 5.9
Salinity	mean ± SD	13 ± 1.5	N/A
	minimum – maximum	10 – 18	N/A
<i>p</i> O ₂ (mbar)	mean ± SD	196 ± 16	N/A
	minimum – maximum	123 – 214	N/A
Chlorophyll <i>a</i> (μl L ⁻¹)	mean ± SD	1.4 ± 0.6	1.8 ± 0.7
	minimum – maximum	0.4 – 7.5	0.5 – 7.1
Turbidity (NTU)	mean ± SD	5.1 ± 3.9	3.1 ± 4.3
	minimum – maximum	1.9 – 55	0.2 – 47
NO ₃ ⁻ (μmol L ⁻¹)	mean ± SD	0.5 ± 0.5	0.8 ± 0.6
	minimum – maximum	- 0.5 – 3.6	- 2 – 3.5
PO ₄ ³⁻ (μmol L ⁻¹)	mean ± SD	0.3 ± 0.2	0.2 ± 0.1
	minimum – maximum	> 0.0 – 0.8	> 0.0 – 0.7

SD stands for standard deviation; N/A for not available

3.1.3 Identification of three event-based system changes

A detailed analysis of the meteorological and hydrographic conditions during the deployment revealed three events, identified by the conspicuous changes in CTD-O₂ measurements and wind conditions and by the numerical model. These events are referred to as FINN-I – III and are described in the following. Spearman correlation coefficients (*r_s*) were calculated for each event under the conditions described in Sect. 2.2.5.

3.1.3.1 Advection of saline waters with a strong mineralization signal – FINN-I

The FINN-I event lasted ~ 30 h (09 – 10 September 2019) and consisted of a rapid advection of saline waters from an external source, resulting in an increase in bottom salinity by ~ 5, measured at both landers. The increased salinity was accompanied by a steep decrease in O₂ such that saturations of ~ 60 % was quickly reached (Figure 4d, e). The advection event occurred only below a water depth of ~ 2 – 3 m, such that the water temperature and O₂ measured at 3 m above the sediment showed a clear difference from measurements at 1 m above the sediment (Figure 5). This temporary stratification was also visible in the distribution of salinity in the water column, simulated by the numerical model (Figure 6, top). The stratification was also evidenced in snapshots from the numerical model simulations of the conditions before, within, and after the event (Figure 6a – c). It can thus be concluded that the

advection of the water mass triggered a temporally restricted stratification of the water column. In addition, the alongshore water velocity, as a measured variable, was characterized by a quick reversal of the flow direction, with the highest water velocities in both alongshore directions reaching $\pm 0.35 \text{ m s}^{-1}$. Since wind speeds were moderate during the event, the fast water velocities and their reversal were not primarily caused by local wind speeds. Instead, a water mass nearby from the northwest accounted for the observed water velocity, $p\text{O}_2$, and salinity dynamics and was identified by the high-temporal three-dimensional model simulation of the water flow. The water mass originated from $\sim 20 \text{ m}$ water depth and had a higher density (salinity of ~ 20), and abruptly transported a $p\text{CO}_2$ signal of up to $1000 \mu\text{atm}$ (Figure 4a). By contrast, the $p\text{CH}_4$ showed only negligible changes. Due to the sharp occurrence of the event and the significant changes in the conditions of the water column, several correlations with a strong effect size were identified in the correlation analysis (Figure 8).

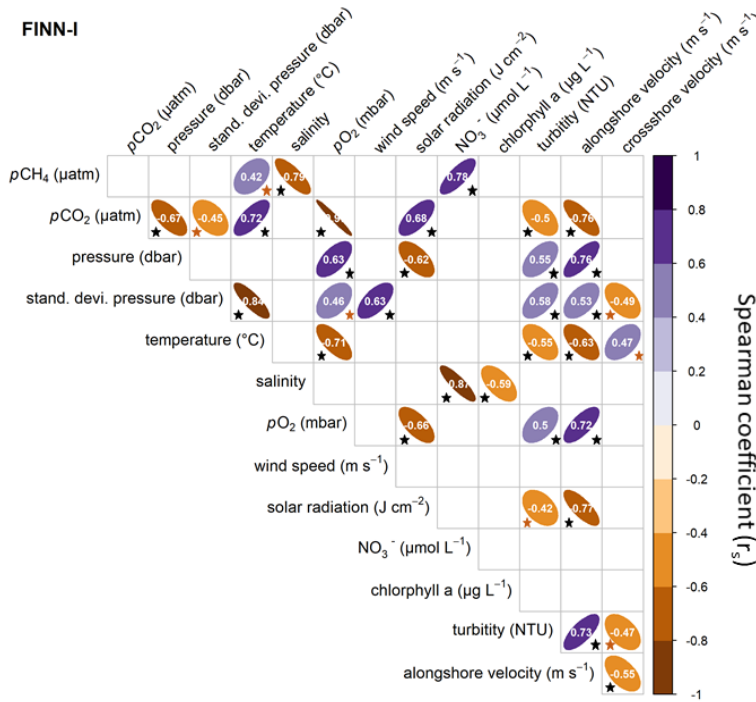


Figure 8: Spearman correlation coefficients (r_s) between the measured variables at lander 1 and auxiliary data for the period corresponding to FINN-I. A significance level of 0.001 was applied to remove non-correlating relationships (empty fields). Cohen's convention was used to interpret the effect size (Cohen, 1988). Black stars represent a large effect size and hence a strong correlation, and brown stars represent a medium effect size.

3.1.3.2 A storm event – FINN-II

A prolonged storm event between 15 and 19 September 2019 formed the boundary of event FINN-II. Maximum wind speeds of up to 19 m s^{-1} and high alongshore water velocities during the storm resulted in a well-mixing water column (Figure 6, top). The high wind speeds

also caused strong fluctuations in the hydrostatic pressure, as measured by the CTD-O₂ instrument, as well as a persistently high calculated standard deviation of the water pressure (Figure 4f). The analysis of absolute differences in the measured pressure showed a maximum wave height of ~ 80 cm. By contrast, the responses of temperature, salinity, and $p\text{CO}_2$, were minor. Although $p\text{CH}_4$ was variable and showed a distinct peak, no clear pattern in response to the storm could be detected. Nevertheless, turbidity increased in response to wind speed and fluctuations in the water pressure. This positive correlation was evidenced by the correlation analysis, both for the single event (Figure 9) and for the entire time series. There, positive correlations of turbidity with wind speed ($r_s = 0.6$) and the standard deviation of the water pressure ($r_s = 0.72$) were found (Figure 7).

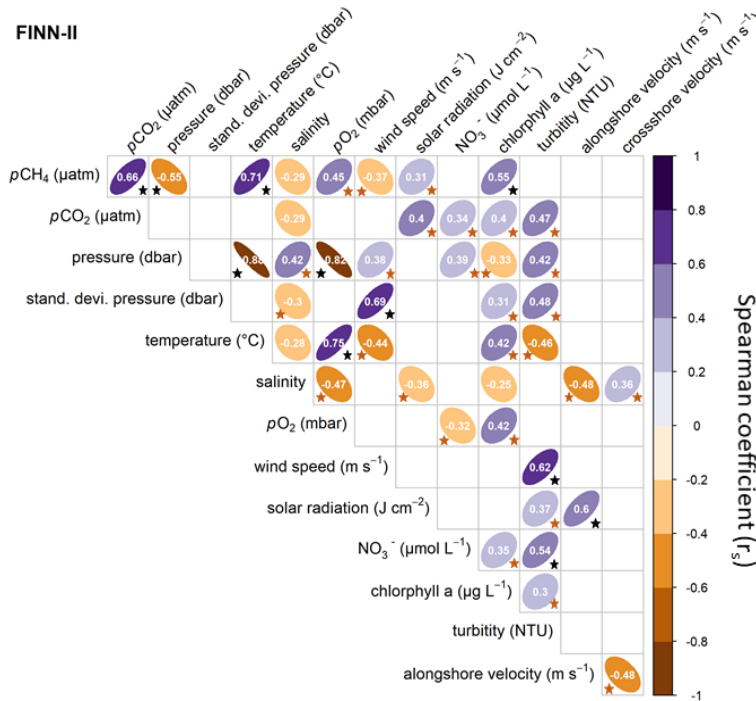


Figure 9: Spearman correlation coefficients (r_s) between the measured variables at lander 1 and auxiliary data, for the period corresponding to FINN-II. A significance level of 0.001 was applied to remove non-correlating relationships (empty fields). Cohen's convention was used to interpret the effect size (Cohen, 1988). Black stars represent a large effect size and hence a strong correlation, and brown stars a medium effect size.

3.1.3.3 A stagnation event – FINN-III

The third event occurred at the end of a 4- to 5-day period of prolonged low wind speeds of $< 5 \text{ m s}^{-1}$ when salinity reached a plateau following an increase (Figure 4d). Water column measurements of temperature and O₂ showed differences between 1 and 3 m above the sediment (Figure 5). Specifically, the temperature was ~ 0.4 °C colder and the O₂ saturation $\sim 20 - 30$ % lower at 1 m than at 3 m above the sediment. These observations were consistent with the CTD-O₂ time series at lander 1, which showed a slow decrease in O₂ during FINN-

III (Figure 4e). Consequently, stagnant conditions and decoupling between bottom and surface waters prevailed in the water column. This was confirmed by the numerical model, in which the salinity was higher at the bottom than at the water surface (Figure 6, top). The partial pressures of the GHGs increased during the stagnation period, with pronounced differences between the two landers with respect to $p\text{CO}_2$ and $p\text{CH}_4$. Thus, while $p\text{CO}_2$ showed a rather steep increase, the increase in $p\text{CH}_4$ was slower and more linear compared to the other peaks during the deployment. Since the signal from $p\text{CO}_2$ was interrupted, only the difference in $p\text{CH}_4$ between the two landers at the end of the deployment could be determined and was 10 – 50 μatm , with higher values at lander 1. The correlation analysis revealed several significant relations, e.g., $p\text{CH}_4$ correlated positively with temperature and $p\text{CO}_2$ negatively with $p\text{O}_2$ (Figure 10).

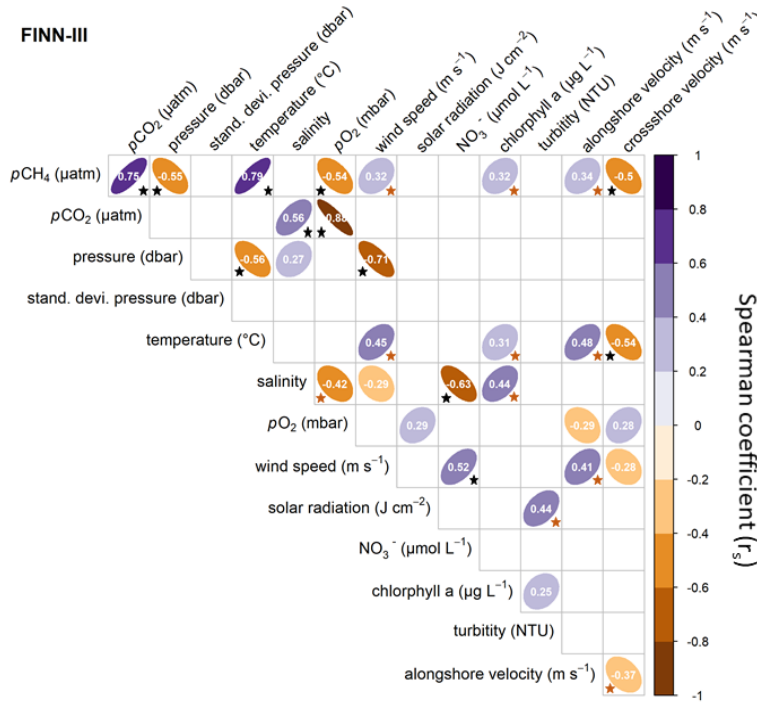


Figure 10: Spearman correlation coefficients (r_s) between the measured variables at lander 1 and auxiliary data, for the period corresponding to FINN-III. A significance level of 0.001 was applied to remove non-correlating relationships (empty fields). Cohen's convention was used to interpret the effect size (Cohen, 1988). Black stars represent a large effect size and hence a strong correlation, and brown stars a medium effect size.

3.2 The Drammendorf field survey

The content and the figures of Section 3.2 were in part published in Pönisch et al., 2023. Nutrient release and flux dynamics of CO₂, CH₄, and N₂O in a coastal peatland driven by actively induced rewetting with brackish water from the Baltic Sea, Biogeosciences, 20 (2), 295–323, <https://doi.org/10.5194/bg-20-295-2023>. The following paragraphs were changed for linguistic and conceptual reasons to conform with the overall style of this dissertation.

This survey was conducted during the transition from drained to flooded conditions, i.e., from ~ 6 months before (2019) to ~ 12 months after (2019/2020) rewetting. GHG fluxes were determined before and after rewetting, and intensive discrete sampling of the water column after flooding of the peatland and inner bay was also conducted from a small working boat.

Flooding of the peatland resulted in the immediate formation of a permanent water column and a drastic change between pre- and post-flooding conditions. A further effect was the establishment of continuous water exchange between the peatland stations and stations of the inner bay (*Kubitzer Bodden*), which was reflected by the statistically (data not shown) indistinguishable differences between surface water temperature, salinity, and O₂ at those stations (Figure 11a – c). The absence of temperature and salinity differences between the surface and bottom waters over the year (data not shown) suggested that vertical exchange processes and mixing were pronounced. However, local and temporary gradients were still possible, as a significant difference in O₂ between surface and bottom waters was measured in summer.

Table 6: Summary of the measured and calculated variables of the Drammendorf field survey. **(a)** Seasonal summary of the measured surface water means \pm standard deviations (SD) in the peatland after rewetting (n = the number of observations) and **(b)** the derived GHG fluxes determined in chamber measurements and wind-based parameterization before and after rewetting.

(a)	Winter 2019 (December – February)		Spring 2020 (March – May)		Summer 2020 (June – August)		Autumn 2020 (September – December)	
	mean \pm SD	n	mean \pm SD	n	mean \pm SD	n	mean \pm SD	n
Temperature (°C)	3.7 \pm 1.3	45	12.0 \pm 4.2	35	19.9 \pm 2.4	30	12.9 \pm 6.6	30
Salinity	6.7 \pm 0.7	45	8.2 \pm 0.7	35	9.0 \pm 0.5	30	8.2 \pm 0.3	30
O ₂ (mg L ⁻¹)	11.2 \pm 0.7	45	11.7 \pm 1.9	35	8.6 \pm 1.9	30	9.3 \pm 1.4	30
Chlorophyll <i>a</i> (µg L ⁻¹)	8.6 \pm 10.8	24	40.0 \pm 26.4	12	74.0 \pm 29.0	10	30.6 \pm 37.5	10
DOC (µmol L ⁻¹)	N/A	N/A	14.8 \pm 2.1	18	17.0 \pm 6.1	27	12.1 \pm 3.5	29
NO ₃ ⁻ (µmol L ⁻¹)	100.0 \pm 57.7	45	25.2 \pm 46.0	35	0.1 \pm 0.1	29	3.7 \pm 4.0	30
NO ₂ ⁻ (µmol L ⁻¹)	1.5 \pm 0.6	45	0.4 \pm 0.44	35	0.2 \pm 0.1	29	1.0 \pm 1.0	30
NH ₄ ⁺ (µmol L ⁻¹)	30.0 \pm 26.1	45	2.3 \pm 1.6	35	5.5 \pm 6.5	29	18.8 \pm 19.5	30
PO ₄ ³⁻ (µmol L ⁻¹)	0.4 \pm 0.4	45	0.3 \pm 0.3	35	0.5 \pm 0.3	29	0.4 \pm 0.3	30
CH ₄ (nmol L ⁻¹)	48.0 \pm 49.5	46	300.5 \pm 414.3	35	1502.4 \pm 693.4	30	733.7 \pm 699.2	30
N ₂ O (nmol L ⁻¹)	85.5 \pm 152.5	46	15.4 \pm 5.0	35	7.0 \pm 1.4	30	14.3 \pm 4.0	30
<i>p</i> CO ₂ (µatm)	1403.9 \pm 674.8	46	925.6 \pm 868.6	35	4016.7 \pm 2120.0	30	2197.1 \pm 1771.4	30
pH	7.7 \pm 0.2	46	8.0 \pm 0.3	35	7.4 \pm 0.3	30	7.6 \pm 0.3	30
C _T (µmol kg ⁻¹)	2153.6 \pm 121.1	46	2471.1 \pm 223.7	35	2539.1 \pm 225.3	30	2273.4 \pm 313.0	30
A _T (µmol kg ⁻¹)	2154.4 \pm 155.1	46	2614.9 \pm 209.6	35	2546.0 \pm 240.0	30	2290.6 \pm 272.7	30

(b) Summary of GHG fluxes and statistical comparison of pre- and post-rewetting measurements, by using summer and autumn seasons each from June to November 2019 and 2020, respectively.

	Location	Pre-rewetting		Post-rewetting		<i>p</i>
		mean \pm SD	n	mean \pm SD	n	
CO ₂ flux (g m ⁻² h ⁻¹)	transect and area (≠ formerly dry)	0.29 \pm 0.82	330	0.26 \pm 0.29	450	n.s.
CO ₂ flux (g m ⁻² h ⁻¹)	ditch	0.28 \pm 0.13	87	0.32 \pm 0.28	92	n.s.
CH ₄ flux (mg m ⁻² h ⁻¹)	transect and area (≠ formerly dry)	0.13 \pm 1.01	97	1.74 \pm 7.59	320	***
CH ₄ flux (mg m ⁻² h ⁻¹)	ditch	11.37 \pm 37.54	85	8.54 \pm 26.91	92	***

SD stands for standard deviation; N/A for not available; the three asterisks *** indicate $p < 0.001$, and n.s. stands for not significant

3.2.1 Surface water properties (temperature, salinity, O₂, DOC, and chlorophyll *a*)

Since the height of the water column at the peatland was only ~ 0.5 m, the water warmed early and strongly during the year (Figure 11a). The O₂ concentration was characterized by values that fluctuated around saturated conditions, with oversaturation occurring in spring (Figure 11c). DOC and chlorophyll *a* concentrations were highest in summer and higher than at the stations of the inner bay (Figure 11d – e).

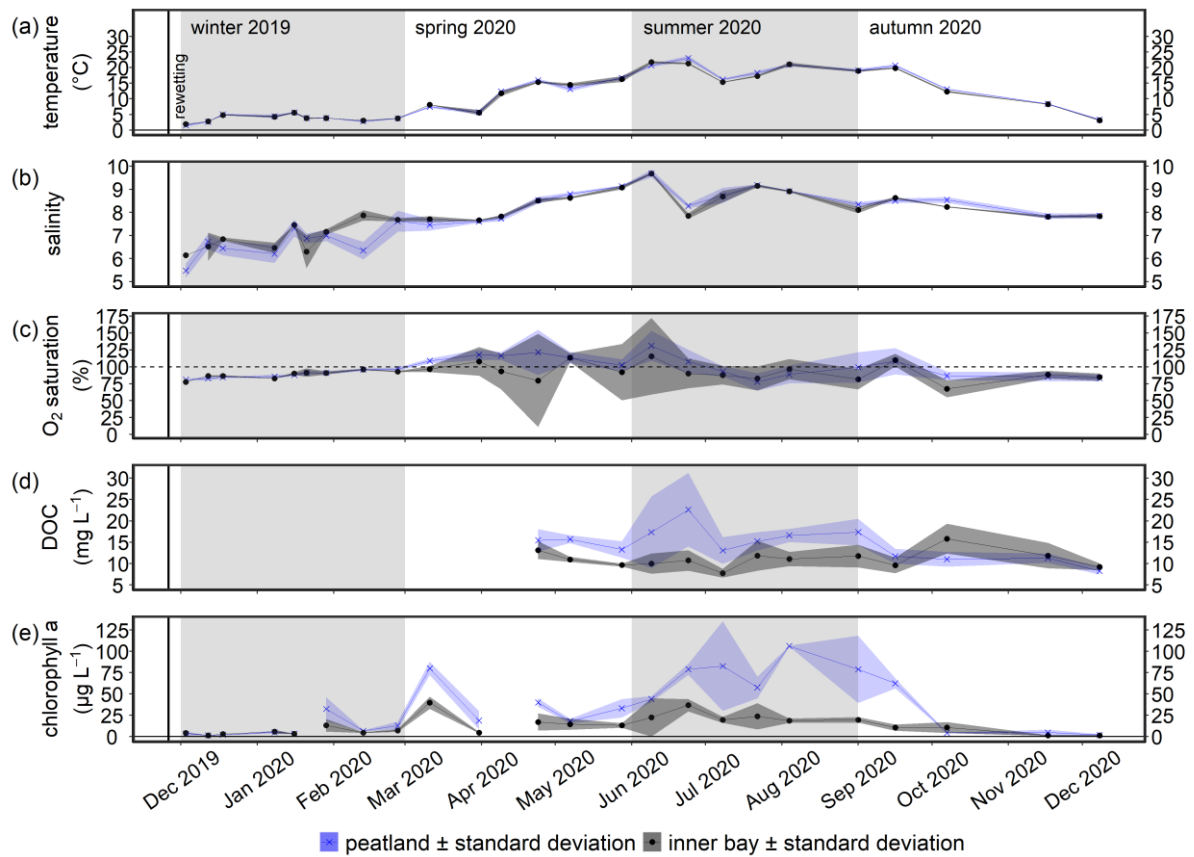


Figure 11: Time series of the mean (a) temperature, (b) salinity, (c) O₂ saturation, (d) DOC concentration, and (e) chlorophyll *a* concentration (\pm standard deviations) in the surface water after rewetting, as measured from December 2019 to December 2020. Data from the flooded peatland are shown in blue and data from the inner bay in black. The vertical black line indicates the rewetting event.

3.2.2 The inorganic carbon system in the surface water after rewetting

The variables C_T, A_T, and pH increased until spring (Figure 12) while *p*CO₂ decreased (Figure 13a), coinciding with a slight increase in salinity during the same period (Figure 11b). From spring onwards, however, the components of the CO₂ system differed in their behavior, with C_T and A_T remaining relatively constant in the inner bay but reaching significantly higher values in the peatland ($p < 0.05$), including maximum values in summer. The pH was also characterized by significant seasonal differences, with lower values and a minimum in

summer in the peatland ($p < 0.05$). C_T and A_T values in the inner bay and in the peatland aligned in autumn whereas the pH remained significantly different ($p < 0.05$). The mean pCO_2 (calculated from C_T and pH) of the surface water in winter was $1050.0 \pm 55.7 \mu\text{atm}$ in the inner bay and $1403.9 \pm 674.8 \mu\text{atm}$ (Table 6a) in the peatland (Figure 13) and hence, comparable. The pCO_2 values were high in winter during the first few weeks after inundation and then steadily decreased, with the lowest mean values occurring in spring (peatland) and summer (inner bay). The summer was characterized by increased pCO_2 values in general, including earlier and stronger increases in the peatland than in the inner bay that resulted in significant differences in spring and summer ($p < 0.05$ for both seasons). pCO_2 values were highest in summer with $4016.7 \pm 2120.0 \mu\text{atm}$ (peatland) and $1161.7 \pm 1275.5 \mu\text{atm}$ (inner bay).

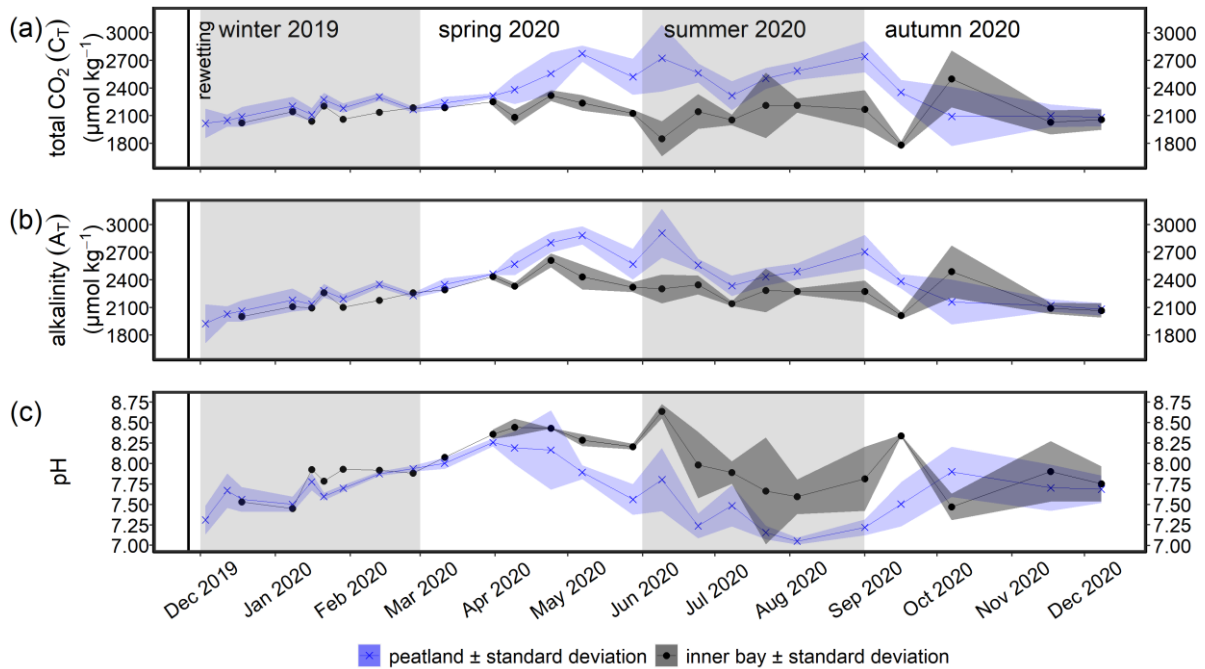


Figure 12: Time series of the mean (a) total CO_2 (C_T), (b) total alkalinity (A_T), and (c) pH (\pm standard deviations) in the surface water after rewetting, as measured from December 2019 to December 2020. Data from the flooded peatland ($n = 6$) are shown in blue and data from the inner bay (until March $n = 1$, thereafter: $n = 2$) in black. The vertical black line indicates the rewetting event.

3.2.3 CH_4 in the surface water after rewetting

During the first few months after flooding (in winter), CH_4 concentrations in the inner bay and the peatland were low and did not differ significantly (Figure 13, Table 6a): $48.0 \pm 49.5 \text{ nmol L}^{-1}$ (peatland) and $81.4 \pm 107.0 \text{ nmol L}^{-1}$ (inner bay). From mid-spring onwards, CH_4 concentrations in the inner bay and the peatland increased such that during summer and autumn 2020 the differences were significant ($p < 0.05$). Mean CH_4 values were

highest in summer: $1502.4 \pm 693.4 \text{ nmol L}^{-1}$ in the peatland and $502.5 \pm 479.3 \text{ nmol L}^{-1}$ in the inner bay. The peatland was also characterized by a considerable short-term variability (i.e., between samplings) in spring and summer, evidenced by four peaks in the CH_4 concentration. A positive significant correlation ($r_s = 0.73$, $n = 72$, $p < 0.001$) was determined in the peatland between the surface water CH_4 concentrations and a water temperature $> 10^\circ\text{C}$ but not $< 10^\circ\text{C}$.

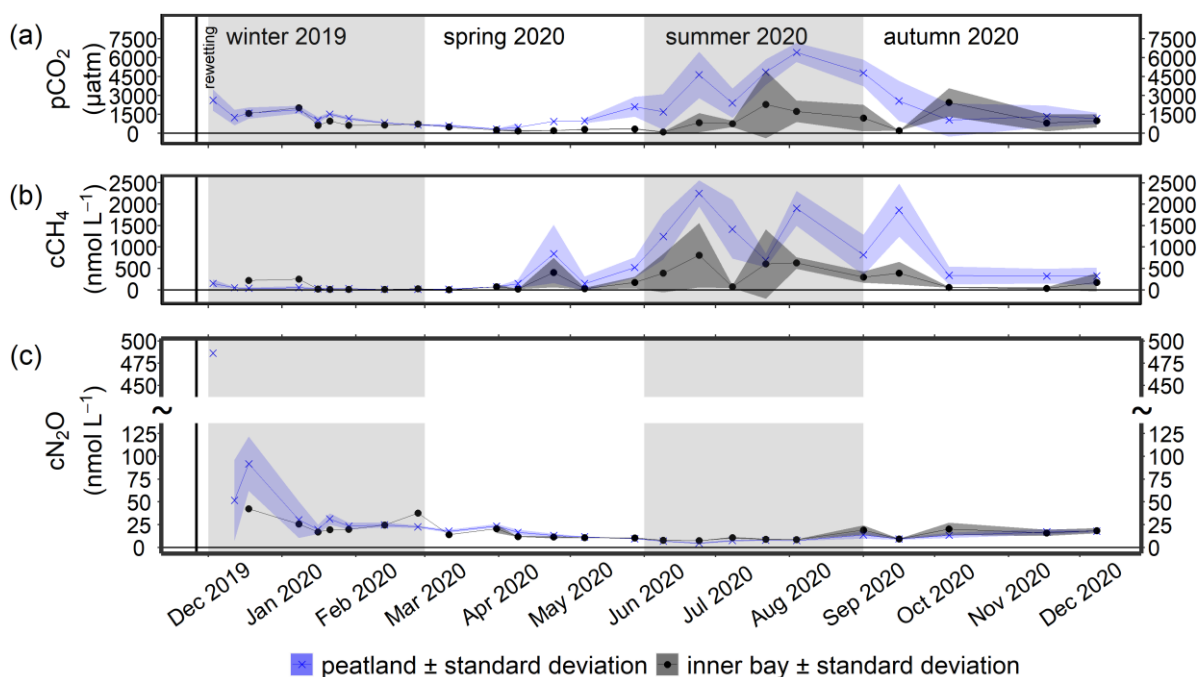


Figure 13: Time series of the mean (a) $p\text{CO}_2$, (b) CH_4 concentration ($c\text{CH}_4$), and (c) N_2O concentration ($c\text{N}_2\text{O}$) (\pm standard deviations) after rewetting in the surface water, as measured from December 2019 to December 2020. Data from the flooded peatland ($n = 6$) are shown in blue and data from the inner bay (until March $n = 1$, thereafter: $n = 2$) in black. The vertical black line indicates the rewetting event.

3.2.4 N_2O in the surface water after rewetting

The highest single N_2O concentration was measured one week after flooding and amounted to $486.3 \text{ nmol L}^{-1}$ and was followed by 4–5 weeks of elevated N_2O concentrations ($19.9 - 91.8 \text{ nmol L}^{-1}$). From spring onwards, N_2O decreased rapidly in the peatland, with the lowest values of $\sim 7 \text{ nmol L}^{-1}$ reached in summer.

3.2.5 Nutrient concentrations after rewetting

In winter, after flooding, the concentrations of all N-nutrients in the peatland were high but they decreased rapidly in spring (Table 6a). The lowest N-nutrient concentrations were measured in summer and were partly below detection limit, with NH_4^+ and NO_2^- then

increasing again in autumn. PO_4^{3-} concentrations followed a different pattern, with the highest concentrations determined in summer and fewer fluctuations throughout the year.

3.2.6 Pre- and post-rewetting GHG fluxes (CO_2 , CH_4 , N_2O)

Determining GHG fluxes to assess the effect of flooding with brackish water was challenging because of the drastically changed sampling conditions after rewetting and the need for two different methods to capture the different spatial extents (Figure 1d, e). Thus, GHG fluxes after rewetting were simplified by pooling data from (i) fluxes measured with chambers at the transect (Figure 1e), (ii) fluxes derived from the wind-based parameterization at the transect (i.e., Sect. 2.7; Wanninkhof, 2014), and (iii) fluxes derived from the wind-based parameterization at stations covering the spatial extent of the flooded peatland (Figure 1d). With this pooled approach (Sect. 2.3), the GHG fluxes covered both a small-scale-resolved transect and a spatially resolved component, making the data representative of the peatland.

Terrestrial CO_2 fluxes before rewetting, during summer and autumn 2019, were highly variable, ranging from -3.3 to $3.0 \text{ g m}^{-2} \text{ h}^{-1}$ with a mean \pm SD of $0.29 \pm 0.82 \text{ g m}^{-2} \text{ h}^{-1}$ (Figure 14a, Table 6b). Within the ditch, pre-rewetting CO_2 fluxes ranged from -0.008 to $0.6 \text{ g m}^{-2} \text{ h}^{-1}$ but on average were comparable to the fluxes determined at the terrestrial (dry) stations. After rewetting, formerly terrestrial CO_2 fluxes decreased in amplitude (-0.5 to $1.4 \text{ g m}^{-2} \text{ h}^{-1}$), while the average fluxes in the summer and autumn were mostly unchanged compared to the pre-rewetting fluxes (Table 6b). In the ditch, the mean and minimum post-rewetting CO_2 fluxes were within the range of those determined pre-rewetting (mean: $0.26 \pm 0.29 \text{ g m}^{-2} \text{ h}^{-1}$, min: $-0.02 \text{ g m}^{-2} \text{ h}^{-1}$) but the maximum flux ($1.1 \text{ g m}^{-2} \text{ h}^{-1}$) was almost twice as high as the pre-rewetting flux measured in the ditch (max: $0.6 \text{ g m}^{-2} \text{ h}^{-1}$).

Pre-rewetting CH_4 fluxes (mean \pm SD) in summer and autumn 2019 varied between -0.9 – $8.4 \text{ mg m}^{-2} \text{ h}^{-1}$ (terrestrial) and -1.1 – $193.6 \text{ mg m}^{-2} \text{ h}^{-1}$ (drainage ditch). While mean terrestrial CH_4 fluxes were $0.13 \pm 1.01 \text{ mg m}^{-2} \text{ h}^{-1}$, the mean fluxes in the ditch were $11.4 \pm 37.5 \text{ mg m}^{-2} \text{ h}^{-1}$ and thus two orders of magnitude higher (Table 6b). In summer and autumn 2020, after rewetting, average CH_4 fluxes on formerly terrestrial land increased slightly but significantly ($1.74 \pm 7.59 \text{ mg m}^{-2} \text{ h}^{-1}$), whereas in the ditch they decreased considerably ($8.5 \pm 26.9 \text{ mg m}^{-2} \text{ h}^{-1}$). Flux amplitudes at the ditch station before and after rewetting were comparable (Figure 14b).

Data on N₂O fluxes were available only for the period after rewetting. In the first year after rewetting, the mean annual flux in the peatland was $0.02 \pm 0.1 \text{ mg m}^{-2} \text{ h}^{-1}$ (Figure 14c). The highest N₂O flux of $0.4 \text{ mg m}^{-2} \text{ h}^{-1}$ occurred one week after rewetting, with a continuous decrease over the following 4 – 5 weeks. Thereafter, N₂O fluxes remained consistently close to zero, and N₂O uptake was measured during the summer.

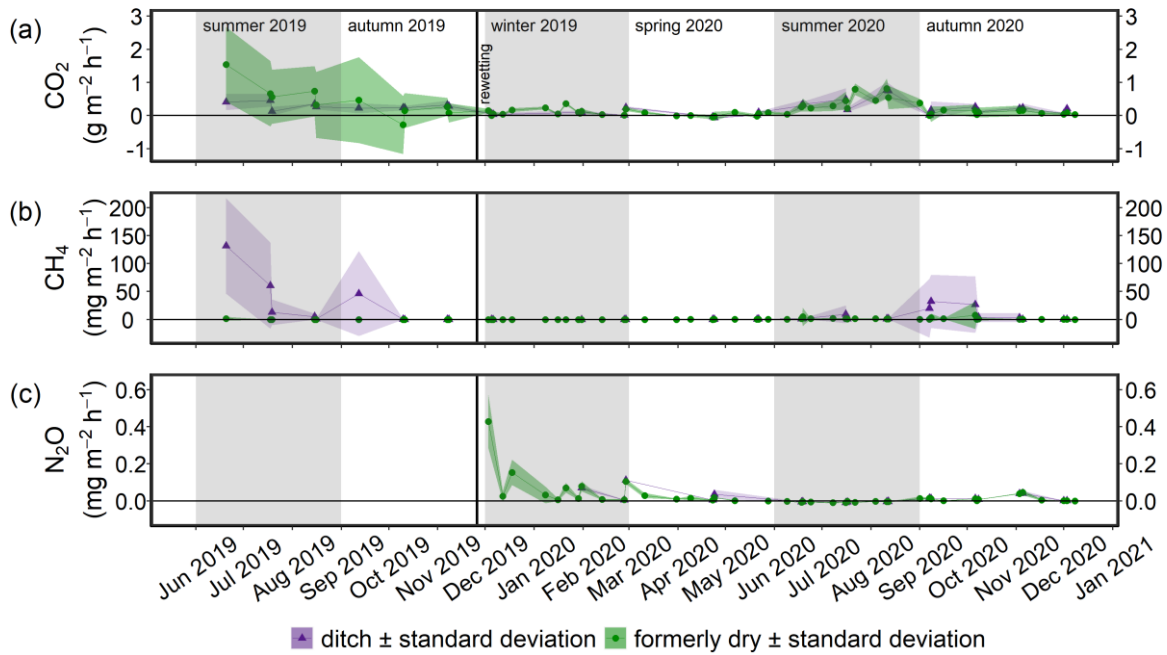


Figure 14: Time series of the mean (a) CO₂, (b) CH₄, and (c) N₂O fluxes (\pm standard deviations) from June 2019 to December 2020. Fluxes of the permanently water-filled drainage ditch are shown in purple, and fluxes derived from the flooded, formerly dry peatland in green. In both cases, the two methods (i.e., fluxes measured using chambers and fluxes derived from wind-parameterization) were applied. The vertical black line indicates the rewetting event.

3.3 The Drammendorf lander survey

This survey, conducted in the summer of 2021 (June – August), included deployment of the two landers in the central peatland and the connecting ditch between the peatland and the *Kubitzer Bodden*. In contrast to the field study (Sect. 3.2), the objective of the sensor measurements was to determine the temporal variability of GHG partial pressures ($p\text{CO}_2$, $p\text{CH}_4$), nutrients, O₂, and physical variables, as well as its driver, by measuring at high temporal resolution. In addition, supplementary discrete samples were taken from a small working boat.

3.3.1 Time series of the variables at lander 1 and lander 2

Wind speeds were persistently weak to moderate at the study site, with a mean of 3.4 m s^{-1} (Figure 15j) and ranging from 0.2 to 10 m s^{-1} , indicating that no storm events occurred during

the deployment. Precipitation during deployment was low, with a mean of 0.08 mm h^{-1} (corresponding to $\text{L m}^{-2} \text{ h}^{-1}$).

The water column temperature measured by the two landers showed considerable agreement in average and standard deviation (Table 7) as well as in the pronounced daily cycles (Figure 15c). Within the period of simultaneous data coverage of both CTD- O_2 sensors, only small differences in salinity were determined (Figure 15d). In early July, salinity dropped by 2 – 3, separating two periods of relatively stable salinity conditions. Bottle data for salinity supported the strong agreement between the two landers. Considered together, the similar temperatures and salinities indicated a distinctive water exchange between the sites and hence with the *Kubitzer Bodden*. To demonstrate the exchange, we analyzed the pressure differences between the two landers at 10-min intervals by calculating an average of the high-resolution data every 10 min. The differences between the two sites served as a proxy for water height compensation or the rate of water exchange, also including the periods of fast changes in the water column height. The differences were only $\pm 10 \text{ cm}$ (minimum/maximum) or $\pm 5 \text{ cm}$ (0.98th percentile/0.02th percentile), respectively. These results suggested that adjustment of the water level between the two landers was quasi-simultaneous, due to the strong hydrological connection. The same conclusion emerged from the field survey. In general, the water column height during the deployment at both sites was characterized by frequent changes on the order of several cm (i.e., $\sim 5 - 15 \text{ cm}$; Figure 15e). This resulted in common inflows and outflows through the dike opening (lander 2) and counteracted stagnant conditions in the peatland (lander 1). Major changes in the water level in a relatively short period of time during the lander deployment were also observed. For example, in late July, the water column at both sites rose by 0.46 m within 11.5 h (following a period of decreasing water column height).

Oxygen saturations were characterized by large short-term fluctuation on a daily scale (Sect. 3.3.2), with saturation values ranging from ~ 0 to 180 %, indicating strong alternations between undersaturated and oversaturated conditions (Figure 15f). Despite occasional low O_2 values, the measurements indicated a predominantly oxygenated water column, with slightly lower mean O_2 values at lander 2 (Table 7).

The $p\text{CO}_2$ varied considerably at both landers during the deployment, including strong, multi-day, sinusoidal fluctuations (Figure 15a) and short-scale fluctuations < 1 day (Sect. 3.3.2, Table 1). The values were consistently low (i.e., $< 4000 \mu\text{atm}$) at the beginning of the

deployment (early June) compared to the rest of the deployment, but then increased for the most part thereafter at both locations. The direction of change in the CO₂ signal on a multi-day scale was the same at the two sites. While both landers indicated comparable variability in the $p\text{CO}_2$ (i.e., standard deviation), the mean at lander 1 was $> 1000 \mu\text{atm}$ higher. At both landers, there was a negative correlation between $p\text{CO}_2$ and O₂ saturation ($r_s = -0.58$, $r_s = -0.56$), with a strong effect size (Figure 16). A comparison of the $p\text{CO}_2$ calculated from the bottle C_T and pH data with the $p\text{CO}_2$ measured by the sensors showed good agreement at both landers, with a difference of only -2% (a minus sign means bottle data values lower than those of the sensors) but also larger discrepancies of up to 45% . The median of the differences of the nine comparisons was 13% for lander 1 and 12% for lander 2.

The $p\text{CH}_4$ signals were characterized by strong, complex fluctuations that included multi-day variability during the deployment and short-term fluctuations (< 1 day), with periods of overlap. The mean $p\text{CH}_4$ from lander 2 was slightly higher than that from lander 1 (Figure 15b, Table 7). A correlation analysis showed that $p\text{CH}_4$ at both lander correlated positively with temperature ($r_s = 0.30$, $r_s = 0.19$) and salinity ($r_s = 0.37$, $r_s = 0.30$) and negatively with wind speed ($r_s = -0.31$, $r_s = -0.29$; Figure 16). The comparison of the bottle data, in which $p\text{CH}_4$ was calculated from the CH₄ concentration (cCH₄), with the $p\text{CH}_4$ determined by the sensors showed good agreement with a discrepancy of only -21% , but also predominantly higher divergences reaching a maximum of 595% . The median of the differences of the nine comparisons was 83% for lander 1 and 77% for lander 2 hence, most divergences were $< 100 \%$.

A comparison between the two landers with respect to the mean chlorophyll *a* concentrations and turbidity showed slight differences, with higher values measured at lander 1 (Table 7). The time series of chlorophyll *a* revealed a more fluctuating pattern in the second half of the deployment, coinciding with a rapid decrease in salinity, by about 3 within ~ 1 day, followed by prolonged lower values until the end of the deployment. Accordingly, chlorophyll *a* as determined at both landers showed a significant negative correlation with salinity ($r_s = -0.25$, $r_s = -0.51$; Figure 16). Chlorophyll *a* also correlated negatively with pressure, with a medium effect size, at both landers ($r_s = -0.34$, $r_s = -0.44$). Turbidity was positively related to the wind speeds measured at lander 1 ($r_s = 0.36$).

Mean phosphate values at the two landers were comparable although they were measured during different periods of operation. Measurements at lander 1 ranged from 0.55 to

3.43 $\mu\text{mol L}^{-1}$, with a plateau of elevated values for ~ 12 days in late June (Figure 15i, Table 7). The sensor data were consistent with the bottle data.

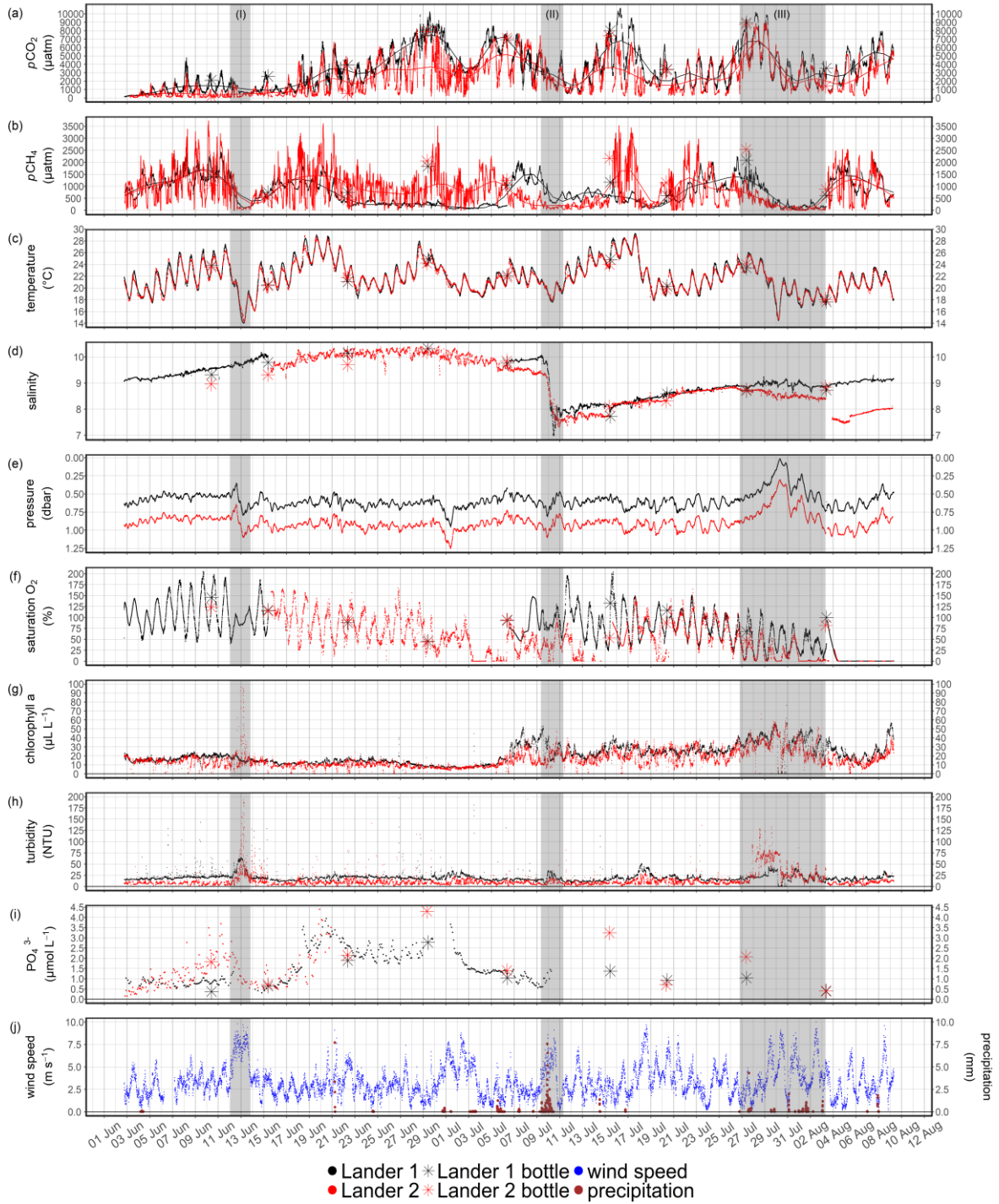


Figure 15: High-resolution time series from lander 1 (black) and lander 2 (red). Results from discrete bottle data are indicated by asterisks, together with the color of the respective lander. (a – j) Post-processed data of (a) $p\text{CO}_2$ (μatm), (b) $p\text{CH}_4$ (μatm), (c) water temperature ($^{\circ}\text{C}$), (d) salinity, (e) O_2 saturation (%), (f) pressure (depth; dbar), (g) chlorophyll a concentration ($\mu\text{L L}^{-1}$), (h) turbidity (NTU), (i) PO_4^{3-} concentration ($\mu\text{mol L}^{-1}$), (j) wind speed (m s^{-1}), and precipitation (mm). The sensor signals of $p\text{CO}_2$ and $p\text{CH}_4$ were additionally smoothed, as represented by the black and red lines, respectively. The gray rectangles highlight three periods of system changes.

Table 7: Summary of the mean, standard deviation, minimum and maximum (as 0.98th and 0.02th percentiles) of available data from lander 1 and lander 2. The mean, minimum and maximum of the calculated daily variability are also shown (Sect. 3.3.2). The CH₄ concentration (nmol L⁻¹) was calculated from *p*CH₄ (μatm). NO₃⁻ concentrations could not be determined due to strong interferences from CDOM.

		Lander 1	Lander 2
<i>p</i> CO ₂ (μatm)	mean ± SD	3399.1 ± 2348.0	2339.7 ± 2008.4
	0.98 th pct – 0.02 th pct	295.0 – 8937.8	97.4 – 7164.3
	mean (min – max) of daily variability	3730.8 (172.8 – 8535.0)	4066.9 (357.6 – 7891.0)
<i>p</i> CH ₄ (μatm)	mean ± SD	754.3 ± 543.1	843.0 ± 708.8
	0.98 th pct – 0.02 th pct	74.3 – 1982.1	22.8 – 2681.3
	mean (min – max) of daily variability	720.2 (93.3 – 1715.5)	1769.6 (168.7 – 3475.2)
cCH ₄ (nmol L ⁻¹)	mean ± SD	1049.1 ± 754.5	1186.9 ± 948.4
	0.98 th pct – 0.02 th pct	108.4 – 2677.0	42.7 – 3568.6
	mean (min – max) of daily variability	N/A	N/A
Temperature (°C)	mean ± SD	21.9 ± 2.7	21.8 ± 2.6
	0.98 th pct – 0.02 th pct	16.9 – 28.1	16.6 – 27.6
	mean (min – max) of daily variability	4.2 (1.6 – 8.5)	4.0 (1.4 – 8.0)
Pressure (mbar)	mean ± SD	0.59 ± 0.11	0.89 ± 0.12
	0.98 th pct – 0.02 th pct	0.23 – 0.76	0.51 – 1.08
	mean (min – max) of daily variability	0.16 (0.04 – 0.39)	0.15 (0.04 – 0.39)
Salinity	mean ± SD	9.0 ± 0.6*	9.0 ± 0.9*
	0.98 th pct – 0.02 th pct	7.9 – 10.0*	7.5 – 10.3*
	mean (min – max) of daily variability	0.3 (0.07 – 2.40)*	0.4 (0.06 – 1.95)*
Saturation O ₂ (%)	mean ± SD	75.9 ± 46.6*	53.6 ± 40.8*
	0.98 th pct – 0.02 th pct	0.1 – 179.5*	~ 0 – 144.0*
	mean (min – max) of daily variability	77.9 (0.1 – 180.0)*	70.1 (0.01 – 142.7)*
Chlorophyll <i>a</i> (μl L ⁻¹)	mean ± SD	21.3 ± 10.3	16.4 ± 9.8
	0.98 th pct – 0.02 th pct	7.1 – 47.3	4.5 – 41.0
	mean (min – max) of daily variability	16.1 (1.9 – 76.2)	28.1 (4.1 – 187.8)
Turbidity (NTU)	mean ± SD	19.7 ± 9.9	12.9 ± 14.8
	0.98 th pct – 0.02 th pct	9.5 – 41.8	2.7 – 70.2
	mean (min – max) of daily variability	43.4 (3.5 – 323.2)	44.9 (4.2 – 200.5)
NO ₃ ⁻ (μmol L ⁻¹)	mean ± SD	N/A	N/A
	0.98 th pct – 0.02 th pct	N/A	N/A
	mean (min – max) of daily variability	N/A	N/A
PO ₄ ³⁻ (μmol L ⁻¹)	mean ± SD	1.59 ± 0.83*	1.37 ± 0.86*
	0.98 th pct – 0.02 th pct	0.55 – 3.43*	0.24 – 3.68*
	mean (min – max) of daily variability	0.59 (0.03 – 2.19)*	1.22 (0.27 – 3.28)*

SD stands for standard deviation; pct stands for percentile; N/A for not available; data marked with the asterisk * are not comparable due to different time coverage.

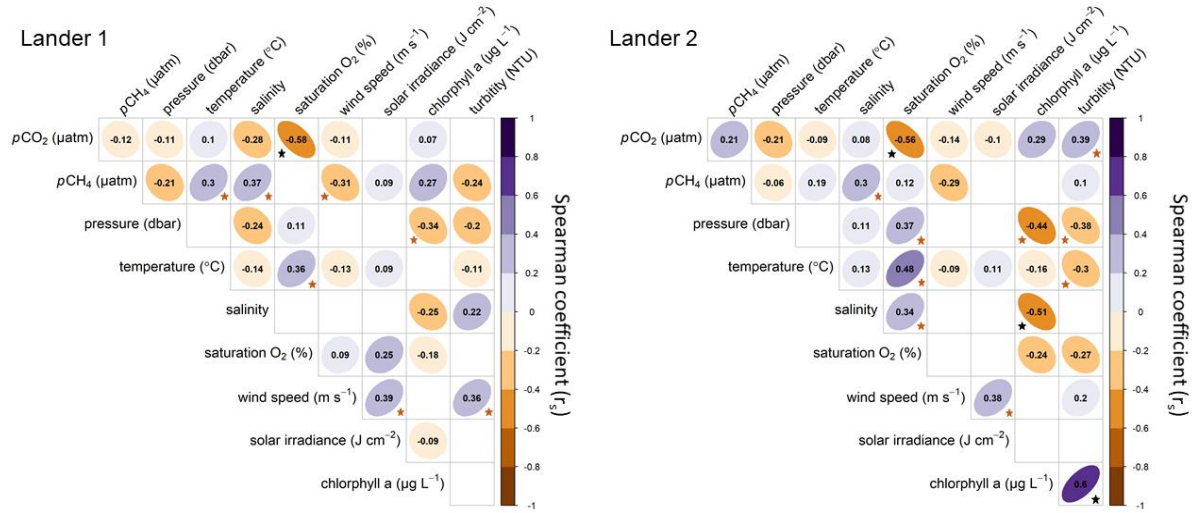


Figure 16: Spearman correlation coefficients (r_s) between the measured variables determined by both landers, wind speed and solar irradiance. A significance level of 0.001 was applied to remove non-correlating relationships (empty fields). The Cohen convention was used to interpret the effect size (Cohen, 1988). Black stars represent a large effect size and hence a strong correlation, and brown stars a medium effect size. Wind speeds were retrieved from the *Putbus* station (WMO-ID 10093) and solar irradiance from *Rostock-Warnemünde* (WMO-ID 10170; both DWD).

3.3.2 Short-term variability and diurnal cycles

The variables $p\text{CO}_2$, $p\text{CH}_4$, temperature, and O_2 were characterized by pronounced short-term variability and diurnal cyclicity with regular sinusoidal fluctuations that were intermittently superimposed by other fluctuations, especially GHG signals (Figure 15). Based on these observations and to assess the strength of the diurnal variability, the mean diurnal variability was calculated. The high-resolution data were divided into 24-h intervals, each starting at midnight, and then for each interval (i.e., day) the difference between the minimum and maximum was determined. Subsequent determination of the mean, minimum, and maximum yielded an approximation of diurnal variability (Table 7). The mean daily range for $p\text{CO}_2$ of $\sim 4000 \mu\text{atm}$ was substantial. However, it differed during the deployment, with minimum and maximum daily variability ranging from $\sim 200 \mu\text{atm}$ to $\sim 8500 \mu\text{atm}$ and comparable patterns at the two landers (Table 7). For $p\text{CH}_4$, the diurnal variability was also pronounced, but with larger differences between the two landers: $\sim 700 \mu\text{atm}$ at lander 1 and $\sim 1800 \mu\text{atm}$ at lander 2. The observed minimum and maximum during the deployment ranged from $\sim 100 \mu\text{atm}$ to $\sim 3500 \mu\text{atm}$ (both at lander 2). In addition, the daily average temperature varied by $\sim 4 ^{\circ}\text{C}$ and O_2 saturation by $\sim 80 \%$.

The relationships among the daily variability of the variables were examined by analyzing the distribution of the values in the course of a day (Figure 17). $p\text{CO}_2$ had an inverse pattern compared to temperature and O_2 , with the highest and lowest mean $p\text{CO}_2$ occurring in the early morning (05:00 UTC) and in the late afternoon (17:00 UTC), respectively. The daily

cycle of $p\text{CH}_4$ was less pronounced but also included high values in the early morning ($\sim 04:00$ UTC) and low values in the late afternoon ($\sim 18:00$ UTC). Wind speed similarly followed a diurnal cycle, with higher speeds during the day and at midday. Since wind is used for the parameterization of the air-sea exchange, it influences determinations of GHG emissions.

The remaining variables (i.e., salinity, pressure, chlorophyll a , turbidity) showed either a slight or non-diurnal behavior. The relatively high mean daily variability of chlorophyll a and turbidity (Table 7) included a large number of spikes (Figure 15g, h).

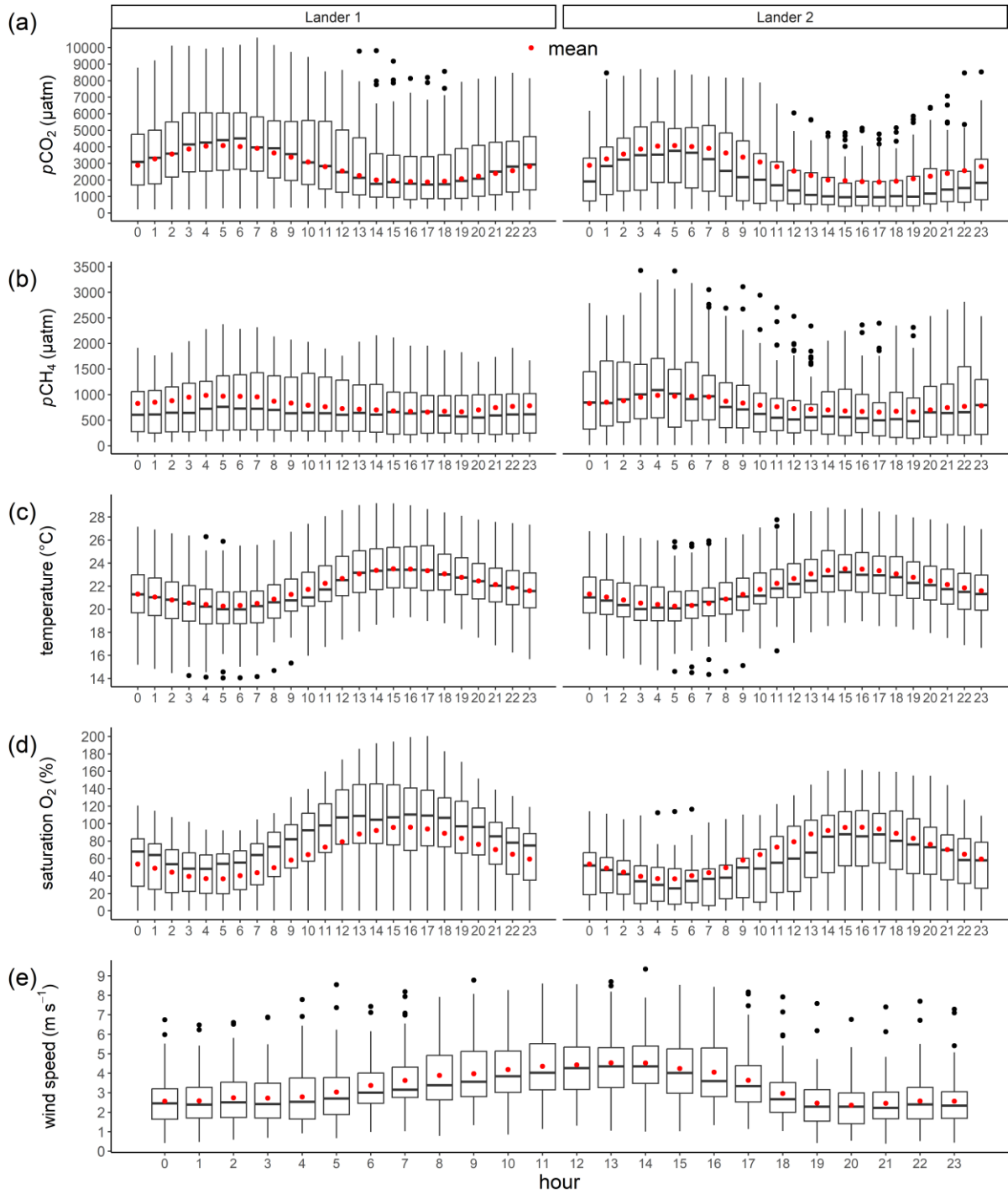


Figure 17: Distribution and mean values of $p\text{CO}_2$, $p\text{CH}_4$, temperature, O_2 , and wind speed calculated for each hour of the daily cycle over 24 h during the deployment, highlighting diurnal patterns. The box plots show the median and the 25/75 % quantiles; the whiskers indicate the 5/95 % percentiles, and the red points the mean values.

3.3.3 Identification of three event-based system changes

Analyses of wind speeds and CTD- O_2 measurements resulted in the identification of three events (Figure 15), numbered (I), (II), and (III) and described in the following. Since they serve as the time periods for detailed analyses of GHG drivers only in the flooded peatland,

only data from lander 1 were used. Correlation analyses were conducted exclusively for each event.

3.3.3.1 Storm event – (I)

A short-lived period with sustained high-wind speeds of up to $9 - 10 \text{ m s}^{-1}$ occurred between 12 and 13 June 2021. After an initial decline, the water level rose by $\sim 0.4 \text{ m}$ due to the inflow of water from the *Kubitzer Bodden*, which led to a water volume 2.4 -fold larger than during normal water level conditions. There was also a fast drop in water temperature of $\sim 13 \text{ }^{\circ}\text{C}$, while salinity remained unaffected. Turbidity increased, forming a pronounced peak of $\sim 60 \text{ NTU}$. The partial pressures of CO_2 and CH_4 decreased considerably, and the amplitude of the daily cyclicity of both GHGs and of O_2 was significantly reduced for several days after the event. A number of correlations with strong and medium effect sizes were identified (Figure 18), including a positive correlation of wind speed with turbidity ($r_s = 0.48$) as well as negative correlations of $p\text{CO}_2$ ($r_s = -0.66$) and $p\text{CH}_4$ ($r_s = -0.87$) with pressure and their positive correlation with temperature ($r_s = 0.60$ and 0.86 , respectively).

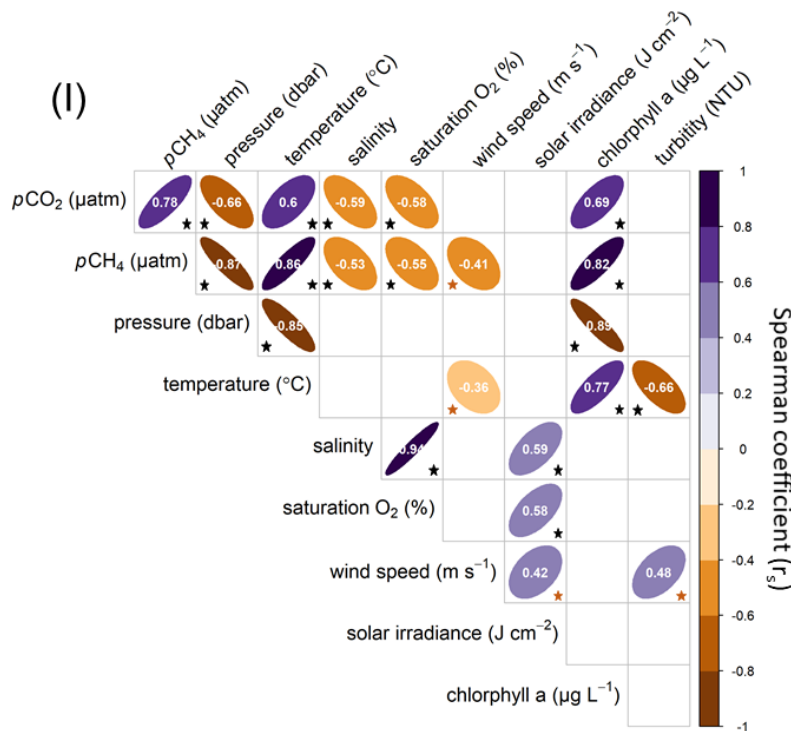


Figure 18: Spearman correlation coefficients (r_s) between the measured variables at lander 1, wind speed, and solar irradiance, limited to time period (I). A significance level of 0.001 was applied to remove non-correlating relationships (empty fields). Cohen's convention was used to interpret the effect size (Cohen, 1988). Black stars represent a large effect size and hence a strong correlation, and brown stars a medium effect size. Wind speeds were retrieved from *Putbus* station (WMO-ID 10093) and solar irradiance from *Rostock-Warnemünde* (WMO-ID 10170; both DWD).

3.3.3.2 Fast salinity decrease – (II)

The second event occurred in early July and lasted ~ 48 h. It was characterized by an accumulated precipitation of $\sim 76 \text{ L m}^{-2}$ ($1.6 \text{ L m}^{-2} \text{ h}^{-1}$) that resulted in a rapid (~ 24 h) decrease in salinity (by $\sim 2 - 3$) as well as a concomitant outflow of water towards the *Kubitzer Bodden*. The freshwater input also triggered a slight temperature decrease. The data from lander 1 showed a larger decrease in salinity, reflecting the central position of the lander in the shallow flooded area (Figure 15d). The low salinity prevailed long after the event and only slowly returned to higher values. During event (II), the chlorophyll *a* concentration and the turbidity increased, while the mean partial pressures and daily cyclicality of GHGs decreased. The $p\text{CH}_4$ level correlated positively with temperature ($r_s = 0.42$; Figure 19).

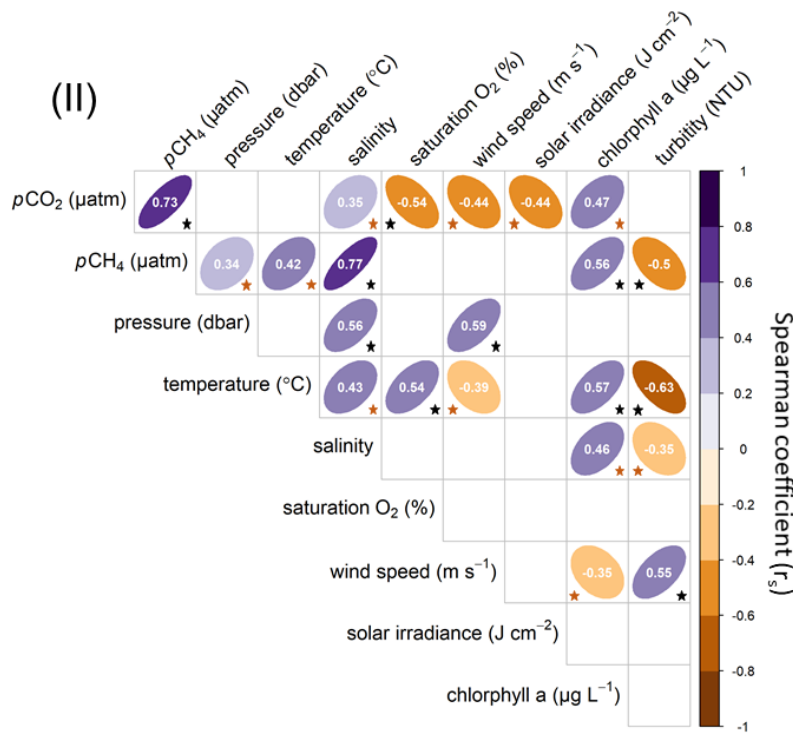


Figure 19: Spearman correlation coefficients (r_s) between the measured variables at lander 1, wind speed, and solar irradiance, limited to time period (II). A significance level of 0.001 was applied to remove non-correlating relationships (empty fields). Cohen's convention was used to interpret the effect size (Cohen, 1988). Black stars represent a large effect size and hence a strong correlation, and brown stars a medium effect size. Wind speeds were retrieved from *Putbus* station (WMO-ID 10093) and solar irradiance from *Rostock-Warnemünde* (WMO-ID 10170; both DWD).

3.3.3.3 Water outflow – (III)

In late July, an outflow of water from the peatland caused the water column as detected by the CTD- O_2 sensor to reach ~ 0 m, thus draining larger areas of the rewetted peatland. This drop in water level reduced the water volume by a factor of 5 – 6 compared to the normal water level. Nevertheless, the sensors were consistently covered with water. The outflow was slow and extended over several days, with a subsequent water inflow. Nighttime temperatures

were cold the day before the minimum water level was reached. The drop in the water level triggered decreases in $p\text{CH}_4$ (correlation with wind; $r_s = -0.64$; Figure 20) and $p\text{CO}_2$ as well as a suppression of the amplitude of the diurnal cycles of both GHGs (Figure 15).

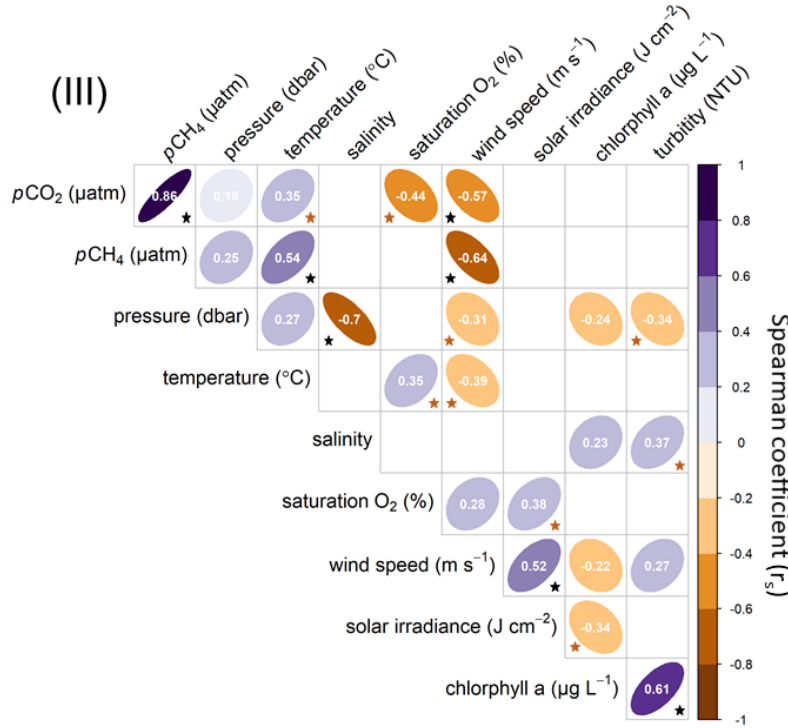


Figure 20: Spearman correlation coefficients (r_s) between the measured variables at lander 1, wind speed, and solar irradiance, limited to time period (III). A significance level of 0.001 was applied to remove non-correlating relationships (empty fields). Cohen's convention was used to interpret the effect size (Cohen, 1988). Black stars represent a large effect size and hence a strong correlation, and brown stars a medium effect size. Wind speeds were retrieved from *Putbus* station (WMO-ID 10093) and solar irradiance from *Rostock-Warnemünde* (WMO-ID 10170; both DWD).

3.3.4 GHG fluxes derived from high-resolution data at lander 1 and lander 2

GHG fluxes for CO_2 and CH_4 were derived from the entire high-resolution sensor data using a gas transfer velocity model parameterized by wind speeds (Wanninkhof, 2014). For further interpretation, these fluxes were compared with the measurements derived from the Drammendorf field study. In addition, GHG fluxes were calculated using the same approach but based on different scenarios: from bottle data only, during the daytime, and at nighttime. These results are summarized in Table 8.

Since the $p\text{CO}_2$ values were predominantly above atmospheric equilibrium during the deployment, a mean (\pm standard deviation) CO_2 flux of $0.151 \pm 0.180 \text{ g m}^{-2} \text{ h}^{-1}$ and $0.092 \pm 0.180 \text{ g m}^{-2} \text{ h}^{-1}$ was determined for lander 1 and lander 2, respectively, with persistently higher fluxes at lander 1 (Table 8, Figure 21). Nevertheless, a brief CO_2 uptake was registered at both landers at the beginning of the deployment, in early June (Figure 21).

The range of measured $p\text{CH}_4$ values indicated a permanent oversaturation compared to the atmospheric values. Consequently, the resulting air-sea flux was $0.480 \pm 0.514 \text{ mg m}^{-2} \text{ h}^{-1}$ and $0.536 \pm 0.609 \text{ mg m}^{-2} \text{ h}^{-1}$ for lander 1 and lander 2, respectively (Table 8). The differences between daytime and nighttime GHG fluxes (CO_2 and CH_4) were large, due to the diurnal cycles of the gas partial pressures and wind speeds (Figure 17). Hence, GHG fluxes were 2.1 – 2.3-fold higher for $p\text{CO}_2$ and 2.3 – 3.0-fold higher for $p\text{CH}_4$ during the day than at night, depending on the position of the lander (Table 8).

Table 8: Greenhouse gas fluxes calculated for both lander positions and by using different data sets. The fluxes were calculated based on the sensor data⁽¹⁾ (bold) and, for comparison, using the bottle data⁽²⁾. GHG fluxes were also calculated based on the sensor data for daytime⁽³⁾ and nighttime⁽³⁾ in order to show the impact of diurnal effects. The sensor data for daytime and nighttime were averaged by $\pm 1 \text{ h}$. Data from the Drammendorf field survey were used to calculate the ASE for the corresponding period in 2020⁽⁴⁾ (column “data from 2020”). For maximum comparability, the ASE based on the sensor data (lander survey) for the period between 09:00 and 15:00 UTC (the main sampling period in the Drammendorf field survey) was calculated⁽⁵⁾. The calculation procedure of (1) – (5) is described in Sect 2.4.4.

		Sensor data ⁽¹⁾	Bottle data ⁽²⁾	Daytime ⁽³⁾ 12:00 UTC	Nighttime ⁽³⁾ 00:00 UTC	Data from 2020 ^{(4)*}	Sensor data ⁽⁵⁾ (from 2021)
Lander 1 – CO_2 ($\text{g m}^{-2} \text{ h}^{-1}$)	Mean \pm SD	0.151 ± 0.180	0.163 ± 0.079	0.224 ± 0.211	0.098 ± 0.138	N/A	N/A
	0.98 th pct – 0.02 th pct	$-0.002 - 0.673$	N/A	N/A	N/A		
Lander 2 – CO_2 ($\text{g m}^{-2} \text{ h}^{-1}$)	Mean \pm SD	0.092 ± 0.132	0.104 ± 0.100	0.122 ± 0.155	0.059 ± 0.081	N/A	N/A
	0.98 th pct – 0.02 th pct	$-0.023 - 0.465$	N/A	N/A	N/A		
Both lander – CO_2 ($\text{g m}^{-2} \text{ h}^{-1}$)	Mean \pm SD	0.122 ± 0.161	N/A	0.173	0.078	0.322 ± 0.218	0.167 ± 0.190
Lander 1 – CH_4 ($\text{mg m}^{-2} \text{ h}^{-1}$)	Mean \pm SD	0.480 ± 0.514	0.560 ± 0.216	0.820 ± 0.683	0.276 ± 0.318	N/A	N/A
	0.98 th pct – 0.02 th pct	$0.015 - 2.137$	NA	N/A	N/A		
Lander 2 – CH_4 ($\text{mg m}^{-2} \text{ h}^{-1}$)	Mean \pm SD	0.536 ± 0.609	0.655 ± 0.400	0.789 ± 0.760	0.348 ± 0.410	N/A	N/A
	0.98 th pct – 0.02 th pct	$0.010 - 2.410$	N/A	N/A	N/A		
Both lander – CH_4 ($\text{mg m}^{-2} \text{ h}^{-1}$)	Mean \pm SD	0.508 ± 0.564	N/A	0.805	0.312	1.961 ± 6.591	0.755 ± 0.682

SD stands for standard deviation; pct stands for percentile; N/A for not available; data marked with the asterisk * originated from the Drammendorf field survey

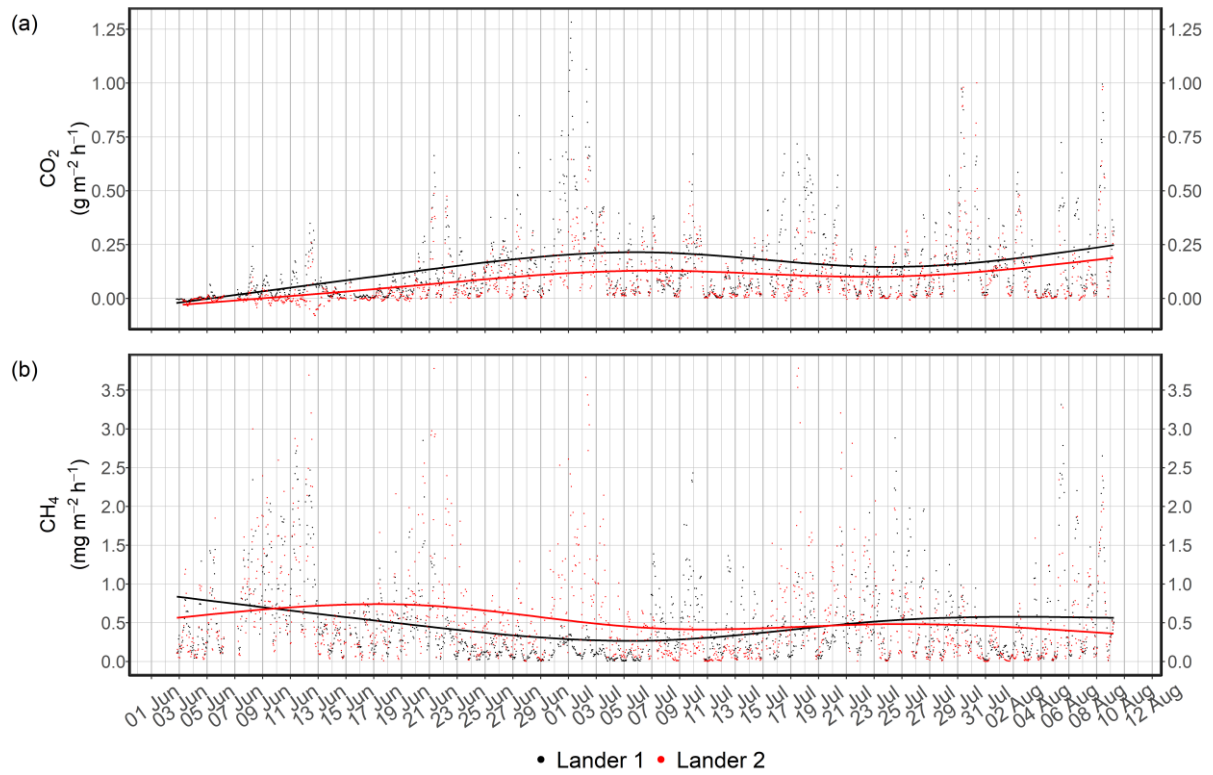


Figure 21: Calculated GHG fluxes for CO₂ and CH₄ at both landers using the wind parameterization approach of Wanninkhof (2014). Smoothing was used to highlight the trend and differences between the data from the two landers.

4. Discussion

4.1 The Hütelmoor lander survey

The objective of the Hütelmoor lander survey was to investigate GHG distributions in a shallow coastal area, which has been insufficiently described so far. Stationary lander measurements in combination with modeling were used to gain a temporal and spatial understanding in the distribution of the measured variables that allowed the study of coastal drivers of GHG dynamics.

4.1.1 GHG and nutrient distribution in the nearshore area

Coastal GHG conditions are remarkably heterogeneous because the coast, as the interface between terrestrial and marine environments, is influenced by a variety of processes acting at different spatial and temporal scales, including inputs from rivers, high turnover rates of C and nutrients, water column mixing, enhanced shear stress at the sediment surface, and lateral transport processes. High-resolution measurements obtained for around one month in the autumn of 2019 provided detailed information on these processes. The mean (\pm standard deviation) $p\text{CO}_2$ determined at lander 1 and lander 2 was $486 \pm 181 \mu\text{atm}$ and $465 \pm 111 \mu\text{atm}$, respectively (Table 5). In order to assess the variability of the $p\text{CO}_2$, measured ~ 400 m offshore, values from a reference area in a more central and adjacent area of the Baltic Sea was used for comparison. For this purpose, the mean surface water $p\text{CO}_2$ was calculated from regular transects of a ferry line for the same period, with data retrieved from the Surface Ocean CO_2 Atlas (SOCAT, <https://www.socat.info>, last access: 21 November 2022; Bakker et al., 2016). A sub-transect of the ferry line within a box of Cartesian coordinates (the Mecklenburg Bight, MEB) was selected, as the MEB is described in Schneider and Müller (2018). The mean $p\text{CO}_2$ determined at the MEB was $453 \pm 49 \mu\text{atm}$, which was lower and, in particular, less variable than the measurements of the landers. The $p\text{CO}_2$ measured at the lander were lower than the $\sim 700 \mu\text{atm}$ reported for a shallow Finnish coastal region or even higher values in the Finish archipelagoes, although measurements were made at the end of a heat wave (Humborg et al., 2019). Consequently, the $p\text{CO}_2$ levels in the shallow waters at the Hütelmoor area appear to be in between the more open waters of the Baltic Sea and the more enclosed waters such as an archipelago.

The mean CH_4 concentration calculated from the $p\text{CH}_4$ at lander 1 (a calculation for lander 2 was not possible due to missing salinity measurements) was ~ 3 times higher than that of the

MEB ($45 \pm 24 \text{ nmol L}^{-1}$ compared to $14 \pm 8 \text{ nmol L}^{-1}$). The measured concentration at the Finnish coast in September 2018 was $> 30 \text{ nmol L}^{-1}$ and that at a freshwater-influenced (salinity < 5) Finnish archipelago 70 nmol L^{-1} ; thus, the value determined at lander 1 was within the typical coastal range (Humborg et al., 2019). Although CH_4 concentrations at lander 1 varied by one order of magnitude ($17 - 143 \text{ nmol L}^{-1}$), the range was lower than that derived from high-resolution data obtained in shallow water of the Baltic Sea ($< 4 \text{ m}$) near Askö Island (Roth et al., 2022). There, variability in August was $53 - 460 \text{ nmol L}^{-1}$, measured in a habitat with vegetation comparable to that in the Hütelmoor study area but located in a more northern and enclosed environment. Two previous studies of coastal CH_4 conditions were available that roughly covered the area of the lander deployments and relied on discrete samples: (i) in summer 2017, a mean concentration of $25.3 \pm 9.3 \text{ nmol L}^{-1}$ was determined (Jurasinski et al., 2018), corresponding to the lower range than that measured at lander 1, and (ii) from March 2016 to June 2017, a larger discrete sampling campaign yielded a mean concentration of $27 \pm 29 \text{ nmol L}^{-1}$ (in a range of $5 - 162 \text{ nmol L}^{-1}$), consistent with the high-resolution data presented here (Kreuzburg, 2019). In the latter study, during a pronounced salinity gradient between ~ 9 in surface water and ~ 19 in bottom water, the accumulation of CH_4 reached a maximum of 162 nmol L^{-1} in September. This value is consistent with the maximum value of 111 nmol L^{-1} measured over the course of the lander deployment, which also coincided with a stagnation event.

Measuring coastal nutrient concentrations is important because coastal regions, particularly archipelagos, play an important role in reducing nutrient fluxes from land to the open Baltic Sea, with reductions of nitrogen and phosphorous inputs from land of 16 % and 52 %, respectively (Asmala et al., 2017). However, sensor-based measurements of NO_3^- concentrations in the Baltic Sea are challenging due to the complex composition of its waters. For example, NO_3^- determination is affected by colored dissolved organic matter (CDOM) and by the increased scattering that occurs due to the high turbidity and re-suspension. These time-varying effects can lead to sensor responses in the absence of a change in NO_3^- concentrations. PO_4^{3-} measurements were in high accordance with the bottle data and were less problematic than NO_3^- measurements, but the autonomous data were limited due to a hardware failure. Nevertheless, the available data showed an increase in the PO_4^{3-} concentration during a period of stagnation and, simultaneously with a depletion of O_2 (Figure 4). The release of PO_4^{3-} could be due to the mineralization of OM or due to release from

anoxic sediments (Mort et al., 2010), but no information on O₂ conditions in the sediments was available.

4.1.2 Drivers of nearshore variability

The GHG partial pressures were characterized by high temporal variability, which was resolved by the sensor measurements. Changes in the $p\text{CO}_2$ occurred over the short-term, e.g., in the magnitude of 700 – 830 μatm within 6.5 – 12 h, while those in CH₄ were also pronounced but occurred over slightly longer time scales and more frequently (Figure 4a, b). For example, CH₄ varied over ranges of $\sim 92 - 123 \text{ nmol L}^{-1}$ (60 – 80 μatm) and 107 – 138 nmol L^{-1} (70 – 90 μatm) within 12 – 17 h and 21 – 27 h at lander 1 and lander 2, respectively. In the literature, temporal variations in $p\text{CO}_2$ and CH₄ in coastal regions within a few hours have also been reported. In the case of $p\text{CO}_2$, dynamics were described as diurnal fluctuations driven mainly by biological factors (Honkanen et al., 2021). However, the latter fluctuations had a much lower amplitude than those recorded in this study. Diurnal cyclicity coupled to solar irradiance was not detected in the Hütelmoor survey, which is not unusual given the lower solar irradiance in September. In other studies, the variability of CH₄ in bottom waters in the vicinity of the Hütelmoor area (Jurasinski et al., 2018; Kreuzburg, 2019) was also described as dynamic.

In this Hütelmoor survey and based on the high-resolution measurements, three event-based changes that led to GHG changes within hours were identified and are described below; they are likely examples of controlling coastal GHG variability.

4.1.2.1 Advection of saline waters with a strong mineralization signal – FINN-I

The advection event (FINN-I) was shaped by a rapid increase in bottom salinity, by ~ 5 , with a sharp slope during its appearance and disappearance (Figure 4d). This was accompanied by a bottom water O₂ decrease, during which time the lowest values of $\sim 60 \%$ saturation were measured, while the temperature changed only marginally. Within the ~ 30 -h lasting event, alongshore currents reached high velocities and a fast reversal in direction. However, since wind speeds were low to moderate, local wind was probably not the main driver of the advective transport. The numerical model simulation indicated that the advective signal reached the lander only below a water depth of 2 – 3 m, as the incoming water had a higher density (Figure 6). The origin of the signal was identified by the three-dimensional flow information from the model calculation as a water mass from the deeper northwestern part, from where water was transported toward the landers from a water depth of ~ 20 m with a

salinity of ~ 20 . The result was a temporal stratification of the water column and $p\text{CO}_2$ values of up to $1000 \mu\text{atm}$ in bottom waters, but with negligible changes in $p\text{CH}_4$. The latter can probably be explained by the fact that the water masses were still oxygenated.

Thus, a water mass that transported a mineralization signal characterized by the high $p\text{CO}_2$ values of the original water mass ultimately reached the coastal area. In the case of a mixing of the water mass with the shallow water column can lead to supersaturated CO_2 conditions in the surface waters. This observation resembled nearshore upwelling events recently described for the Baltic Sea (e.g., Jacobs et al., 2021). For example, a similar pattern was described for a coastal environment where $p\text{CO}_2$ reached $> 800 \mu\text{atm}$, although not as close to the coast as in this study and occurring during a summer heat wave (Humborg et al., 2019). The salinity, O_2 , and $p\text{CO}_2$ of FINN-I had a two-part structure associated with a fast reversal of the water velocity (Figure 4). According to the numerical model, another, local waterfront was pushed toward the coast from the northwest with slightly altered O_2 and $p\text{CO}_2$ values. O_2 and $p\text{CO}_2$ values altered as the water mass likely resided in slightly deeper water for a few hours, where they may have been subject to ongoing biochemical processes or mixing.

4.1.2.2 A storm event – FINN-II

Sustained high wind speeds for ~ 4 days characterized this event. During this period, maximum wind speeds reached $\sim 19 \text{ m s}^{-1}$ (Figure 4l), which was high in relation to commonly recorded local values, as winds with this velocity have only been measured 18 times since 2010 (X. Lange, IOW, personal communication, 2022). The high winds triggered a high alongshore water velocity and large fluctuations in the water pressure. The standard deviation of the pressure was persistently high (Figure 4f) and indicated turbulent surface water conditions, with a derived wave height of $\sim 80 \text{ cm}$. The surface dynamics (i.e., waves) led to a well-mixed water column, which was confirmed by the modeled salinity distribution in the water column (Figure 6). Turbidity, measured at the bottom waters, increased and correlated with wind speed, water pressure, and the standard deviation of the pressure during FINN-II (Figure 9). The storm event likely resulted in turbulence at the sediment surface and thus in fluffy layer transport and sediment re-suspension. The latter is an important process inducing pore water interactions that could lead to chemical exchanges (e.g., OM, GHGs, nutrients) between water and sediment (e.g., Massel, 2001; Beer et al., 2005). However, the strong water mixing was not accompanied by a clear signal for $p\text{CO}_2$ or NO_3^- . Indeed, the NO_3^- correlation with turbidity appears to be a valid observation, as NO_3^-

could have been released from the pore water, but the optical determination could also reflect the presence of CDOM, which could have been significantly affected by the resuspension. A similar pattern of non-response to re-suspension was observed for $p\text{CH}_4$; since methane is mostly produced in anoxic sediments, its release during re-suspension was expected. However, CH_4 did not correlate positively either with wind speed or turbidity (Figure 9). In contrast, an anti-correlation of CH_4 with the water pressure was determined. This observation is related to the CH_4 accumulation in the sediment during periods of increased water pressure and a release from the pore water in response to a relaxation due to a lower water pressure. However, this effect has been predominantly described for tidal systems (e.g., Linke et al., 2010; Römer et al., 2016). In fact, the described effect of a changing pressure on the CH_4 release was less pronounced when the correlation of the entire time series during the Hütelmoor deployment was considered (Figure 7).

4.1.2.3 A stagnation event – FINN-III

A long stagnation phase at the end of the deployment included a ~ 5 -day period of stable temperature, salinity, and pressure values as well as a low wind speed (Figure 4). During this event (FINN-III), a decoupling between bottom and surface waters and the formation of vertical temperature, salinity, and O_2 gradients were observed (Figure 6), with lower O_2 levels measured at the landers than 3 m above the sediment (Figure 5). Stagnation may allow local processes to become more established, resulting in small-scale gradients due to accumulation or depletion processes. This was likely the case for $p\text{CH}_4$, which increased linearly according with a slope that was different from previous peaks. The increase suggested the local mineralization of OM in anoxic environments and the accumulation of CH_4 in bottom waters during calm conditions. Furthermore, $p\text{CH}_4$ increased faster at lander 1, resulting in values different from those at lander 2 at the end of this event. This was attributed to the location of lander 1 in a position closer to potential peat deposits and ~ 1 m deeper than lander 2. It can be assumed that CH_4 production was (i) driven by the higher OM availability, as peat releases DOC from pore water (Tiemeyer et al., 2016), and (ii) anoxic conditions in the sediment established earlier and to a larger extent. An indication was delivered by the measurements 1 m above the sediment at each lander (Figure 5) showed that O_2 at lander 1 was more depleted.

High CH_4 concentrations were also detected in a coastal area in the southern region of the North Sea, where gassy sediments and peat deposits were associated with these elevated

concentrations (Borges et al., 2016). There, these high bottom-near concentrations also resulted in high CH₄ emissions because the shallow and well-mixed water column led to an effective transfer of CH₄ from the seafloor to the surface water, and CH₄ could hardly be oxidized (Borges et al., 2016). Thus, CH₄ could also be released to the atmosphere during conceivable mixing of the water column at the end of FINN-III.

Spatial differences among the landers were also detected for PO₄³⁻, NO₃⁻, chlorophyll *a*, and *p*CO₂ during this period, suggesting that the responsible processes can be locally quite heterogeneous, even within a distance of only ~ 700 m. This is in accordance with a previous study in this area that reported cross-slope gradients with slightly different salinities and temperatures after a short period of stagnation close to the shore and with low spatial extension (Jurasinski et al., 2018). Therefore, knowledge of these local processes and their drivers is important for the characterization of sinks and sources and for a better estimation of the role of coasts as sources of GHG release into the atmosphere.

4.1.3 Implications of these lander deployments

The sensor measurements have captured the prevailing heterogeneity, at least during a limited time period in summer 2019. Discrete samples would insufficiently describe such measured temporal dynamics, but can be important to verify the sensor data, exemplified by O₂ measurements at lander 2. A recent study found that up to 50 discrete samples per day are required to resolve such a scale of coastal dynamics (Roth et al., 2022). The implementation of a numerical model in the Hütelmoor study provided important information, such as regarding the conditions in the water column or large-scale transport processes, and hence supported the stationary measurements and demonstrated the power of interdisciplinary approaches in investigations of coastal dynamics.

The CO₂ observations suggested event-based changes in the water column as the driver of the dynamic conditions of the nearshore water column during low-productivity seasons. This implied that coastal CO₂ is driven in part by rapid transport signals (i.e., mineralization) from deeper parts of the adjacent Baltic Sea. While turbulent and well-mixed conditions had no effect, stagnant conditions and local processes such as mineralization likely controlled CO₂ during stagnation. However, in contrast to the straightforward dynamics and drivers of CO₂, in the case of CH₄ they were ambiguous, such that long-term studies and/or the incorporation of other information might be necessary. For example, CH₄ did not respond consistently to turbulent water conditions and re-suspension at the sediment surface, as observed during the

deployment. The correlation analysis revealed a weak relationship of CH₄ with the water column height, as described as an important process controlling bottom CH₄ concentrations in tidal systems (e.g., Linke et al., 2010; Römer et al., 2016). In addition, CH₄ increased during calm water conditions, which was likely released from the porewater. The correlation analysis of the individual periods FINN-I – III (Figure 8, Figure 9, Figure 10) indicated that temperature is an important driver of CH₄ concentrations in the shallow waters of the Hütelmoor area, as a positive correlation between the two was determined in all three events and it was the only correlation common to all of them. This temperature control was identified as an important driver of coastal CH₄ production in shallow nearshore waters (e.g., Bange et al., 1998; Heyer and Berger, 2000) and these observations imply that global warming increases coastal CH₄ emissions, as also proposed by Humborg et al. (2019).

4.2 Drammendorf field survey

The content of section 4.2 was partially published in Pönisch et al., 2023. Nutrient release and flux dynamics of CO₂, CH₄, and N₂O in a coastal peatland driven by actively induced rewetting with brackish water from the Baltic Sea, Biogeosciences, 20 (2), 295–323, <https://doi.org/10.5194/bg-20-295-2023>. The respective paragraphs have been changed for linguistic and conceptual reasons to conform with the overall style of this dissertation.

In the following, before GHG responses during the transition from dry to flooded conditions and the effects of brackish water are evaluated, the characteristics of the post-flooding water column situation are described.

4.2.1 Development of the CO₂ system after flooding

The CO₂ system (C_T , A_T , pH, pCO_2) of the study area is shaped by a variety of processes, which were influenced by transport mechanisms or local processes, acting on different temporal and spatial scales (Wolf-Gladrow et al., 2007; Kuliński et al., 2017; Schneider and Müller, 2018). Carbon fixation and the formation of OM decrease C_T and lower pCO_2 , by simultaneously increasing the pH. The mineralization of OM, including that derived from other sources (i.e., in situ primary production, inundated vegetation after flooding, or underlying peat deposits), in turn increases the C_T and A_T concentrations as well as the pCO_2 and lowers the pH. A_T can be further transported with brackish water originating from the more central Baltic Sea or can be added by a freshwater supply (Beldowski et al., 2010; Müller et al., 2016). A water column pCO_2 above atmospheric equilibrium, as observed during most of the study period, results in a loss of CO₂ from the water column and a decrease in C_T .

Two major developments in the surface water CO₂ system were identified and are discussed in the following: (i) in winter 2019/2020, the CO₂ systems of the peatland and the inner bay hardly differed; (ii) from spring to autumn, the CO₂ systems of the peatland and the inner bay differed significantly, with higher $p\text{CO}_2$, C_T , and A_T values and a lower pH in the peatland that coincided with an enrichment of chlorophyll *a* concentration.

4.2.1.1 The initial conditions in the winter after flooding

The marine environment of the peatland and adjacent *Kubitzer Bodden* in winter 2019/2020 can be described together, because the respective CO₂ systems differed only marginally (Figure 12, Figure 13a). The first few weeks after rewetting were characterized by high nutrient concentrations, a continuous increase in A_T , C_T , and pH, and a decrease in $p\text{CO}_2$. The increase in C_T and A_T coincided with a steady increase in salinity (Figure 11), in line with the general increase of A_T with increasing salinity that is known for the western Baltic Sea (e.g. Kuliński et al., 2022). The measured A_T background was higher than expected from the linear A_T -salinity relationship described for the open Baltic Sea (Beldowski et al., 2010; Müller et al., 2016). Presumably, the higher A_T was associated with local CaCO₃ weathering or was the product of leaching from the recently inundated peat and anoxic processes such as SO₄²⁻ reduction.

The winter was further shaped by an unusually early, brief onset of primary production during mid/end of January that amplified the decline in $p\text{CO}_2$ until spring (Figure 11). In addition to other drivers of the decrease in $p\text{CO}_2$ until spring, such as $p\text{CO}_2$ oversaturation, the brief onset in primary production was triggered by an early increase in water temperature and by the high nutrient availability.

4.2.1.2 The productive phase (spring to autumn) and high $p\text{CO}_2$

From mid-spring to late summer, the nitrogen-limited surface water of the peatland had high mean chlorophyll *a* concentrations, with a single recording of up to 106.0 µg L⁻¹ (Figure 11, Table 6). In addition, O₂ saturation shifted from over- to undersaturated conditions, while $p\text{CO}_2$ increased but was also variable (Figure 13a). These observations indicated simultaneous production and mineralization processes in the peatland that kept the concentrations of N-nutrients (except for PO₄³⁻) low. However, the mineralization of OM in the water column, sediment, and soil dominated over production, resulting in a high $p\text{CO}_2$, lowered pH and enhanced A_T and C_T concentrations. This stronger mineralization, especially during the warm summer months, led to an increase in DOC concentrations, with a maximum in June/July that

coincided with maximum surface water temperatures. The enhanced mineralization in the peatland was likely facilitated by the higher OM availability from high decomposition rates of fresh plant substrate from inundated plant residuals (Glatzel et al., 2008; Hahn-Schöfl et al., 2011). In addition, the aerobic and anaerobic oxidation of CH₄ produced in anoxic zones may have increased CO₂ production, especially during increased water temperatures (Treude et al., 2005; Dean et al., 2018), due to the availability of SO₄²⁻ and O₂.

4.2.2 The development of CH₄ after flooding

Two major developments in surface water methane concentrations were identified and are discussed in the following: (i) a short-term, very moderate increase in CH₄ concentrations directly after rewetting in winter 2019/2020 and (ii) an increase in CH₄ concentrations mainly from spring to autumn that was significantly larger and more variable in the peatland than in the inner bay and correlated with water temperature.

4.2.2.1 The initial conditions in the winter after flooding

Winter CH₄ concentrations in the surface water were low (Figure 13b), although sufficient OM was available for CH₄ formation. Flooding of the organic-rich peat and the unremoved vegetation and its subsequent die-back provided OM for methanogenesis (Heyer and Berger, 2000; Parish et al., 2008) hence, in the winter after rewetting the availability of OM was apparently not a limiting factor. Therefore, the low CH₄ concentrations were associated with the low water temperature, as a factor that controls microbial processes such as CH₄ production. A study in a nearby shallow coastal area of the Baltic Sea, between the islands of *Rügen* and *Hiddensee*, showed that water temperature was the major factor in emissions, with low rates associated with low temperatures (Heyer and Berger, 2000). Along with temperature control, the rewetting transported SO₄²⁻, which as a TEA promoted the establishment of SRB able to outcompete methane-producing microorganisms (methanogens) for substrates (Segers and Kengen, 1998; Jørgensen, 2006; Segarra et al., 2013). Methanogenesis may also have been suppressed by the availability of other TEAs, such as NO₃⁻ (Jørgensen, 2006), which reached concentrations of $\sim 100 \pm 58 \mu\text{mol L}^{-1}$ in the winter. In addition to competitive mineralization and temperature control, CH₄ concentrations may have been reduced by aerobic and anaerobic oxidation (Heyer and Berger, 2000; Reeburgh, 2007; Knittel and Boetius, 2009; Steinle et al., 2017). Overall, rewetting with brackish water during the cold winter apparently limited methanogenesis and stimulated effective oxidation, resulting in low CH₄ concentrations.

4.2.2.2 The productive phase (spring to autumn) and high CH₄ concentrations

From spring to autumn, water temperature increased, accompanied by enhanced CH₄ concentrations. Temperature is crucial in controlling CH₄ cycling in shallow nearshore waters (Bange et al., 1998; Heyer and Berger, 2000; Borges et al., 2018), and this control was also described for permanently inundated wetlands (e.g., Koebsch et al., 2015) and for a peatland close to our study site during the first year after rewetting (Hahn et al., 2015). Consequently, the temperature increase was assumed to be one of the main causes of the increased CH₄ concentrations. However, CH₄ concentrations in the flooded peatland were significantly higher than in the inner bay (Figure 13b; Pönisch et al., 2023), suggesting the availability of OM as another important driver of peatland CH₄ concentrations in summer. This assumption is in accordance with incubation experiments conducted in a degraded fen grassland, in which the accumulation of fresh plant litter in a new sediment layer after flooding resulted in high rates of CH₄ and CO₂ production (Hahn-Schöfl et al., 2011). A further potential source of OM availability was the sedimentation of freshly produced OM originating from primary production, as described for shallow areas in the Baltic Sea (Bange et al., 1998) and for a shallow bight in the North Sea, which in the latter case led to a yearly peak in the seasonal CH₄ cycle (Borges et al., 2018). Although OM-poor sediments were not a feature of the Drammendorf site, a role of primary production in the enhanced CH₄ concentrations in the OM-rich peatland was likely, given the significant positive correlation of the surface CH₄ concentration and the chlorophyll *a* concentration ($r_s = 0.41$, $n = 56$, $p < 0.05$).

4.2.3 The role of brackish water in GHG fluxes – a system shift

In general, with the rewetting of drained peatlands and the increased water levels, water-saturated zones in the peat soil become larger, such that the decomposition of OM is no longer oxygen-induced and relies on alternative TEAs, for example NO₃⁻ and SO₄²⁻, leading to a reduction in CO₂ emissions (Strack, 2008; Dean et al., 2018). With the reduced O₂ availability and a depletion of TEAs in anoxic zones, methanogenesis is established. Thus, rewetting with freshwater is often associated with high CH₄ emissions (Hahn et al., 2015), which counteracts the goal of GHG (CO₂) reduction. However, the Drammendorf peatland was flooded with brackish water, such that SO₄²⁻ was readily available after flooding. As noted above, SO₄²⁻ reduces CH₄ emissions as it allows SRB to outcompete methanogenic archaea (Bartlett et al., 1987; Capone and Kiene, 1988; Oremland, 1988; Jørgensen, 2006). Consequently, CH₄ emissions should be lower than in peatlands rewetted with freshwater.

4.2.3.1 Sustained high CO₂ fluxes

Average summer/autumn CO₂ fluxes after rewetting had a mean of $0.26 \pm 0.29 \text{ g m}^{-2} \text{ h}^{-1}$ and thus remained relatively high compared to those fluxes from 2019 (Table 6b). They were also two orders of magnitude higher than in a nearby coastal peatland recently influenced by brackish water inflow, where ecosystem respiration was investigated (Koebsch et al., 2020). The main reason for the persistently high CO₂ fluxes in Drammendorf in the first year after rewetting was probably the decomposition of submerged vegetation and fresh, easily degradable substrates (Hahn-Schöfl et al., 2011). Another source of the high CO₂ emissions after flooding may have been the mineralization of OM from the primary production driven by the high initial nutrient availability. Aerobic and anaerobic oxidation (Dean et al., 2018) of CH₄ can also release CO₂. CO₂ emissions at Drammendorf are expected to decrease in the future, likely because substrates become exhausted, and a new ecosystem will be established (Kreyling et al., 2021), with developing of algae fostering CO₂ fixation. Another observation was the decreased amplitude of CO₂ fluxes at formerly dry stations after their rewetting with brackish water. This resulted in a die-back of the highly productive grassland vegetation that was established before rewetting. Therefore, the elevated water table was likely the main driver of the reduced amplitude of CO₂ fluxes, as the rates of photosynthesis and ecosystem respiration sharply decreased after rewetting, as also described for a nearby coastal peatland (Koebsch et al., 2013). The die-back at Drammendorf likely occurred faster than after rewetting with freshwater (Hahn-Schöfl et al., 2011).

4.2.3.2 Moderate increase of the CH₄ fluxes

Despite the high surface-water concentrations of CH₄ in the peatland and their inter-seasonal and spatial variability (Figure 13b), rewetting with brackish water resulted in CH₄ emissions considerably lower than those from temperate fens rewetted with freshwater, where CH₄ emissions strongly increased (Augustin and Chojnicki, 2008; Couwenberg et al., 2011; Hahn et al., 2015; Franz et al., 2016; Jurasinski et al., 2016). Average CH₄ fluxes in Drammendorf on formerly terrestrial locations increased significantly, by one order of magnitude, after rewetting, but the overall increase from 0.13 ± 1.01 to $1.74 \pm 7.59 \text{ mg m}^{-2} \text{ h}^{-1}$ (Figure 14, Table 6b) was lower than that reported for freshwater rewetted fens under similar climatological boundary conditions (e.g., Hahn et al., 2015; Franz et al., 2016). For example, even several years after rewetting, the annual CH₄ budgets of a shallow lake on a formerly drained fen ranged from 1.5 to 6.0 $\text{mg m}^{-2} \text{ h}^{-1}$ (numbers derived from Franz et al., 2016). The CH₄ fluxes from Drammendorf were also lower than the emissions from coastal shallow

waters of the Baltic Sea, where fluxes of 39.9–104.2 mg m⁻² h⁻¹ were measured in June/July (Heyer and Berger, 2000). For the same months, mean CH₄ fluxes at the formerly dry stations in the Drammendorf study site were 0.5 – 4.9 mg m⁻² h⁻¹. Nevertheless, it must be stressed that Drammendorf was a source of CH₄ already in its drained state, especially within the drainage ditch, where CH₄ fluxes were comparable to the ~ 0.2 mg m⁻² h⁻¹ reported from an undrained fen (Danevčič et al., 2010).

The lower CH₄ emissions from the brackish rewetted Drammendorf peatland than from freshwater-rewetted systems can be attributed to the availability of TEAs, especially SO₄²⁻, which (i) may have contributed to a suppression in methanogenesis by competitive inhibition (Segers and Kengen, 1998; Jørgensen, 2006; Segarra et al., 2013) or (ii) fostered AOM as an effective pathway to reduce CH₄ emissions, or (iii) by promoting fast aerobic CH₄ oxidation mediated by oxygen-rich water. Similarly, the high variability in the CH₄ concentrations may have been related to the changing rates of AOM, as the process is sensitive to the introduction of O₂ such as mediated by sporadic wind-driven re-suspension (Treude et al., 2005). Since Drammendorf is shallow and is probably regularly subjected to wind-driven re-suspension, spatially and temporally dynamic AOM can be assumed. Moreover, higher CH₄ concentrations in the peatland than in the inner bay (Figure 13b) in combination with the high lateral water exchange due to frequent changes in the water level should have driven a net advective export of CH₄-enriched water to the inner bay. This would have further contributed to the low peatland CH₄ emissions and the observed high variability.

4.2.3.3 Low annual N₂O flux after rewetting

The rewetted peatland was a source of N₂O in the first year after rewetting, although the mean annual N₂O flux of 0.02 ± 0.07 mg m⁻² h⁻¹ was very low (Figure 14c). This was expected because permanent inundation leads to anoxic conditions in peat and prevents the formation of N₂O (Succow and Joosten, 2001; Strack, 2008). In general, N₂O fluxes in rewetted peatlands are of the same order of magnitude as in pristine peatlands (Minkkinen et al., 2020), suggesting that rewetting is a very effective measure to reduce N₂O emissions. The literature values range from 0.01 and 0.02 mg m⁻² h⁻¹ for rewetted and undrained boreal peatlands, respectively (Minkkinen et al., 2020), to 0.08 mg m⁻² h⁻¹ for a rewetted riparian wetland near a freshwater meadow (Kandel et al., 2019). Although it is difficult to compare the N₂O fluxes determined in this study with those from other sites with different salinities, hydrologies, and

histories of usage, the mean annual post-rewetting values of Drammendorf were in the lower range of the N₂O fluxes previously reported for rewetted and pristine peatlands.

4.2.4 Nutrient dynamics after rewetting

After rewetting, NO₃⁻, NO₂⁻, and NH₄⁺ concentrations were high in winter and autumn (Table 6a), which could be attributed to the mineralization of OM followed by nitrification (Voss et al., 2010) or to a release from the peat soil. By contrast, the low dissolved inorganic nitrogen concentrations during spring and summer coincided with the strong presence of a phototrophic community (high chlorophyll *a* concentrations) and reflected N consumption by plants and phytoplankton. Nevertheless, compared to the *Kubitzer Bodden* the peatland nutrient concentrations (nitrogen species and phosphate) were generally higher, especially during periods of low phototrophic activity (data not shown). The Drammendorf peatland therefore acted as a source of nutrients, by transporting dissolved compounds to the adjacent *Kubitzer Bodden* (Pönisch et al., 2023). The higher nutrient concentrations in the peatland were associated with previous mineralization of the upper peat layers and the accumulation of nutrients in the soil (Zak and Gelbrecht, 2007; Cabezas et al., 2012). After rewetting and the establishment of water-saturated soils, nutrient concentrations increase in the porewater and ultimately in the overlying water (van de Riet et al., 2013; Harpenslager et al., 2015; Zak et al., 2017), which was probably also the case in Drammendorf. This potential for leaching depends on different factors, but highly degraded peat can store and release more nutrients than less degraded ones (Cabezas et al., 2012).

4.3 The Drammendorf lander survey

4.3.1 Temporal and spatial variation of CO₂ and CH₄ distribution at lander 1 and lander 2

The deployment of two landers equipped with sensors for high-resolution measurements of physicochemical variables, including *p*CO₂ and *p*CH₄, in a challenging coastal peatland revealed large temporal and spatial variations. Temporal variations occurred on multi-day or diurnal scales or dependent on specific events. Spatial differences in the peatland were reflected in variables dominated by biological processes. Unfortunately, the absence of a study covering a comparable area and with comparable data resolution hinders comparisons, but in general the measured variations were much more pronounced than at coastal areas.

The time series of the measured physical parameters (i.e., temperature and salinity) showed strong fluctuations on multi-day and diurnal scales (Figure 15c, d). However, the differences between the data series obtained at the two lander positions were very small, due to the strong spatial coupling between the two sites by advective flow, which was an important general characteristic of the study area. The coupling is the product of the short distance between the two landers of ~ 400 m, but it is also due to the pronounced water exchange with the adjacent *Kubitzer Bodden* during the frequent changes in the water level (Figure 15e). This exchange transports brackish water containing SO_4^{2-} into the flooded peatland. Together with the wind-induced mixing of the shallow water column, this resulted in a mostly well-mixed water column, such that long-term anoxic or stagnant conditions in the bottom water cannot be assumed (Figure 15f). This conclusion is consistent with the results of the Drammendorf field study, which covered a longer time period but at a much lower temporal resolution. The hydrologic coupling implied that the peatland became part of the coastal water region as a result of flooding and that the observed biogeochemical patterns in the study area were influenced by processes occurring not only in the rewetted peatland but also in the adjacent *Kubitzer Bodden*.

Thus, as a result of hydrological coupling, the time series of most biogeochemical variables recorded by the two landers were partially coupled, as evidenced by similar responses in the form of multi-day variability and event-based changes (Section 4.3.3). For example, the multi-day variations, especially the decrease in $p\text{CO}_2$ and $p\text{CH}_4$, appeared to be coupled to the increased wind speeds that followed windless phases, with a parallel decrease in temperature. Conversely, GHG concentrations increased again during windless periods, as also indicated by the slightly negative correlations of both GHGs with wind speed (Figure 16). With increasing wind, ASE and water exchange with the *Kubitzer Bodden* were enhanced. This apparently induced both a reduction of the accumulated GHGs to atmospheric/coastal Baltic Sea background conditions and presumably a lower water temperature due to mixing with slightly colder water from the *Kubitzer Bodden* or to colder air temperatures. Superimposed on the multi-day fluctuations were diurnal cycles, discussed in Sect 4.3.2.

However, in contrast to the coupled patterns, spatial differences were detected, especially for $p\text{CO}_2$, $p\text{CH}_4$, and O_2 , and thus for those variables most strongly influenced by biological processes. These spatial differences were mainly reflected in the differences between the means and standard deviations of the data from the two landers (Table 7). While the variability

in $p\text{CO}_2$ was comparable, a higher mean $p\text{CO}_2$ was recorded at lander 1 than at lander 2. The higher values in the central peatland and thus at lander 1 were associated with a higher availability of OM than at lander 2. The possible sources of that higher availability included mineralization of flooded former vegetation/plant residuals (Hahn-Schöfl et al., 2011), degraded peat, and the OM supply from new primary production. A similar situation would be expected for $p\text{CH}_4$, with higher values in the central, OM-enriched area of the peatland (i.e., at lander 1), as the availability of OM is a major driver of CH_4 formation (Heyer and Berger, 2000; Glatzel et al., 2008; Parish et al., 2008; Hahn-Schöfl et al., 2011). However, slightly higher and more variable $p\text{CH}_4$ values were determined at lander 2, consistent with the lower O_2 values (Figure 15). This was likely due to (i) a slightly deeper position of ~ 0.3 m than at lander 1, resulting in faster O_2 depletion/ CH_4 production during calm conditions and (ii) local transport processes from the *Kubitzer Bodden* or the peatland due to the high velocities in the connecting ditch (inflowing/outflowing water), apparently leading to a higher variability. This unique flow regime could have led to local erosion/re-suspension and variable CH_4 release from the soil. Furthermore, because the sediment surface is heterogeneous, it may have contained local hot spots for CH_4 production, which would have affected data from lander 2. Based on a correlation analysis, temperature control of CH_4 as described in the literature (e.g., Bange et al., 1998; Heyer and Berger, 2000) was more pronounced only at lander 1, where local production and decay were likely to have been the dominating processes (Figure 16). In contrast, water movement might have played a larger role at lander 2. Surprisingly, however, at both landers CH_4 correlated negatively, with a medium effect size, with wind speed (Figure 16). Wind can trigger re-suspension, promote pore water flows, and enhance the transport of soluble compounds, including CH_4 accumulated in the soil, into the water column (e.g., Massel, 2001; Beer et al., 2005). In turn, an enhanced wind speed also increases ASE-induced losses to the atmosphere, which would explain the negative correlation.

4.3.2 Diurnal $p\text{CO}_2$ and $p\text{CH}_4$ variability

Solar irradiance causes a diurnal cycle in the physics, chemistry, and biology of water bodies and has a powerful effect in shallow waters. As a result, diurnal cycles of $p\text{CO}_2$ and $p\text{CH}_4$ in shallow waters are coupled to a temperature-controlled cycle (e.g., solubility), air-sea exchange (i.e., wind parametrization), and a biological component enhanced by highly eutrophic conditions (cycle of primary production and mineralization). During lander deployment, the highest GHG partial pressures (CO_2 , CH_4) were measured in the morning

and the lowest in the afternoon, with a much more pronounced cyclicity for $p\text{CO}_2$ (Figure 17). A anti-correlation of the GHG partial pressures with temperature and O_2 cycles was also determined (Figure 17). However, based on the diurnal temperature cyclicity, lower GHG partial pressures would be expected at lower temperatures and vice versa, due to the temperature-dependence of the solubility. Since this was not the case, the reduction in $p\text{CO}_2$ caused by primary production exceeded the expected temperature effect. This was evident during the day, when the biologically controlled $p\text{CO}_2$ minimum coincided with the less influential temperature-controlled diurnal $p\text{CO}_2$ maximum. At night, the opposite occurred, and mineralization-induced enrichment was more important than the cooling-induced lowering of the $p\text{CO}_2$. The dominance of production (and mineralization) was supported by the strong negative correlation with O_2 (Figure 16). This relationship, representing a stronger biological than physical (temperature) control of $p\text{CO}_2$, was also recently described for a shallow area on the Baltic coast near Utö Island in August, but with a much lower maximum amplitude of $108 \mu\text{atm}$ (Honkanen et al., 2021). The cyclicity of $p\text{CH}_4$ in Drammendorf was lower, in line with equally important roles for other controlling parameters such as the water exchange rate or wind speed. Hence, ASE which is parameterized by wind, can contribute to cyclicity if the wind has a diurnal cycle. During lander deployment, wind velocities were higher during the day (classical coastal sea breeze setting; Figure 17e). Since the water volume to water surface ratio was relatively large, the GHG minima (CO_2/CH_4) may also have been due to the increased ASE during the daytime.

4.3.3 Event driven variability in the rewetted peatland

In addition to the multi-day and diurnal variability, three influential system changes (events I – III) occurred during the lander deployment (Figure 15). Like the diurnal cycles, these events occurred rapidly (on the order of hours to days) such that they could only be tracked by high-resolution measurements. Although the flooded peatland is semi-enclosed by a 20 m wide channel, water mass exchange occurs almost exclusively through this channel, such that the *Kubitzer Bodden* acts as a start- and endmember for external signals.

The first event (I) was characterized by elevated wind speeds that led to an inflow of water after a short runoff, a fast drop in temperature of $\sim 13^\circ\text{C}$, a peak in turbidity, and lowered GHG concentrations. The inflow likely resulted in a dilution effect, transporting water with lower GHG concentrations from the *Kubitzer Bodden*. At the same time, the decrease in temperature would have reduced microbial activity, as this relationship has been described

especially in coastal regions (Bange et al., 1998; Heyer and Berger, 2000) and is consistent with the drastically suppressed amplitude of the diurnal cycles of $p\text{CO}_2$ and $p\text{CH}_4$ (Figure 15a, b). During the event, turbidity increased at both lander positions, indicating increased re-suspension. Although re-suspension can trigger the exchange of soluble compounds and GHGs between the soil/sediment and the water column (e.g., Massel, 2001; Beer et al., 2005), this was not reflected in the data (low $p\text{CO}_2$ and $p\text{CH}_4$ during the turbidity maximum). With increased wind speed, ASE increased, such that the ventilation of GHGs to the atmosphere likely contributed to the generally lower GHG partial pressures, although this could not be confirmed by the correlation analysis (Figure 18). The partial pressures of the GHGs and the strength of the diurnal cycles recovered over the course of a few days and, simultaneously, the water temperature returned to pre-event conditions.

The second event (II) demonstrated the impact of freshwater inputs from strong precipitation and resulted in a rapid drop of salinity (within one day) as well as a potential outflow of water due to a positive water balance. The salinity remained low after this event and increased only slowly. The partial pressures of both GHGs declined and had a lower diurnal amplitude. A dilution effect due to the precipitation presumably occurred, while the positive water balance caused the transport of dissolved compounds towards *Kubitzer Bodden*. The precipitation-induced transport of dissolved compounds, including nutrients and OM, from the terrestrial catchment into the peatland water was likely and could have influenced GHG dynamics thereafter.

The third event (III) comprised a sustained outflow, resulting in a water column of ~ 0 m height at lander 1, followed by an inflow of water that restored normal conditions. The very low water levels prevailed for around 24 h, during which time the water temperature, $p\text{CO}_2$, $p\text{CH}_4$, and O_2 decreased, with an additional decline in the diurnal amplitude. The outflow, lower water volume, and ongoing GHG emissions likely caused a decrease in GHG concentrations in the water. In addition, larger areas of the shallow peatland fell dry, so that O_2 may have infiltrated the soil. The added O_2 together with the lower temperature could have reduced CH_4 production after the water level rose, resulting in low CH_4 concentrations in the water column for several days.

4.3.4 Derivation of GHG fluxes from sensor measurements

The fluxes of the GHGs CO₂ and CH₄ were calculated from the high-resolution sensor data, as measurements were made just below the water surface (< 1.25 m), assuming direct coupling of the bottom water with surface water for most of the time. Although a slight CO₂ uptake was recorded in the peatland in early June, accompanied by stable but slightly decreasing chlorophyll *a* concentrations, ASE was clearly dominated by a flux of CO₂ ($0.122 \pm 0.161 \text{ g m}^{-2} \text{ h}^{-1}$; averaged from both landers) from the water to the atmosphere (Table 8, Figure 21). Beginning in early June, the CO₂ fluxes followed an increasing trend until early July, after which they stabilized in parallel with a generally strong increase in the chlorophyll *a* concentration (Figure 15). Overall, CO₂ emissions in the peatland were controlled by the simultaneous occurrence of primary production and mineralization, with the latter predominating. A comparison of the peatland CO₂ fluxes with the fluxes reported in other studies showed that emissions in Drammendorf were around one order of magnitude higher. For example, nine years after flooding with freshwater, CO₂ emissions from a shallow lake that formed on a formerly drained fen varied from $0.018 \text{ g m}^{-2} \text{ h}^{-1}$ (open water) to $0.086 \text{ g m}^{-2} \text{ h}^{-1}$ (emergent vegetation stands; numbers adapted from Franz et al. (2016)).

The CH₄ fluxes derived in this study ($0.508 \pm 0.564 \text{ mg m}^{-2} \text{ h}^{-1}$) were significantly lower than those reported for temperate fens rewetted with freshwater and with comparable boundary conditions (Couwenberg et al., 2011; Hahn et al., 2015; Franz et al., 2016). At the shallow lake mentioned above, CH₄ emissions ranged from $1.48 \text{ mg m}^{-2} \text{ h}^{-1}$ (emergent vegetation stands) to $6.05 \text{ mg m}^{-2} \text{ h}^{-1}$ (open water) even nine years after rewetting (numbers adapted from Franz et al. (2016)). In another study of a dry fen that had been converted to a shallow lake with occasional brackish water impact, the mean CH₄ flux in the first year after rewetting was of $29.68 \text{ mg m}^{-2} \text{ h}^{-1}$ (Hahn et al., 2015).

4.3.4.1 GHG flux development in the peatland in the second year after rewetting

The studies mentioned above reported annual fluxes, whereas the lander survey was conducted only in the summer months, such that comparability was limited. However, since annual CO₂ and CH₄ emissions are normally higher in late summer than in winter, emissions in the Drammendorf study were likely overestimated compared to the annual means. To allow a direct comparison between similar time periods (summers of 2020 and 2021), measurements from the Drammendorf field survey were used. However, despite the high degree of comparable boundary conditions between the surveys, their comparison was limited by the

slightly different sampling height, which in the field survey was ~ 20 cm below the water surface and $\sim 60 - 90$ cm in the case of the lander survey (and thus unknown time-limited effect of possible gradients in the water column, e.g., O_2), and by the different sampling approaches. In addition, since the studies covered only two years, inter-annual variations that do not indicate a trend cannot be excluded. Thus, the comparison can only indicate a possible trend, and further studies are needed.

From the field survey (2020), ~ 190 measurements were obtained: ~ 35 from the peatland and the remaining from the transect in the vicinity of the later position of lander 1. The high-resolution data from the lander survey were adjusted to the conditions of the field study by using a daily average value of the data collected between 09:00 and 15:00 UTC, during which time discrete sampling was conducted. The comparison showed a trend of decreasing CO_2 and CH_4 fluxes by a factor of 1.9 and 2.6, respectively, within one year (Table 8). The reductions were likely due to the ongoing decomposition of OM from flooded plant residues and fresh plant material after rewetting (Heyer and Berger, 2000; Hahn-Schöfl et al., 2011) and to the continued effectiveness of aerobic and anaerobic CH_4 filtering. Despite the limitations mentioned above, the results indicated future reductions in CO_2 and CH_4 fluxes and thus a favorable outcome of rewetting with brackish water with respect to the GHG balance of the peatland.

4.3.4.2 The impact of temporal bias on GHG flux estimates

The studied peatland featured a high heterogeneity, particularly with respect to GHG partial pressures, which were characterized by multi-day (Figure 15) and diurnal variability (Figure 17). The diurnal variability may have introduced a day-night bias in the ASE estimates. To assess the impact of this potential bias, GHG fluxes were calculated from the continuous time series theoretically based (a) only on nighttime and (b) only on daytime samplings (Table 8).

Comparison of these two scenarios with the ASE derived from entire high-resolution data showed higher daytime and lower nighttime fluxes. Daytime and nighttime CO_2 and CH_4 emissions differed by factors of 2.1 – 2.3, and 2.3 – 3.0, respectively, depending on the lander.

These results showed that studies on flooded peatlands and shallow coastal areas (< 2 m) that are based only on bottle data and conducted, as is usually the case, during the daytime may result in biased estimates of CO_2 and CH_4 fluxes, due to the strong impact of diurnal cyclicity. For the Drammendorf peatland, cyclicity was a dominant factor for variables influenced by

biological processes (Sect. 4.3.2). Furthermore, ASE estimates from this area differed, along with possible additional spatial variability (Sect. 4.3.1). These findings highlight the need for sampling strategies that address the time scales governing variability. A suitable approach to capture these short-term temporal variations is the use of high-resolution, autonomous measurement techniques, such as sensor-based or eddy-covariance measurements. The influence of diurnal cycles in the flooded peatland during the winter months was not investigated in this survey.

4.4 Conceptual assessment of the lander system and data verification

The two lander systems were deployed in different environments during two investigations. The deployment in Hütelmoor took place in the clearer shallow water of the Baltic Sea, deployed by a vessel able to reach the shallow water and using battery powered system; the deployment in Drammendorf was in very turbid water and based on landers with a constant power supply and that needed regular maintenance. The concept underlying the use of the lander systems in shallow water studies, possible improvements, and the quality of sensor-based data in combination with discrete water sampling are discussed in the following.

The duration of the Hütelmoor deployment was limited by battery capacity, as is often the case with studies based on sensor measurements. Apart from the fact that battery replacement to extend the deployment time is often not feasible, the batteries used in the survey were expensive and not sustainable (primary cells). Therefore, alternative power supply concepts have to be evaluated to improve autonomous measurements. In the Drammendorf survey, the landers were adapted for a permanent power supply, but this is only available in certain scenarios. Nevertheless, the wired connection had several advantages, including the establishment of a powerline communication for data/scheduler access. In both surveys, the DPU had a major hardware problem during power consumption peaks that resulted in an overload. As a result, the HCycle-PO₄ instruments failed, leading to limited measurements during the Hütelmoor deployment. During the Drammendorf investigation these instruments were deployed with external batteries.

In the Drammendorf lander survey, a direct comparison of the GHG partial pressures derived from the bottle data (i.e., from concentrations) with the sensor measurements (calculated mean of ~ 10 min prior to discrete sampling) showed good agreement in some cases but also large discrepancies (Figure 15a, b). For example, the differences in the $p\text{CO}_2$ values ranged

from – 2 % to 45 %, and those for $p\text{CH}_4$ from – 21 % to 595 %. Calculation and comparison of the GHG fluxes from the bottle data and sensor measurements allowed the impact of these discrepancies to be evaluated: Higher fluxes were obtained from the bottle data than from the sensor measurements (Table 8). Several potential influences complicate the reconciliation of discrete bottle data with continuous sensor data in heterogeneous environments, such as the fast-changing field conditions, difficult sampling, and long sensor response times (Canning et al., 2021). For example, during the Drammendorf survey, the discrete sampling procedure may have resulted in sediment disturbance/re-suspension due to boat mooring or Niskin bottle movements, thus impacting subsequent sampling. In addition, sampling directly at the pump basket/sensor inlet could not be performed satisfactorily. A possible effect of water heterogeneity was also seen in the duplicate determinations (data not shown) of CH_4 from the bottle data, with some differences of > 25 % (corresponding to several 100 nmol L^{-1}), even though the duplicates were from the same batch of a horizontally inserted Niskin bottle. In future deployments, discrete sampling closer to the sensor inlet, e.g., using an automated discrete water sampler, might lead to more reliable comparisons.

The calculated final values for $p\text{CO}_2$ and $p\text{CH}_4$ from the sensors had small uncertainties. For example, the selected calibration for the measurement of $p\text{CO}_2$ was partially exceeded during the Drammendorf survey. Further, the pumps attached to the HydroC- CO_2 and HydroC- CH_4 instruments did not run reliably, most likely due to sediment transport that reduced the water flow across the membranes. A similar uncontrollable pump flow occurred during the CTD- O_2 measurement, resulting in parts of the data having to be discarded. CTD- O_2 pump failures occurred during both lander surveys and were likely related to the shallow water depths (low hydrostatic pressure), which may have caused the entrapment of air bubbles in the instrument.

Improvements in future deployments can be achieved by adjusting the pumps for HydroC- CO_2 , HydroC- CH_4 , and CTD- O_2 instruments. For example, all sensors should be equipped with a central water inlet or individual revised pumps that are more resistant to environmental influences. In addition, water flow at the instruments should be monitored or self-cleaning pump systems used. The inclusion of other, non-pumped loggers, such as for CTD- O_2 determinations, can supplement and validate the sensor data. Potential fouling on these loggers can be reduced by using UV lamps, such as those deployed during the lander surveys (very short UV irradiation is sufficient).

5. Summary

Shallow water zones and rewetted peatlands can play essential roles in OM sequestration, but current estimates of their contribution are not supported by long-term data with adequate resolution. Moreover, knowledge of the temporal and spatial variability of the processes controlling the distribution of $p\text{CO}_2$ and $p\text{CH}_4$ is limited. Therefore, identifying local nearshore sinks and sources of atmospheric GHGs remains an important task. This dissertation addresses the release of GHGs from nearshore sediments with peat deposits under long (Hütelmoor) and short (Drammendorf) seawater exposure. Most of the measurements were of high temporal resolution and were made using new, advanced lander platforms. A particular focus was the actively induced rewetting of a drained coastal peatland. Its permanent hydrological connection with the Baltic Sea allowed investigation of the influence of brackish water on the distribution of GHGs. Here, the governing processes are largely unknown, but will henceforth influence the marine nearshore carbon balance.

The Hütelmoor survey combined stationary high-resolution measurements at the sediment surface with additional water column measurements and numerical model simulations. The latter simulated the salinity and temperature distribution of the water column as well as cross-scale water movement processes. The field data revealed the considerable temporal dynamics of the GHG distribution, with concentration changes of up to one order of magnitude within a few hours (i.e., 7 – 27 h) that were partly triggered by event-based changes in the water column. Three of those changes were identified: (i) an advection of water masses that transported salt-enriched and CO_2 -enriched (up to $1000 \mu\text{atm-CO}_2$) water, (ii) a storm with wind speeds of up to 19 m s^{-1} that resulted in sediment re-suspension and likely affected pore water interactions, and (iii) a stagnant period with bottom-water O_2 depletion and the accumulation of CO_2 and CH_4 . Given the shallow water column of $\sim 6 \text{ m}$, such events might lead to a supersaturation of the surface water with GHGs, allowing the study area to act as a short-term source of atmospheric GHGs.

The GHG response to the rewetting of a coastal peatland with brackish water was evaluated by determining GHG emissions before, during the first year, and during the second year of the rewetting at the Drammendorf study site, as summarized in Figure 22. In general, the literature values for CO_2 uptake or release from peatlands rewetted by freshwater vary widely and depend, e.g., on previous use, prevailing vegetation, the water level, and the duration of rewetting (Figure 22, top). Before rewetting, the studied peatland was a source of CO_2 , with

comparable fluxes from the dry soil and the ditch (Figure 22, middle). After rewetting with brackish water, fluxes were in the same magnitude as under drained conditions (Figure 22, bottom). In the second year after rewetting (lander survey), CO₂ emissions decreased by a factor of 1.9, but representing only a potential trend. Nevertheless, emissions were higher than in studies that examined peatlands flooded by freshwater. The main driver of emissions after rewetting was likely the high OM availability from the residual vegetation (no topsoil removal prior to rewetting) and the high rate of primary production in the water column. Measurements with temporal high-resolution showed strong fluctuation of *p*CO₂, expressed as multi-day, diurnal, and event-based variability. Spatial differences in variables controlled dominantly by biological processes were also a feature of the flooded peatland.

The rewetting of peatlands with freshwater usually results in high CH₄ emissions occurring under anoxic conditions (Figure 22, top). Before rewetting, Drammendorf was a source of CH₄, especially from its water-filled ditches (Figure 22, middle). After rewetting, CH₄ fluxes increased by one order of magnitude (Figure 22, bottom), but tended to lower values in the second year, with CH₄ fluxes decreasing by a factor of 2.6. Despite the immediate increase after rewetting, the CH₄ emissions were low compared to those reported from peatlands rewetted with freshwater, suggesting that rewetting with brackish or seawater could minimize CH₄ emissions. The lower emissions were associated with the suppressed formation of CH₄ and the promotion of its aerobic and anaerobic oxidation, due to the availability of O₂ (i.e., well-mixed water column) and SO₄²⁻ in the water column. The high-resolution investigation also revealed strong multi-day, short-term (< 1 day), and event-based variability in the CH₄ distribution.

This study of a heterogeneous coastal area and a peatland with limited field accessibility faced several challenges, such as the need for extensive technical infrastructure or conditions negatively affecting data acquisition due to inadequately adapted methods. The latter was particularly pronounced in the peatland and both the discrete sample analysis and the state-of-the-art sensor measurements were compromised by turbid water conditions and particle/sediment transport. This resulted in a lower data quality in some cases. Nevertheless, robust post-processing of sensor data was achieved in conjunction with discrete water samples that were also used to verify the sensor data. Furthermore, the reduced data quality was of less concern when considering the observed amplitudes of the fluctuations at the two study sites. Thus, the chosen methodological approach ultimately proved to be a very robust

strategy. Moreover, the observed temporal and spatial heterogeneity of the GHG distributions emphasizes the need to pursue comparable approaches and implement long-term monitoring strategies for coastal research.

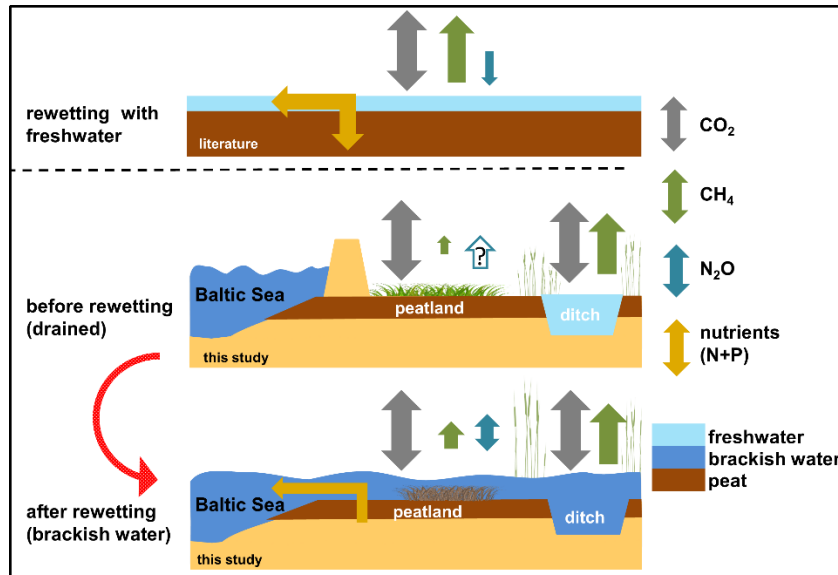


Figure 22: Summary of the results in Drammendorf. Schematic overview of (a) literature-based GHG fluxes after rewetting with freshwater, (b) measured GHG fluxes in the drained condition, and (c) measured GHG fluxes after rewetting with brackish water.

6. Outlook

Studies of nearshore areas and rewetted coastal peatlands are usually constrained by financial and methodological challenges. However, the research conducted for this dissertation shows that an approach based on high temporal resolution measurements and discrete sampling enables investigations of the processes controlling the distribution of nearshore CO₂ and CH₄. In addition to adjustments aimed at improving the reliability of sensor-based measurements in shallow water (e.g., of the pumps; Sect. 4.4), future studies will benefit from coupling point measurements from landers with modeling techniques. The advantages conferred by these improvements include the following: First, sensor deployment is costly and the sensors must be operated by skilled personnel whereas modeling can cover larger shallow water areas and the results verified by sensor measurements. Second, extreme events (tipping points), some of which have been identified in this work and have determined the coastal heterogeneity, can be better detected and located. Guided by model predictions (e.g., storm), targeted sensor-based measurements could be made at already installed platforms by switching them from low-power (i.e., battery saving) to high-resolution mode to track the event. A fundamental requirement is that the sensor-based measurements from the landers can be reliably retrieved in real time. This cross-scale approach could lead to the creation of an autonomous monitoring network for coastal zones that explicitly includes niche areas, such as flooded coastal peatlands.

7. References

- Archer, D.: Fate of fossil fuel CO₂ in geologic time, *J. Geophys. Res.*, 110, <https://doi.org/10.1029/2004JC002625>, 2005.
- Asmala, E., Carstensen, J., Conley, D. J., Slomp, C. P., Stadmark, J., and Voss, M.: Efficiency of the coastal filter: Nitrogen and phosphorus removal in the Baltic Sea, *Limnol. Oceanogr.*, 62, S222-S238, <https://doi.org/10.1002/lno.10644>, 2017.
- Augustin, J. and Chojnicki, B.: Austausch von klimarelevanten Spurengasen, Klimawirkung und Kohlenstoffdynamik in den ersten Jahren nach Wiedervernässung von degradiertem Niedermoorgrünland, *Berichte des Leibniz-Institut für Gewässerökologie und Binnenfischerei*, 50–61, 2008.
- BACC II Author Team: Second Assessment of Climate Change for the Baltic Sea Basin, Regional Climate Studies, Springer, Berlin, <https://doi.org/10.1007/978-3-319-16006-1>, 2015.
- Bakker, D. C. E., Pfeil, B., Landa, C. S., Metzl, N., O'Brien, K. M., Olsen, A., Smith, K., Cosca, C., Harasawa, S., Jones, S. D., Nakaoka, S.-I., Nojiri, Y., Schuster, U., Steinhoff, T., Sweeney, C., Takahashi, T., Tilbrook, B., Wada, C., Wanninkhof, R., Alin, S. R., Balestrini, C. F., Barbero, L., Bates, N. R., Bianchi, A. A., Bonou, F., Boutin, J., Bozec, Y., Burger, E. F., Cai, W.-J., Castle, R. D., Chen, L., Chierici, M., Currie, K., Evans, W., Featherstone, C., Feely, R. A., Fransson, A., Goyet, C., Greenwood, N., Gregor, L., Hankin, S., Hardman-Mountford, N. J., Harlay, J., Hauck, J., Hoppema, M., Humphreys, M. P., Hunt, C. W., Huss, B., Ibáñez, J. S. P., Johannessen, T., Keeling, R., Kitidis, V., Körtzinger, A., Kozyr, A., Krasakopoulou, E., Kuwata, A., Landschützer, P., Lauvset, S. K., Lefèvre, N., Lo Monaco, C., Manke, A., Mathis, J. T., Merlivat, L., Millero, F. J., Monteiro, P. M. S., Munro, D. R., Murata, A., Newberger, T., Omar, A. M., Ono, T., Paterson, K., Pearce, D., Pierrot, D., Robbins, L. L., Saito, S., Salisbury, J., Schlitzer, R., Schneider, B., Schweitzer, R., Sieger, R., Skjelvan, I., Sullivan, K. F., Sutherland, S. C., Sutton, A. J., Tadokoro, K., Telszewski, M., Tuma, M., van Heuven, S. M. A. C., Vandemark, D., Ward, B., Watson, A. J., and Xu, S.: A multi-decade record of high-quality fCO₂ data in version 3 of the Surface Ocean CO₂ Atlas (SOCAT), *Earth Syst. Sci. Data*, 8, 383–413, <https://doi.org/10.5194/essd-8-383-2016>, 2016.
- Bange, H. W.: Nitrous oxide and methane in European coastal waters, *Estuarine, Coastal and Shelf Science*, 70, 361–374, <https://doi.org/10.1016/j.ecss.2006.05.042>, 2006.
- Bange, H. W., Bartell, U. H., Rapsomanikis, S., and Andreae, M. O.: Methane in the Baltic and North Seas and a reassessment of the marine emissions of methane, *Global Biogeochem. Cycles*, 8, 465–480, <https://doi.org/10.1029/94GB02181>, 1994.
- Bange, H. W., Bergmann, K., Hansen, H. P., Kock, A., Koppe, R., Malien, F., and Ostrau, C.: Dissolved methane during hypoxic events at the Boknis Eck time series station (Eckernförde Bay, SW Baltic Sea), *Biogeosciences*, 7, 1279–1284, <https://doi.org/10.5194/bg-7-1279-2010>, 2010.
- Bange, H. W., Dahlke, S., Ramesh, R., Meyer-Reil, L.-A., Rapsomanikis, S., and Andreae, M. O.: Seasonal Study of Methane and Nitrous Oxide in the Coastal Waters of the Southern Baltic Sea, *Estuarine, Coastal and Shelf Science*, 47, 807–817, <https://doi.org/10.1006/ecss.1998.0397>, 1998.
- Bartlett, K. B., Bartlett, D. S., Harriss, R. C., and Sebacher, D. I.: Methane emissions along a salt marsh salinity gradient, *Biogeochemistry*, 4, 183–202, <https://doi.org/10.1007/BF02187365>, 1987.
- Beer, D. de, Wenzhöfer, F., Ferdelman, T. G., Boehme, S. E., Huettel, M., van Beusekom, J. E. E., Böttcher, M. E., Musat, N., and Dubilier, N.: Transport and mineralization rates in North Sea sandy intertidal sediments, Sylt-Rømø Basin, Wadden Sea, *Limnol. Oceanogr.*, 50, 113–127, <https://doi.org/10.4319/lo.2005.50.1.0113>, 2005.

- Beldowski, J., Löffler, A., Schneider, B., and Joensuu, L.: Distribution and biogeochemical control of total CO₂ and total alkalinity in the Baltic Sea, *Journal of Marine Systems*, 81, 252–259, <https://doi.org/10.1016/j.jmarsys.2009.12.020>, 2010.
- Bittig, H. C., Fiedler, B., Scholz, R., Krahmann, G., and Körtzinger, A.: Time response of oxygen optodes on profiling platforms and its dependence on flow speed and temperature, *Limnol. Oceanogr. Methods*, 12, 617–636, <https://doi.org/10.4319/lom.2014.12.617>, 2014.
- Bittig, H. C. and Körtzinger, A.: Tackling Oxygen Optode Drift: Near-Surface and In-Air Oxygen Optode Measurements on a Float Provide an Accurate in Situ Reference, *Journal of Atmospheric and Oceanic Technology*, 32, 1536–1543, <https://doi.org/10.1175/JTECH-D-14-00162.1>, 2015.
- Bižić, M., Grossart, H.-P., and Ionescu, D.: Methane Paradox, In: eLS. John Wiley & Sons, Ltd: Chichester, 1–11, <https://doi.org/10.1002/9780470015902.a0028892>, 2020.
- Boetius, A., Ravensschlag, K., Schubert, C. J., Rickert, D., Widdel, F., Gieseke, A., Amann, R., Jørgensen, B. B., Witte, U., and Pfannkuche, O.: A marine microbial consortium apparently mediating anaerobic oxidation of methane, *Nature*, 407, 623–626, <https://doi.org/10.1038/35036572>, 2000.
- Borges, A. V., Champenois, W., Gypens, N., Delille, B., and Harlay, J.: Massive marine methane emissions from near-shore shallow coastal areas, *Scientific reports*, 6, 27908, <https://doi.org/10.1038/srep27908>, 2016.
- Borges, A. V., Speeckaert, G., Champenois, W., Scranton, M. I., and Gypens, N.: Productivity and Temperature as Drivers of Seasonal and Spatial Variations of Dissolved Methane in the Southern Bight of the North Sea, *Ecosystems*, 21, 583–599, <https://doi.org/10.1007/s10021-017-0171-7>, 2018.
- Brisch, A.: Erkundung von Torfmächtigkeit und Vegetation in zwei potenziellen Wiedervernässungsgebieten bei Ramin und Grosow (Rügen), Unpublished expert opinion by Naturschutzstiftung Deutsche Ostsee, 2015.
- Buer, A.-L., Gyraite, G., Wegener, P., Lange, X., Katarzyte, M., Hauk, G., and Schernewski, G.: Long term development of Bathing Water Quality at the German Baltic coast: spatial patterns, problems and model simulations, *Marine Pollution Bulletin*, 135, 1055–1066, <https://doi.org/10.1016/j.marpolbul.2018.08.048>, 2018.
- Cabezas, A., Gelbrecht, J., Zwirnmann, E., Barth, M., and Zak, D.: Effects of degree of peat decomposition, loading rate and temperature on dissolved nitrogen turnover in rewetted fens, *Soil Biology and Biochemistry*, 48, 182–191, <https://doi.org/10.1016/j.soilbio.2012.01.027>, 2012.
- Canning, A. R., Fietzek, P., Rehder, G., and Körtzinger, A.: Technical note: Seamless gas measurements across the land–ocean aquatic continuum – corrections and evaluation of sensor data for CO₂, CH₄ and O₂ from field deployments in contrasting environments, *Biogeosciences*, 18, 1351–1373, <https://doi.org/10.5194/bg-18-1351-2021>, 2021.
- Capone, D. G. and Kiene, R. P.: Comparison of microbial dynamics in marine and freshwater sediments: Contrasts in anaerobic carbon catabolism, *Limnol. Oceanogr.*, 33, 725–749, <https://doi.org/10.4319/lo.1988.33.4part2.0725>, 1988.
- Carpenter, J. H.: The accuracy of the Winkler method for dissolved oxygen analysis, *Limnol. Oceanogr.*, 10, 135–140, <https://doi.org/10.4319/lo.1965.10.1.0135>, 1965.
- Carter, B. R., Radich, J. A., Doyle, H. L., and Dickson, A. G.: An automated system for spectrophotometric seawater pH measurements, *Limnol. Oceanogr. Methods*, 11, 16–27, <https://doi.org/10.4319/lom.2013.11.16>, 2013.
- Cohen, J.: Statistical power analysis for the behavioral sciences, Erlbaum, ISBN 0-8058-0283-5, 1988.
- Couwenberg, J., Thiele, A., Tanneberger, F., Augustin, J., Bärisch, S., Dubovik, D., Liashchinskaya, N., Michaelis, D., Minke, M., Skuratovich, A., and Joosten, H.: Assessing greenhouse gas emissions

from peatlands using vegetation as a proxy, *Hydrobiologia*, 674, 67–89, <https://doi.org/10.1007/s10750-011-0729-x>, 2011.

Crutzen, P. J.: Methane's sinks and sources, *Nature*, 350, 380–381, <https://doi.org/10.1038/350380a0>, 1991.

Danevčič, T., Mandic-Mulec, I., Stres, B., Stopar, D., and Hacin, J.: Emissions of CO₂, CH₄ and N₂O from Southern European peatlands, *Soil Biology and Biochemistry*, 42, 1437–1446, <https://doi.org/10.1016/j.soilbio.2010.05.004>, 2010.

Dean, J. F., Middelburg, J. J., Röckmann, T., Aerts, R., Blauw, L. G., Egger, M., Jetten, M. S. M., Jong, A. E. E. de, Meisel, O. H., Rasigraf, O., Slomp, C. P., in't Zandt, M. H., and Dolman, A. J.: Methane Feedbacks to the Global Climate System in a Warmer World, *Rev. Geophys.*, 56, 207–250, <https://doi.org/10.1002/2017RG000559>, 2018.

Deppenmeier, U.: The unique biochemistry of methanogenesis, *Progress in nucleic acid research and molecular biology*, 71, 223–283, [https://doi.org/10.1016/s0079-6603\(02\)71045-3](https://doi.org/10.1016/s0079-6603(02)71045-3), 2002.

Dickson, A. and Riley, J.: The estimation of acid dissociation constants in seawater media from potentiometric titrations with strong base. I. The ionic product of water — Kw, *Marine Chemistry*, 7, 89–99, [https://doi.org/10.1016/0304-4203\(79\)90001-X](https://doi.org/10.1016/0304-4203(79)90001-X), 1979.

Dickson, A. G.: An exact definition of total alkalinity and a procedure for the estimation of alkalinity and total inorganic carbon from titration data, *Deep Sea Research Part A. Oceanographic Research Papers*, 28, 609–623, [https://doi.org/10.1016/0198-0149\(81\)90121-7](https://doi.org/10.1016/0198-0149(81)90121-7), 1981.

Dickson, A. G.: Standard potential of the reaction: AgCl(s) + 1/2H₂(g) = Ag(s) + HCl(aq), and the standard acidity constant of the ion HSO₄⁻ in synthetic sea water from 273.15 to 318.15 K, *The Journal of Chemical Thermodynamics*, 22, 113–127, [https://doi.org/10.1016/0021-9614\(90\)90074-Z](https://doi.org/10.1016/0021-9614(90)90074-Z), 1990.

Dickson, A. G., Afghan, J. D., and Anderson, G. C.: Reference materials for oceanic CO₂ analysis: a method for the certification of total alkalinity, *Marine Chemistry*, 80, 185–197, [https://doi.org/10.1016/S0304-4203\(02\)00133-0](https://doi.org/10.1016/S0304-4203(02)00133-0), 2003.

Dickson, A. G., Sabine, C. L. and Christian, J. R. (Eds.): Guide to best practices for ocean CO₂ measurements, North Pacific Marine Science Organization, ISBN 1-897176-07-4, 2007.

Dlugokencky, E., Crotwell, A., Mund, J., Crotwell, M., and Thoning, K.: Atmospheric Methane Dry Air Mole Fractions from the NOAA ESRL Carbon Cycle Cooperative Global Air Sampling Network, 1983–2018, <https://doi.org/10.15138/VNCZ-M766>, 2019a.

Dlugokencky, E., Crotwell, A., Mund, J., Crotwell, M., and Thoning, K.: Atmospheric Methane Dry Air Mole Fractions from the NOAA ESRL Carbon Cycle Cooperative Global Air Sampling Network, 1983–2018, <https://doi.org/10.15138/wkgj-f215>, 2019b.

Doney, S. C.: The growing human footprint on coastal and open-ocean biogeochemistry, *Science* (New York, N.Y.), 328, 1512–1516, <https://doi.org/10.1126/science.1185198>, 2010.

Duhamel, S., Nogaro, G., and Steinman, A. D.: Effects of water level fluctuation and sediment–water nutrient exchange on phosphorus biogeochemistry in two coastal wetlands, *Aquat Sci*, 79, 57–72, <https://doi.org/10.1007/s00027-016-0479-y>, 2017.

Dutaur, L. and Verchot, L. V.: A global inventory of the soil CH₄ sink, *Global Biogeochem. Cycles*, 21, 1–9, <https://doi.org/10.1029/2006GB002734>, 2007.

Ehhalt, D. H.: The atmospheric cycle of methane, *Tellus A: Dynamic Meteorology and Oceanography*, 26, 58, <https://doi.org/10.3402/tellusa.v26i1-2.9737>, 2022.

Enders, K., K  ppler, A., Bini  sch, O., Feldens, P., Stollberg, N., Lange, X., Fischer, D., Eichhorn, K.-J., Pollehne, F., Oberbeckmann, S., and Labrenz, M.: Tracing microplastics in aquatic environments

based on sediment analogies, *Scientific reports*, 9, 15207, <https://doi.org/10.1038/s41598-019-50508-2>, 2019.

Feely, R. A., Sabine, C. L., Lee, K., Berelson, W., Kleypas, J., Fabry, V. J., and Millero, F. J.: Impact of anthropogenic CO₂ on the CaCO₃ system in the oceans, *Science* (New York, N.Y.), 305, 362–366, <https://doi.org/10.1126/science.1097329>, 2004.

Fiedler, B., Fietzek, P., Vieira, N., Silva, P., Bittig, H. C., and Körtzinger, A.: In Situ CO₂ and O₂ Measurements on a Profiling Float, *Journal of Atmospheric and Oceanic Technology*, 30, 112–126, <https://doi.org/10.1175/JTECH-D-12-00043.1>, 2013.

Field, J. G. (Ed.): *Oceans 2020*, Island Press, ISBN 1559634693, 2002.

Fietzek, P., Fiedler, B., Steinhoff, T., and Körtzinger, A.: In situ Quality Assessment of a Novel Underwater pCO₂ Sensor Based on Membrane Equilibration and NDIR Spectrometry, *Journal of Atmospheric and Oceanic Technology*, 31, 181–196, <https://doi.org/10.1175/JTECH-D-13-00083.1>, 2014.

Franz, D., Koebisch, F., Larmanou, E., Augustin, J., and Sachs, T.: High net CO₂ and CH₄ release at a eutrophic shallow lake on a formerly drained fen, *Biogeosciences*, 13, 3051–3070, <https://doi.org/10.5194/bg-13-3051-2016>, 2016.

Friedlingstein, P., O'Sullivan, M., Jones, M. W., Andrew, R. M., Gregor, L., Hauck, J., Le Quéré, C., Luijkx, I. T., Olsen, A., Peters, G. P., Peters, W., Pongratz, J., Schwingshackl, C., Sitch, S., Canadell, J. G., Ciais, P., Jackson, R. B., Alin, S. R., Alkama, R., Arneeth, A., Arora, V. K., Bates, N. R., Becker, M., Bellouin, N., Bittig, H. C., Bopp, L., Chevallier, F., Chini, L. P., Cronin, M., Evans, W., Falk, S., Feely, R. A., Gasser, T., Gehlen, M., Gkritzalis, T., Gloege, L., Grassi, G., Gruber, N., Gürses, Ö., Harris, I., Hefner, M., Houghton, R. A., Hurtt, G. C., Iida, Y., Ilyina, T., Jain, A. K., Jersild, A., Kadono, K., Kato, E., Kennedy, D., Klein Goldewijk, K., Knauer, J., Korsbakken, J. I., Landschützer, P., Lefèvre, N., Lindsay, K., Liu, J., Liu, Z., Marland, G., Mayot, N., McGrath, M. J., Metzl, N., Monacchi, N. M., Munro, D. R., Nakaoka, S.-I., Niwa, Y., O'Brien, K., Ono, T., Palmer, P. I., Pan, N., Pierrot, D., Pocock, K., Poulter, B., Resplandy, L., Robertson, E., Rödenbeck, C., Rodriguez, C., Rosan, T. M., Schwinger, J., Séférian, R., Shutler, J. D., Skjelvan, I., Steinhoff, T., Sun, Q., Sutton, A. J., Sweeney, C., Takao, S., Tanhua, T., Tans, P. P., Tian, X., Tian, H., Tilbrook, B., Tsujino, H., Tubiello, F., van der Werf, G. R., Walker, A. P., Wanninkhof, R., Whitehead, C., Willstrand Wranne, A., Wright, R., Yuan, W., Yue, C., Yue, X., Zaehle, S., Zeng, J., and Zheng, B.: Global Carbon Budget 2022, *Earth Syst. Sci. Data*, 14, 4811–4900, <https://doi.org/10.5194/essd-14-4811-2022>, 2022.

Frolking, S., Talbot, J., Jones, M. C., Treat, C. C., Kauffman, J. B., Tuittila, E.-S., and Roulet, N.: Peatlands in the Earth's 21st century climate system, *Environ. Rev.*, 19, 371–396, <https://doi.org/10.1139/a11-014>, 2011.

Gattuso, J.-P., Epitalon, J.-M., Lavigne, H., and Orr, J.: seacarb: Seawater Carbonate Chemistry, <https://CRAN.R-project.org/> <https://CRAN.R-project.org/package=seacarb> (last access: 06 February 2022), R package version 3.2.15, 2019.

Gelesh, L., Marshall, K., Boicourt, W., and Lapham, L.: Methane concentrations increase in bottom waters during summertime anoxia in the highly eutrophic estuary, Chesapeake Bay, U.S.A, *Limnol. Oceanogr.*, 61, S253–S266, <https://doi.org/10.1002/lno.10272>, 2016.

Glatzel, S., Forbrich, I., Krüger, C., Lemke, S., and Gerold, G.: Environmental controls of greenhouse gas release in a restoring peat bog in NW Germany, *Biogeosciences Discussions, European Geosciences*, 213–242, <https://doi.org/10.5194/bg-5-213-2008>, 2008.

Grasshoff, K., Kremling, K., and Ehrhardt, M.: *Methods of Seawater Analysis*, Wiley-VCH, ISBN 3527295895, 2009.

Gräwe, U. and Burchard, H.: Storm surges in the Western Baltic Sea: the present and a possible future, *Clim Dyn*, 39, 165–183, <https://doi.org/10.1007/s00382-011-1185-z>, 2012.

- Grossart, H.-P., Frindte, K., Dziallas, C., Eckert, W., and Tang, K. W.: Microbial methane production in oxygenated water column of an oligotrophic lake, *Proceedings of the National Academy of Sciences of the United States of America*, 108, 19657–19661, <https://doi.org/10.1073/pnas.1110716108>, 2011.
- Gülzow, W., Gräwe, U., Kedzior, S., Schmale, O., and Rehder, G.: Seasonal variation of methane in the water column of Arkona and Bornholm Basin, western Baltic Sea, *Journal of Marine Systems*, 139, 332–347, <https://doi.org/10.1016/j.jmarsys.2014.07.013>, 2014.
- Hahn, J., Köhler, S., Glatzel, S., and Jurasinski, G.: Methane Exchange in a Coastal Fen in the First Year after Flooding - A Systems Shift, *PloS one*, 10, 1–25, <https://doi.org/10.1371/journal.pone.0140657>, 2015.
- Hahn-Schöfl, M., Zak, D., Minke, M., Gelbrecht, J., Augustin, J., and Freibauer, A.: Organic sediment formed during inundation of a degraded fen grassland emits large fluxes of CH₄ and CO₂, *Biogeosciences*, 8, 1539–1550, <https://doi.org/10.5194/bg-8-1539-2011>, 2011.
- Hansell, D. A. and Carlson, C. A.: *Biogeochemistry of marine dissolved organic matter*, Academic Press, ISBN 9780124071537, 2014.
- Harpenslager, S. F., van den Elzen, E., Kox, M. A., Smolders, A. J., Ettwig, K. F., and Lamers, L. P.: Rewetting former agricultural peatlands: Topsoil removal as a prerequisite to avoid strong nutrient and greenhouse gas emissions, *Ecological Engineering*, 84, 159–168, <https://doi.org/10.1016/j.ecoleng.2015.08.002>, 2015.
- HELCOM: State of the Baltic Sea – Second HELCOM holistic assessment 2011-2016. Baltic Sea Environment, www.helcom.fi/baltic-sea-trends/holistic-assessments/state-of-the-baltic-sea-2018/reports-and-materials/ (last access 01 February 2023), HELCOM, 2018.
- Heyer, J. and Berger, U.: Methane Emission from the Coastal Area in the Southern Baltic Sea, *Estuarine, Coastal and Shelf Science*, 51, 13–30, <https://doi.org/10.1006/ecss.2000.0616>, 2000.
- Honkanen, M., Müller, J. D., Seppälä, J., Rehder, G., Kielosto, S., Ylöstalo, P., Mäkelä, T., Hatakka, J., and Laakso, L.: The diurnal cycle of pCO₂ in the coastal region of the Baltic Sea, *Ocean Sci.*, 17, 1657–1675, <https://doi.org/10.5194/os-17-1657-2021>, 2021.
- Houghton, R. A. and Hackler, J. L.: Carbon Flux to the Atmosphere from Land-Use Changes: 1850 to 1990, <https://doi.org/10.3334/CDIAC/lue.ndp050>, 2001.
- Humborg, C., Geibel, M. C., Sun, X., McCrackin, M., Mörtz, C.-M., Stranne, C., Jakobsson, M., Gustafsson, B., Sokolov, A., Norkko, A., and Norkko, J.: High Emissions of Carbon Dioxide and Methane From the Coastal Baltic Sea at the End of a Summer Heat Wave, *Front. Mar. Sci.*, 6, <https://doi.org/10.3389/fmars.2019.00493>, 2019.
- IPCC: Climate Change 2013: The Physical Science Basis. Contribution of Working Group I to the Fifth Assessment Report of the Intergovernmental Panel on Climate Change, [Stocker, T.F., D. Qin, G.-K. Plattner, M. Tignor, S.K. Allen, J. Boschung, A. Nauels, Y. Xia, V. Bex and P.M. Midgley (eds.)], Cambridge University Press, United Kingdom and New York, 2013.
- Jacobs, E., Bittig, H. C., Gräwe, U., Graves, C. A., Glockzin, M., Müller, J. D., Schneider, B., and Rehder, G.: Upwelling-induced trace gas dynamics in the Baltic Sea inferred from 8 years of autonomous measurements on a ship of opportunity, *Biogeosciences*, 18, 2679–2709, <https://doi.org/10.5194/bg-18-2679-2021>, 2021.
- Johnson, K. S., Coletti, L. J., Jannasch, H. W., Sakamoto, C. M., Swift, D. D., and Riser, S. C.: Long-Term Nitrate Measurements in the Ocean Using the in situ Ultraviolet Spectrophotometer: Sensor Integration into the APEX Profiling Float, *Journal of Atmospheric and Oceanic Technology*, 30, 1854–1866, <https://doi.org/10.1175/JTECH-D-12-00221.1>, 2013.

Joosten, H. and Clarke, D.: Wise use of mires and peatlands, Background and principles including a framework for decision-making, Internat. Mire Conservation Group, ISBN 9519774483, 2002.

Jørgensen, B. B. (Ed.): Bacteria and Marine Biogeochemistry, in: Marine Geochemistry, https://doi.org/10.1007/3-540-32144-6_5, 2006.

Jørgensen, B. B., Weber, A., and Zopfi, J.: Sulfate reduction and anaerobic methane oxidation in Black Sea sediments, Deep Sea Research Part I: Oceanographic Research Papers, 48, 2097–2120, [https://doi.org/10.1016/S0967-0637\(01\)00007-3](https://doi.org/10.1016/S0967-0637(01)00007-3), 2001.

Jurasinski, G., Günther, A. B., Huth, V., Couwenberg, J., and Glatzel, S.: Paludiculture – productive use of wet peatlands., Ecosystem services provided by paludiculture – Greenhouse gas emissions, 79–94, 2016.

Jurasinski, G., Janssen, M., Voss, M., Böttcher, M. E., Brede, M., Burchard, H., Forster, S., Gosch, L., Gräwe, U., Gründling-Pfaff, S., Haider, F., Ibenthal, M., Karow, N., Karsten, U., Kreuzburg, M., Lange, X., Leinweber, P., Massmann, G., Ptak, T., Rezanezhad, F., Rehder, G., Romoth, K., Schade, H., Schubert, H., Schulz-Vogt, H., Sokolova, I. M., Strehse, R., Unger, V., Westphal, J., and Lennartz, B.: Understanding the Coastal Ecocline: Assessing Sea–Land Interactions at Non-tidal, Low-Lying Coasts Through Interdisciplinary Research, Front. Mar. Sci., 5, <https://doi.org/10.3389/fmars.2018.00342>, 2018.

Kaat, A. and Joosten, H.: Factbook for UNFCCC policies on peat carbon emissions, Internat. Mire Group, 2009.

Kandel, T. P., Lærke, P. E., Hoffmann, C. C., and Elsgaard, L.: Complete annual CO₂, CH₄, and N₂O balance of a temperate riparian wetland 12 years after rewetting, Ecological Engineering, 127, 527–535, <https://doi.org/10.1016/j.ecoleng.2017.12.019>, 2019.

Karl, D. M., Beversdorf, L., Björkman, K. M., Church, M. J., Martinez, A., and DeLong, E. F.: Aerobic production of methane in the sea, Nature Geosci, 1, 473–478, <https://doi.org/10.1038/ngeo234>, 2008.

Karstens, S., Jurasinski, G., Glatzel, S., and Buczko, U.: Dynamics of surface elevation and microtopography in different zones of a coastal Phragmites wetland, Ecological Engineering, 94, 152–163, <https://doi.org/10.1016/j.ecoleng.2016.05.049>, 2016.

Knittel, K. and Boetius, A.: Anaerobic oxidation of methane: progress with an unknown process, Annual review of microbiology, 63, 311–334, <https://doi.org/10.1146/annurev.micro.61.080706.093130>, 2009.

Koebisch, F., Glatzel, S., Hofmann, J., Forbrich, I., and Jurasinski, G.: CO₂ exchange of a temperate fen during the conversion from moderately rewetting to flooding, J. Geophys. Res. Biogeosci., 118, 940–950, <https://doi.org/10.1002/jgrg.20069>, 2013.

Koebisch, F., Gottschalk, P., Beyer, F., Wille, C., Jurasinski, G., and Sachs, T.: The impact of occasional drought periods on vegetation spread and greenhouse gas exchange in rewetted fens, Philosophical transactions of the Royal Society of London. Series B, Biological sciences, 375, 20190685, <https://doi.org/10.1098/rstb.2019.0685>, 2020.

Koebisch, F., Jurasinski, G., Koch, M., Hofmann, J., and Glatzel, S.: Controls for multi-scale temporal variation in ecosystem methane exchange during the growing season of a permanently inundated fen, Agricultural and Forest Meteorology, 204, 94–105, <https://doi.org/10.1016/j.agrformet.2015.02.002>, 2015.

Kreuzburg, M.: Impacts of Holocene peat deposits on nearshore biogeochemical processes and trace gas production, https://doi.org/10.18453/rosdok_id00002569, 2019.

Kreuzburg, M., Ibenthal, M., Janssen, M., Rehder, G., Voss, M., Naumann, M., and Feldens, P.: Submarine Continuation of Peat Deposits From a Coastal Peatland in the Southern Baltic Sea and its Holocene Development, *Front. Earth Sci.*, 6, <https://doi.org/10.3389/feart.2018.00103>, 2018.

Kreyling, J., Tanneberger, F., Jansen, F., van der Linden, S., Aggenbach, C., Blüml, V., Couwenberg, J., Emsens, W.-J., Joosten, H., Klimkowska, A., Kotowski, W., Kozub, L., Lennartz, B., Liczner, Y., Liu, H., Michaelis, D., Oehmke, C., Parakenings, K., Pleyl, E., Poyda, A., Raabe, S., Röhl, M., Rücker, K., Schneider, A., Schrautzer, J., Schröder, C., Schug, F., Seeber, E., Thiel, F., Thiele, S., Tiemeyer, B., Timmermann, T., Urich, T., van Diggelen, R., Vegelin, K., Verbruggen, E., Wilmking, M., Wrage-Mönnig, N., Wołejko, L., Zak, D., and Jurasinski, G.: Rewetting does not return drained fen peatlands to their old selves, *Nature communications*, 12, 5693, <https://doi.org/10.1038/s41467-021-25619-y>, 2021.

Kuliński, K., Rehder, G., Asmala, E., Bartosova, A., Carstensen, J., Gustafsson, B., Hall, P. O. J., Humborg, C., Jilbert, T., Jürgens, K., Meier, H. E. M., Müller-Karulis, B., Naumann, M., Olesen, J. E., Savchuk, O., Schramm, A., Slomp, C. P., Sofiev, M., Sobek, A., Szymczycha, B., and Undeman, E.: Biogeochemical functioning of the Baltic Sea, *Earth Syst. Dynam.*, 13, 633–685, <https://doi.org/10.5194/esd-13-633-2022>, 2022.

Kuliński, K., Schneider, B., Hammer, K., Machulik, U., and Schulz-Bull, D.: The influence of dissolved organic matter on the acid–base system of the Baltic Sea, *Journal of Marine Systems*, 132, 106–115, <https://doi.org/10.1016/j.jmarsys.2014.01.011>, 2014.

Kuliński, K., Schneider, B., Szymczycha, B., and Stokowski, M.: Structure and functioning of the acid–base system in the Baltic Sea, *Earth Syst. Dynam.*, 8, 1107–1120, <https://doi.org/10.5194/esd-8-1107-2017>, 2017.

Lang, K., Schuldes, J., Klingl, A., Poehlein, A., Daniel, R., and Brunea, A.: New mode of energy metabolism in the seventh order of methanogens as revealed by comparative genome analysis of “*Candidatus methanoplasma termitum*”, *Applied and environmental microbiology*, 81, 1338–1352, <https://doi.org/10.1128/AEM.03389-14>, 2015.

Lange, X., Klingbeil, K., and Burchard, H.: Inversions of Estuarine Circulation Are Frequent in a Weakly Tidal Estuary With Variable Wind Forcing and Seaward Salinity Fluctuations, *J. Geophys. Res. Oceans*, 125, <https://doi.org/10.1029/2019JC015789>, 2020.

Linke, P., Sommer, S., Rovelli, L., and McGinnis, D. F.: Physical limitations of dissolved methane fluxes: The role of bottom-boundary layer processes, *Marine Geology*, 272, 209–222, <https://doi.org/10.1016/j.margeo.2009.03.020>, 2010.

Liu, H. and Lennartz, B.: Short Term Effects of Salinization on Compound Release from Drained and Restored Coastal Wetlands, *Water*, 11, 1549, <https://doi.org/10.3390/w11081549>, 2019.

Livingston, G. P. and Hutchinson, G.: Enclosure-based measurement of trace gas exchange: applications and sources of error., In: Matson, P.A. and Harris, R.C., Eds., *Biogenic trace gases: measuring emissions from soil and water.*, Blackwell Science Ltd., Oxford, UK., 14–51, 1995.

LU M-V: Konzept zum Schutz und zur Nutzung der Moore, Fortschreibung des Konzeptes zur Bestandssicherung und zur Entwicklung der Moore in Mecklenburg- Vorpommern (Moorschutzkonzept), Ministerium für Landwirtschaft und Umwelt Mecklenburg Vorpommern. Available online at http://service.mvnet.de/_php/download.php?datei_id=11159, last access 13 December 2022, 2009.

Mäkilä, M. and Saarnisto, M. (Eds.): *Peatlands and Climate Change, Chapter1: Carbon accumulation in boreal peatlands during the Holocene–Impacts of climate variations*, 2008.

Martikainen, P. J., Nykänen, H., Crill, P., and Silvola, J.: Effect of a lowered water table on nitrous oxide fluxes from northern peatlands, *Nature*, 366, 51–53, <https://doi.org/10.1038/366051a0>, 1993.

- Massel, S. R.: Circulation of groundwater due to wave set-up on a permeable beach, *Oceanologia*, 43, 279–290, 2001.
- McLeod, E.: A blueprint for blue carbon: Toward an improved understanding of the role of vegetated coastal habitats in sequestering CO₂, *Front. Ecol. Environ.*, 7, 362–370, 2011.
- Millero, F. J.: Carbonate constants for estuarine waters, *Mar. Freshwater Res.*, 61, 139, <https://doi.org/10.1071/MF09254>, 2010.
- Minkinen, K., Ojanen, P., Koskinen, M., and Penttilä, T.: Nitrous oxide emissions of undrained, forestry-drained, and rewetted boreal peatlands, *Forest Ecology and Management*, 478, 118494, <https://doi.org/10.1016/j.foreco.2020.118494>, 2020.
- Moore, T. R., Roulet, N. T., and Waddington, J. M.: Uncertainty in Predicting the Effect of Climatic Change on the Carbon Cycling of Canadian Peatlands, *Climatic Change*, 40, 229–245, <https://doi.org/10.1023/A:1005408719297>, 1998.
- Mort, H. P., Slomp, C. P., Gustafsson, B. G., and Andersen, T. J.: Phosphorus recycling and burial in Baltic Sea sediments with contrasting redox conditions, *Geochimica et Cosmochimica Acta*, 74, 1350–1362, <https://doi.org/10.1016/j.gca.2009.11.016>, 2010.
- Müller, J. D., Bastkowski, F., Sander, B., Seitz, S., Turner, D. R., Dickson, A. G., and Rehder, G.: Metrology for pH Measurements in Brackish Waters—Part 1: Extending Electrochemical pH_T Measurements of TRIS Buffers to Salinities 5–20, *Front. Mar. Sci.*, 5, <https://doi.org/10.3389/fmars.2018.00176>, 2018.
- Müller, J. D. and Rehder, G.: Metrology of pH Measurements in Brackish Waters—Part 2: Experimental Characterization of Purified meta-Cresol Purple for Spectrophotometric pH_T Measurements, *Front. Mar. Sci.*, 5, <https://doi.org/10.3389/fmars.2018.00177>, 2018.
- Müller, J. D., Schneider, B., and Rehder, G.: Long-term alkalinity trends in the Baltic Sea and their implications for CO₂-induced acidification, *Limnol. Oceanogr.*, 61, 1984–2002, <https://doi.org/10.1002/lno.10349>, 2016.
- Myhre, G., Shindell, D., Bréon, F.-M., Collins, W., Fuglestad, J., Huang, J., Koch, D., Lamarque, J.-F., Lee, D., Mendoza, B., Nakajima, A., Robock, A., Stephens, G., Takemura, T. and Zhang, H. (Eds.): *Anthropogenic and Natural Radiative Forcing*, Cambridge University Press, <https://doi.org/10.1017/CBO9781107415324.018>, 2014.
- Nixon, S. W.: Coastal marine eutrophication: A definition, social causes, and future concerns, *Ophelia*, 41, 199–219, <https://doi.org/10.1080/00785236.1995.10422044>, 1995.
- Oertel, C., Matschullat, J., Zurba, K., Zimmermann, F., and Erasmi, S.: Greenhouse gas emissions from soils—A review, *Geochemistry*, 76, 327–352, <https://doi.org/10.1016/j.chemer.2016.04.002>, 2016.
- Omstedt, A., Gustafsson, E., and Wesslander, K.: Modelling the uptake and release of carbon dioxide in the Baltic Sea surface water, *Continental Shelf Research*, 29, 870–885, <https://doi.org/10.1016/j.csr.2009.01.006>, 2009.
- Oremland, R. (Ed.): *Biogeochemistry of methanogenic bacteria*, J. Wiley & Sons, 1988.
- Parish, F., Sirin, A., Charman, D., Joosten, H., and Minayeva, T.: *Assessment on peatlands, biodiversity, and climate change, Main Report*, Global Environment Centre, Kuala Lumpur & Wetlands International, Wageningen, ISBN 9789834375102, 2008.
- Pönisch, D. L.: *Methodenentwicklung und –anwendung zur Analytik von Methan und Lachgas in Seewasser*, Leibniz Institute for Baltic Sea Research Warnemünde (IOW), Master thesis, 2018.

Pönisch, D. L., Breznikar, A., Gutekunst, C. N., Jurasinski, G., Voss, M., and Rehder, G.: Nutrient release and flux dynamics of CO₂, CH₄, and N₂O in a coastal peatland driven by actively induced rewetting with brackish water from the Baltic Sea, *Biogeosciences*, 20, 295–323, <https://doi.org/10.5194/bg-20-295-2023>, 2023.

R Core Team: R: A language and environment for statistical computing, R Foundation for Statistical Computing, Vienna, Austria, <https://www.R-project.org/> (last access: 10 January 2023), 2022.

Reeburgh, W. S.: Oceanic methane biogeochemistry, *Chemical reviews*, 107, 486–513, <https://doi.org/10.1021/cr050362v>, 2007.

Repeta, D. J., Ferrón, S., Sosa, O. A., Johnson, C. G., Repeta, L. D., Acker, M., DeLong, E. F., and Karl, D. M.: Marine methane paradox explained by bacterial degradation of dissolved organic matter, *Nature Geosci*, 9, 884–887, <https://doi.org/10.1038/NGEO2837>, 2016.

Römer, M., Riedel, M., Scherwath, M., Heesemann, M., and Spence, G. D.: Tidally controlled gas bubble emissions: A comprehensive study using long-term monitoring data from the NEPTUNE cabled observatory offshore Vancouver Island, *Geochem. Geophys. Geosyst.*, 17, 3797–3814, <https://doi.org/10.1002/2016GC006528>, 2016.

Rosenberg, R.: Eutrophication—The future marine coastal nuisance?, *Marine Pollution Bulletin*, 16, 227–231, [https://doi.org/10.1016/0025-326X\(85\)90505-3](https://doi.org/10.1016/0025-326X(85)90505-3), 1985.

Roth, F., Sun, X., Geibel, M. C., Prytherch, J., Brüchert, V., Bonaglia, S., Broman, E., Nascimento, F., Norkko, A., and Humborg, C.: High spatiotemporal variability of methane concentrations challenges estimates of emissions across vegetated coastal ecosystems, *Global change biology*, 28, 4308–4322, <https://doi.org/10.1111/gcb.16177>, 2022.

Sabbaghzadeh, B., Arévalo-Martínez, D. L., Glockzin, M., Otto, S., and Rehder, G.: Meridional and Cross-Shelf Variability of N₂O and CH₄ in the Eastern-South Atlantic, *J. Geophys. Res. Oceans*, 126, <https://doi.org/10.1029/2020JC016878>, 2021.

Sabine, C. L., Feely, R. A., Gruber, N., Key, R. M., Lee, K., Bullister, J. L., Wanninkhof, R., Wong, C. S., Wallace, D. W. R., Tilbrook, B., Millero, F. J., Peng, T.-H., Kozyr, A., Ono, T., and Rios, A. F.: The oceanic sink for anthropogenic CO₂, *Science (New York, N.Y.)*, 305, 367–371, <https://doi.org/10.1126/science.1097403>, 2004.

Sakamoto, C. M., Johnson, K. S., and Coletti, L. J.: Improved algorithm for the computation of nitrate concentrations in seawater using an in situ ultraviolet spectrophotometer, *Limnol. Oceanogr.*, 7, 132–143, <https://doi.org/10.4319/lom.2009.7.132>, 2009.

Saunois, M., Stavert, A. R., Poulter, B., Bousquet, P., Canadell, J. G., Jackson, R. B., Raymond, P. A., Dlugokencky, E. J., Houweling, S., Patra, P. K., Ciais, P., Arora, V. K., Bastviken, D., Bergamaschi, P., Blake, D. R., Brailsford, G., Bruhwiler, L., Carlson, K. M., Carrol, M., Castaldi, S., Chandra, N., Crevoisier, C., Crill, P. M., Covey, K., Curry, C. L., Etiope, G., Frankenberg, C., Gedney, N., Hegglin, M. I., Höglund-Isaksson, L., Hugelius, G., Ishizawa, M., Ito, A., Janssens-Maenhout, G., Jensen, K. M., Joos, F., Kleinen, T., Krummel, P. B., Langenfelds, R. L., Laruelle, G. G., Liu, L., Machida, T., Maksyutov, S., McDonald, K. C., McNorton, J., Miller, P. A., Melton, J. R., Morino, I., Müller, J., Murguía-Flores, F., Naik, V., Niwa, Y., Noce, S., O'Doherty, S., Parker, R. J., Peng, C., Peng, S., Peters, G. P., Prigent, C., Prinn, R., Ramonet, M., Regnier, P., Riley, W. J., Rosentreter, J. A., Segers, A., Simpson, I. J., Shi, H., Smith, S. J., Steele, L. P., Thornton, B. F., Tian, H., Tohjima, Y., Tubiello, F. N., Tsuruta, A., Viovy, N., Voulgarakis, A., Weber, T. S., van Weele, M., van der Werf, G. R., Weiss, R. F., Worthy, D., Wunch, D., Yin, Y., Yoshida, Y., Zhang, W., Zhang, Z., Zhao, Y., Zheng, B., Zhu, Q., Zhu, Q., and Zhuang, Q.: The Global Methane Budget 2000–2017, *Earth Syst. Sci. Data*, 12, 1561–1623, <https://doi.org/10.5194/essd-12-1561-2020>, 2020.

- Schmale, O., Schneider von Deimling, J., Gülzow, W., Nausch, G., Waniek, J. J., and Rehder, G.: Distribution of methane in the water column of the Baltic Sea, *Geophys. Res. Lett.*, 37, 1-5, <https://doi.org/10.1029/2010GL043115>, 2010.
- Schmaljohann, R.: Methane dynamics in the sediment and water column of Kiel Harbour (Baltic Sea), *Mar. Ecol. Prog. Ser.*, 131, 263–273, <https://doi.org/10.3354/meps131263>, 1996.
- Schneider, B. and Müller, J. D.: Biogeochemical Transformations in the Baltic Sea, Springer International Publishing, <https://doi.org/10.1007/978-3-319-61699-5>, 2018.
- Schneider, B. and Otto, S.: Organic matter mineralization in the deep water of the Gotland Basin (Baltic Sea): Rates and oxidant demand, *Journal of Marine Systems*, 195, 20–29, <https://doi.org/10.1016/j.jmarsys.2019.03.006>, 2019.
- Schönheit, P., Kristjansson, J. K., and Thauer, R. K.: Kinetic mechanism for the ability of sulfate reducers to out-compete methanogens for acetate, *Arch. Microbiol.*, 132, 285–288, <https://doi.org/10.1007/BF00407967>, 1982.
- Segarra, K. E., Comerford, C., Slaughter, J., and Joye, S. B.: Impact of electron acceptor availability on the anaerobic oxidation of methane in coastal freshwater and brackish wetland sediments, *Geochimica et Cosmochimica Acta*, 115, 15–30, <https://doi.org/10.1016/j.gca.2013.03.029>, 2013.
- Segers, R. and Kengen, S.: Methane production as a function of anaerobic carbon mineralization: A process model, *Soil Biology and Biochemistry*, 30, 1107–1117, [https://doi.org/10.1016/S0038-0717\(97\)00198-3](https://doi.org/10.1016/S0038-0717(97)00198-3), 1998.
- Sierszen, M. E., Morrice, J. A., Trebitz, A. S., and Hoffman, J. C.: A review of selected ecosystem services provided by coastal wetlands of the Laurentian Great Lakes, *Aquatic Ecosystem Health & Management*, 15, 92–106, <https://doi.org/10.1080/14634988.2011.624970>, 2012.
- Small, C. and Nicholls, R. J.: A Global Analysis of Human Settlement in Coastal Zones, *Journal of Coastal Research*, 19, 584–599, 2003.
- Steinle, L., Maltby, J., Treude, T., Kock, A., Bange, H. W., Engbersen, N., Zopfi, J., Lehmann, M. F., and Niemann, H.: Effects of low oxygen concentrations on aerobic methane oxidation in seasonally hypoxic coastal waters, *Biogeosciences*, 14, 1631–1645, <https://doi.org/10.5194/bg-14-1631-2017>, 2017.
- Stokowski, M., Schneider, B., Rehder, G., and Kuliński, K.: The characteristics of the CO₂ system of the Oder River estuary (Baltic Sea), *Journal of Marine Systems*, 211, 103418, <https://doi.org/10.1016/j.jmarsys.2020.103418>, 2020.
- Strack, M. (Ed.): Peatlands and climate change, Internat. Peat Soc, ISBN 978-952-99401-1-0, 2008.
- Succow, M. and Joosten, H. (Eds.): Landschaftsökologische Moorkunde, E. Schweizerbart'sche Verlagsbuchhandlung (Nägele u. Obermiller), ISBN 978-3-510-65198-6, 2001.
- Thauer, R. K., Kaster, A.-K., Seedorf, H., Buckel, W., and Hedderich, R.: Methanogenic archaea: ecologically relevant differences in energy conservation, *Nature reviews. Microbiology*, 6, 579–591, <https://doi.org/10.1038/nrmicro1931>, 2008.
- The Ocean Conference: Factsheet: People and Oceans, Marine Pollution, Biodiversity, Climate Change, United Nations, New York, 2017.
- Tiemeyer, B., Albiac Borraz, E., Augustin, J., Bechtold, M., Beetz, S., Beyer, C., Drösler, M., Ebli, M., Eickenscheidt, T., Fiedler, S., Förster, C., Freibauer, A., Giebels, M., Glatzel, S., Heinichen, J., Hoffmann, M., Höper, H., Jurasinski, G., Leiber-Sauheitl, K., Peichl-Brak, M., Roßkopf, N., Sommer, M., and Zeitz, J.: High emissions of greenhouse gases from grasslands on peat and other organic soils, *Global change biology*, 22, 4134–4149, <https://doi.org/10.1111/gcb.13303>, 2016.

- Treude, T., Krüger, M., Boetius, A., and Jørgensen, B. B.: Environmental control on anaerobic oxidation of methane in the gassy sediments of Eckernförde Bay (German Baltic), *Limnol. Oceanogr.*, 50, 1771–1786, <https://doi.org/10.4319/lo.2005.50.6.1771>, 2005.
- Turunen, J., Tomppo, E., Tolonen, K., and Reinikainen, A.: Estimating carbon accumulation rates of undrained mires in Finland—application to boreal and subarctic regions, *The Holocene*, 12, 69–80, <https://doi.org/10.1191/0959683602hl522rp>, 2002.
- Umweltbundesamt, B.: Factsheet - Moorschutz ist Klimaschutz, Deutsche Emissionshandelsstelle (DEHSt) im Umweltbundesamt. Available online at https://www.dehst.de/SharedDocs/downloads/DE/publikationen/Factsheet_Moore.pdf?__blob=publicationFile&v=6, last access 13 December 2022, 2022.
- Vallius, H.: Permanent Seafloor Anoxia in Coastal Basins of the Northwestern Gulf of Finland, Baltic Sea, *AMBIO: A Journal of the Human Environment*, 35, 105–108, [https://doi.org/10.1579/0044-7447\(2006\)35\[105:PSAICB\]2.0.CO;2](https://doi.org/10.1579/0044-7447(2006)35[105:PSAICB]2.0.CO;2), 2006.
- van de Riet, B. P., Hefting, M. M., and Verhoeven, J. T. A.: Rewetting Drained Peat Meadows: Risks and Benefits in Terms of Nutrient Release and Greenhouse Gas Exchange, *Water Air Soil Pollution*, 224, <https://doi.org/10.1007/s11270-013-1440-5>, 2013.
- Voss, M., Deutsch, B., Liskow, I., Pastuszak, M., Schulte, U., and Sitek, S.: Nitrogen retention in the Szczecin Lagoon, Baltic Sea, *Isotopes in environmental and health studies*, 46, 355–369, <https://doi.org/10.1080/10256016.2010.503895>, 2010.
- Vousdoukas, M. I., Voukouvalas, E., Annunziato, A., Giardino, A., and Feyen, L.: Projections of extreme storm surge levels along Europe, *Clim Dyn*, 47, 3171–3190, <https://doi.org/10.1007/s00382-016-3019-5>, 2016.
- Wanninkhof, R.: Relationship between wind speed and gas exchange over the ocean revisited, *Limnol. Oceanogr. Methods*, 12, 351–362, <https://doi.org/10.4319/lom.2014.12.351>, 2014.
- Wei, T. and Simko, V.: R package 'corrplot': Visualization of a Correlation Matrix, Available from <https://github.com/taiyun/corrplot> (last access: 25 February 2023), R package version 0.92, 2021.
- Weiss, R. F. and Price, B. A.: Nitrous oxide solubility in water and seawater, *Marine Chemistry*, 8, 347–359, [https://doi.org/10.1016/0304-4203\(80\)90024-9](https://doi.org/10.1016/0304-4203(80)90024-9), 1980.
- Whiticar, M. J. (Ed.): *The Biogeochemical Methane Cycle*, https://doi.org/10.1007/978-3-319-54529-5_5-1, 2020.
- Winkler, L. W.: Die Bestimmung des im Wasser gelösten Sauerstoffes, *Ber. Dtsch. Chem. Ges.*, 21, 2843–2854, <https://doi.org/10.1002/cber.188802102122>, 1888.
- Wolf-Gladrow, D. A., Zeebe, R. E., Klaas, C., Körtzinger, A., and Dickson, A. G.: Total alkalinity: The explicit conservative expression and its application to biogeochemical processes, *Marine Chemistry*, 106, 287–300, <https://doi.org/10.1016/j.marchem.2007.01.006>, 2007.
- Zak, D. and Gelbrecht, J.: The mobilisation of phosphorus, organic carbon and ammonium in the initial stage of fen rewetting (a case study from NE Germany), *Biogeochemistry*, 85, 141–151, <https://doi.org/10.1007/s10533-007-9122-2>, 2007.
- Zak, D., Meyer, N., Cabezas, A., Gelbrecht, J., Mauersberger, R., Tiemeyer, B., Wagner, C., and McInnes, R.: Topsoil removal to minimize internal eutrophication in rewetted peatlands and to protect downstream systems against phosphorus pollution: A case study from NE Germany, *Ecological Engineering*, 103, 488–496, <https://doi.org/10.1016/j.ecoleng.2015.12.030>, 2017.
- Zeebe, R. E. and Wolf-Gladrow, D.: *CO₂ in seawater: Equilibrium, kinetics, isotopes*, Elsevier, ISBN 0444505792, 2001.

Data availability and interdisciplinary collaborations

Two manuscripts exist describing the results and data from the Hütelmoor and Drammendorf lander surveys. These are in an advanced editing status and will be published in international journals. In conjunction the associated data will be available under a digital object name (DOI).

Pönisch, D. L., Bittig, H. C., Lange, X., Holtermann, P., Waern, M., and Rehder, G.: Autonomous high-resolution multi-parameter investigation of shallow coastal waters: variability and drivers of CO₂ and CH₄ (in prep.). With Supplementary data for the Hütelmoor lander survey:

- High-resolution lander data on PANGAE: Pönisch, D. L., Bittig, H. C., Rehder, G. (2023): Autonomous high-resolution multi-parameter measurements of marine variables in shallow near-shore waters of the German Baltic Sea to study the variability and drivers of CO₂ and CH₄. PANGAEA, <https://doi.org/10.1594/PANGAEA.956806>
- Flow velocity data on IOW data portal: <https://doi.org/10.12754/data-2023-0007>

Pönisch et al., 2023 (already published; <https://doi.org/10.5194/bg-20-295-2023>). With supplementary data for the Drammendorf field survey:

- Discrete field samples at IOW data portal: <https://doi.org/10.12754/data-2022-0003>
- GHG fluxes at IOW data portal: <https://doi.org/10.12754/data-2022-0004>

Pönisch, D. L., Bittig, H. C., Premaratne, K., Kolbe, M., Schuffenhauer, I., Otto, S., and Rehder, G.: Trace gas variability of CO₂ and CH₄ in a coastal peatland rewetted with brackish water from the Baltic Sea by autonomous high-resolution measurements (in prep). With supplementary data for the Drammendorf lander survey:

- High-resolution lander data on PANGAE: DOI in preparation
- Flow velocity data on IOW data portal: DOI in preparation

Marine coastal research particularly unites different scientific disciplines due to the complex and fast-changing environment resulting, for example, from sediment-water coupling and interactions between open waters and the terrestrial compartment. Thus, coastal research relies on interdisciplinary approaches and therefore the author of this dissertation would like to summarize the collaborations with other researchers involved in the biogeochemical interpretation of this work:

There was a cooperation with Cordula N. Gutekunst (University of Rostock) in the chamber-based determination of GHGs during the Drammendorf field survey, where she led the methodological implementation and data handling. Also, during this field survey, Anne Breznikar (IOW) was the head by calculating nutrient exports and helps with nitrous oxide interpretations. During the Hütelmoor lander survey, support was provided by Xaver Lange (IOW) in the implementation of the numerical modeling approach. Peter Holtermann (IOW) helped with the post-processing of the water velocity data. Furthermore, Henry C. Bittig (IOW) helped with the post-processing of the SBE SUNA V2 spectra.

These interdisciplinary collaborations were important contributions for biogeochemical interpretation, but comprise only a small part of the content of this dissertation and its contributions are estimated to be $\sim 5\%$.

Danksagung

An dieser Stelle möchte ich die Gelegenheit nutzen, um mich bei denjenigen zu bedanken, die mich auf dem Weg der Dissertation begleitet, unterstützt und inspiriert haben.

Ich möchte mich bei meinem Doktorvater, Prof. Dr. Gregor Rehder, für die Möglichkeit, meine Dissertation zu schreiben und für seine intensive Betreuung bedanken. Insbesondere sein Vertrauen in mich, seine Ratschläge sowie die Freiheit bei meinen Projekten haben mich in meiner Entwicklung unterstützt. Des Weiteren danke ich Prof. Dr. Gerald Jurasinski und Prof. Dr. Maren Voß für die hervorragende Ko-Betreuung.

Ich bedanke mich bei allen Mitautor/-innen der Publikation und der Manuskripte, insbesondere bei Anne Breznikar und Cordula N. Gutekunst für ihre fachlichen Begleitungen und für die Unterstützung in der Feldarbeit.

Des Weiteren möchte ich allen Mitarbeiter/-innen des IOW und meiner Arbeitsgruppe danken, die mich bei der Durchführung meiner zum Teil arbeitsgruppenübergreifenden Arbeit mit fachlichem und organisatorischem Rat maßgeblich unterstützt haben. Besonderer Dank geht dabei an Dr. Stefan Otto, Erik Jacobs, Dr. Henry Bittig, Martin Kolbe, Ingo Schuffenhauer, Siegfried Krüger, Dr. Robert Wagner, Dr. Matthias Kreuzburg und Benjamin Schönherr sowie an die Tauchergruppe des IOW.

Weiterhin möchte ich mich herzlich bei Benny Baumann, Mathias Meyer und Nadja Kinski bedanken, für die essentiellen technischen Zuarbeiten an den beiden Landern.

Ich danke meinen Eltern Anke und Lars Pönisch sowie meiner Familie und meinen Freunden, besonders Nils Trautmann und Robert Tröger, die mich unterstützt und geprägt haben. Zuletzt gilt ein besonderer Dank meiner Lebenspartnerin Cindy Hoppe, die mich während der gesamten Zeit motiviert und unterstützt hat und so maßgeblich zum Gelingen meiner Dissertation beigetragen hat.

Vielen Dank!

Curriculum Vitae

Contact information

Daniel Lars Pönisch *15.09.1993 in Dresden

Leibniz Institute for Baltic Sea Research Warnemünde

Trace Gas Biogeochemistry

daniel.poenisch@io-warnemuende.de

Education

01/2019 –	PhD Student, Leibniz Institute for Baltic Sea Research Warnemünde, Working Group Trace Gas Biogeochemistry DFG Research Training Group Baltic TRANSCOAST
11/2016 – 11/2018	Master of Science Chemistry – Universität Rostock, Master Thesis at the Leibniz Institute for Baltic Sea Research Warnemünde
11/2012 – 09/2016	Bachelor of Science Chemistry – Technische Universität Dresden
2012	Abitur – Gotthold-Ephraim-Lessing-Gymnasium Kamenz

Eidesstattliche Versicherung

Doktorandinnen/Doktoranden-Erklärung gemäß § 4 Absatz 1 Buchstaben g und h der Promotionsordnung der Mathematisch-Naturwissenschaftlichen Fakultät der Universität Rostock

Name: Daniel Lars Pönisch, geb. 15.09.1993

Ich habe eine Dissertation zum Thema:

Greenhouse gas release from nearshore sediments with peat deposits under long and short seawater exposure

an der Mathematisch-Naturwissenschaftlichen Fakultät der Universität Rostock angefertigt. Dabei wurde ich von Herr Prof. Dr. Gregor Rehder betreut.

Ich gebe folgende Erklärung ab:

1. Die Gelegenheit zum vorliegenden Promotionsvorhaben ist mir nicht kommerziell vermittelt worden. Insbesondere habe ich keine Organisation eingeschaltet, die gegen Entgelt Betreuerinnen/Betreuer für die Anfertigung von Dissertationen sucht oder die mir obliegenden Pflichten hinsichtlich der Prüfungsleistungen für mich ganz oder teilweise erledigt.
2. Ich versichere hiermit an Eides statt, dass ich die vorliegende Arbeit selbstständig angefertigt und ohne fremde Hilfe verfasst habe. Dazu habe ich keine außer den von mir angegebenen Hilfsmitteln und Quellen verwendet und die den benutzten Werken inhaltlich und wörtlich entnommenen Stellen habe ich als solche kenntlich gemacht.

Rostock, den
